UNIVERSITI TEKNOLOGI MARA

CHARACTERIZATION AND MECHANISTIC INSIGHTS INTO AMOXICILLIN ADSORPTION ON KOH-MODIFIED PALM KERNEL SHELL ACTIVATED CARBON

NUR FARADILA BINTI ANUAR

PhD

September 2026

UNIVERSITI TEKNOLOGI MARA

CHARACTERIZATION AND MECHANISTIC INSIGHTS INTO AMOXICILLIN ADSORPTION ON KOH-MODIFIED PALM KERNEL SHELL ACTIVATED CARBON

NUR FARADILA BINTI ANUAR

Thesis submitted in fulfilment
of the requirements for the degree of
Doctor of Philosophy
(Chemical Engineering)

Faculty of Chemical Engineering

September 2026

CONFIRMATION BY PANEL OF EXAMINERS

I certify that a Panel of Examiners has met on 14th May 2026 to conduct the final examination of Nur Faradila binti Anuar on her Doctor of Philosophy thesis entitled "Characterization and Mechanistic Insight into Amoxicillin Adsorption on KOH-Modified Palm Kernel Shell Activated Carbon" in accordance with Universiti Teknologi MARA Act 1976 (Akta 173). The Panel of Examiners recommends that the student be awarded the relevant degree. The Panel of Examiners was as follows:

Tan Huey Ling, PhD
Associate Professor
Faculty of Chemical Engineering
Universiti Teknologi MARA
(Chairperson)

Siti Wahidah Puasa, PhD
Associate Professor
Faculty of Chemical Engineering
Universiti Teknologi MARA
(Internal Examiner)

Hassimi Abu Hassan, PhD
Professor
Faculty of Engineering and Built Environment
Universiti Kebangsaan Malaysia
(External Examiner)

PROF DR HJH ZURAEDA IBRAHIM
Dean
Institute of Postgraduate Studies
Universiti Teknologi MARA

Date: 18 September 2026

AUTHOR'S DECLARATION

I declare that the work in this thesis was carried out in accordance with the regulations of Universiti Teknologi MARA. It is original and is the results of my own work, unless otherwise indicated or acknowledged as referenced work. This thesis has not been submitted to any other academic institution or non-academic institution for any degree or qualification.

I, hereby, acknowledge that I have been supplied with the Academic Rules and Regulations for Postgraduate, Universiti Teknologi MARA, regulating the conduct of my study and research.

Name of Student	:	Nur Faradila binti Anuar
Student ID. No.	:	2020453312
Programme	:	Doctor of Philosophy (Chemical Engineering) – EH950
Faculty	:	Chemical Engineering
Thesis Title	:	Characterization and Mechanistic Insight into Amoxicillin Adsorption on KOH-Modified Palm Kernel Shell Activated Carbon
Signature of Student	:	……..
Date	:	September 2026

ABSTRACT

Amoxicillin (AMX), a widely used antibiotic, is frequently detected in aquatic environments due to its incomplete removal by conventional wastewater treatment systems, posing significant environmental and public health concerns. Therefore, the development of sustainable and efficient adsorbents from agricultural waste materials has gained increasing attention for pharmaceutical wastewater treatment applications. This thesis presents a comprehensive investigation into the development and mechanistic understanding of a sustainable adsorbent derived from palm kernel shell (PKS) for the removal of AMX. Utilizing PKS, an abundant byproduct of Malaysia's palm oil industry, the study focuses on the synthesis of activated carbon through chemical activation with potassium hydroxide (KOH). The optimized preparation, employing a 1:3 KOH impregnation ratio and thermal activation at 700 ℃, produced a high surface area material (798.35 m^2/g) with enhanced pore volume (0.25 cm^3/g), significantly outperforming untreated biochar. To determine the optimum adsorption conditions, Response Surface Methodology (RSM) based on a Box–Behnken Design (BBD) was applied. The optimum parameters, consisting of 0.5 g of PKSAC in 200 mL of 20 ppm AMX solution at pH 4.0 and 50 minutes of contact time, resulted in an AMX removal efficiency of 86.82%, demonstrating close agreement between the predicted and experimental values obtained from the statistical model. The RSM model was statistically significant with a p-value below 0.0001 and a high regression coefficient (R^2 = 0.9947), confirming the reliability and accuracy of the optimization model. Kinetic and isotherm analyses further revealed that the adsorption process followed pseudo-second-order kinetics and fitted well with the Langmuir isotherm model, indicating monolayer adsorption governed by strong surface interactions with a maximum adsorption capacity of 219.66 mg/g. Critically, Density Functional Theory (DFT) simulations provided molecular-level insight into the adsorption mechanism. Strong interactions were observed between AMX and surface functional groups of PKSAC, primarily governed by hydrogen bonding, electrostatic attraction, and pore-filling mechanisms. In addition, π–π interactions may contribute due to the presence of aromatic structures in both AMX and PKSAC. Among these interactions, surface hydroxyl (OH) groups demonstrated the strongest binding interactions, with the highest adsorption energy recorded at −118.67 kJ/mol and a minimal HOMO–LUMO energy gap of 0.15 eV. These findings underscore the vital role of hydroxyl functionalities in enhancing adsorption affinity and stability. This integrative study, combining material synthesis, experimental optimization, adsorption modelling, and quantum chemical analysis, demonstrates the feasibility of converting agricultural biomass into an effective and low-cost adsorbent. It not only provides a strong foundation for the practical implementation of PKSAC in real wastewater treatment systems but also offers valuable design insights, suggesting that the enrichment of surface hydroxyl groups may serve as a general strategy to improve adsorption performance for a broader range of contaminants.

ACKNOWLEDGEMENT

In the name of Allah, the Most Beneficent and Merciful

Praises and thanks to Allah for granting me the strength, patience, and perseverance to complete this PhD journey.

First and foremost, I would like to express my deepest appreciation to my supervisors, Professor Ir. Dr. Syed Shatir Asghrar Syed Hassan and Dr. Norhasyimi Rahmat, for their invaluable guidance, continuous encouragement, and constructive feedback throughout my research. Their intellectual insights and support have been instrumental in shaping the direction and depth of this work.

Special thanks to my research team, Dr. Siti Zaharah Roslan, Dr. Mohd Saufi Md Zaini, Dr. Mohd Syazwan Mohd Ghazali, Mr. Mohibbah Musa and Mr. Mustafa Mokhtar, for their collaboration, critical discussions, and shared passion in our scholarly pursuits. Your companionship and collective spirit have enriched this academic journey.

My heartfelt gratitude is reserved for my beloved husband, Dr. Darween Rozehan Shah Iskandar Shah, who has been not only my life partner but also an integral part of my research team. From the very beginning of this journey until its completion, you have walked beside me with unwavering support, patience, and love. Your presence in both the academic and personal dimensions of this experience has made all the difference. You understood every challenge before I spoke it and stood strong when I could not. Love, finally, we made it.

To my children, Dian, Dayyan, Damien, Darlene, and Dylan, you are silent witnesses to my sacrifices, late nights, and moments of doubt. Your smiles, hugs, and patience have been my greatest source of motivation.

To my beloved mother, , thank you for your unwavering love, prayers, and support. To my late father, Anuar Ghazali, your words still guide me: study hard, reach the top, but always stay humble. This achievement is dedicated to your memory. To my siblings and in-laws, thank you for your prayers, emotional support, and belief in my capabilities. Your presence in my life is a blessing I deeply cherish.

This thesis is not only the end of academic work but a reflection of the collective support, love, and resilience of the people who have stood by me. May Allah reward each and every one of you for your kindness and support.

To them, I dedicate this thesis. Alhamdulillah

TABLE OF CONTENTS

		Page
CONFIRMATION BY PANEL OF EXAMINERS		**ii**
AUTHOR'S DECLARATION		**iii**
ABSTRACT		**iv**
ACKNOWLEDGEMENT		**v**
TABLE OF CONTENTS		**vi**
LIST OF TABLES		**x**
LIST OF FIGURES		**xii**
LIST OF PLATES		**xiv**
LIST OF SYMBOLS		**xv**
LIST OF ABBREVIATIONS		**xvii**
LIST OF NOMENCLATURES		**xx**
CHAPTER 1 INTRODUCTION		**1**
1.1	Research Background	1
1.2	Problem Statement	6
1.3	Research Objectives	8
1.4	Scope and Limitation of Study	9
	1.4.1 Scope and Limitation of Study	9
	1.4.2 Limitation of the Study	11
1.5	Significance of Study	12
	1.5.1 Society	12
	1.5.2 Knowledge Generation and Human Capital	12
	1.5.3 Government	13
	1.5.4 Environment and Sustainability	13

CHAPTER 2 LITERATURE REVIEW **15**

2.1 Introduction to Antibiotics 15
2.1.1 History and Development of Antibiotics 15
2.1.2 Functions of Antibiotics in Human, Animal and Plant Health 16
2.1.3 Types of Antibiotics and Usage Statistics in Asia and Malaysia 17
2.2 Antibiotics Pollution 19
2.2.1 Sources and Occurrence of Antibiotics Pollution 20
2.2.2 Global and Regional Statistic on Antibiotics Pollution 22
2.2.3 Environmental and Human Health Impact on Antibiotics Pollution 28
2.3 Removal Method for Antibiotics in Water Systems 29
2.4 Adsorption as a Prominent Removal Method: Advantages and Challenges 31
2.5 Adsorption Materials for Antibiotics Removal 33
2.5.1 Conventional and Emerging Adsorbents for Antibiotics 33
2.5.2 Biomass-derived Activated Carbon: Advantages and Challenges 34
2.6 Synthesis of Activated Carbon for Antibiotics Adsorption 35
2.6.1 Preparation of Techniques of Biomass-derived Activated Carbon 35
2.6.2 Influence of Activated Carbon Structure, Surface Chemistry, and Pore Characteristic of Antibiotic Adsorption 57
2.7 Optimization Tools for Antibiotics Adsorption Efficiency 60
2.7.1 Response Surface Methodology (RSM) for Process Optimization 61
2.7.2 Density Functional Theory (DFT) in Adsorption Studies 62
2.8. Adsorption Mechanism of Antibiotics Removal 63
2.9. Influence of Process Condition on Adsorption Performance 64
2.9.1 Influence of pH on Adsorption Performance 64
2.9.2 Influence of Initial Antibiotic Concentration on Adsorption Performance 66
2.9.3 Influence of Adsorbent Dosage on Adsorption Performance 68
2.10 Interaction Mechanism between Amoxicillin (AMX) and Activated Carbon 70
2.11 Summary 71

CHAPTER 3 RESEARCH METHODOLOGY **73**
3.1 Introduction 73
3.2 Operational Framework 74
3.3 Materials 75
3.4 Synthesis of Activated Carbon 76
3.5 Characterization Method 78
3.5.1 pH at the Point of Zero Charge 78
3.5.2 Elemental Analysis (CHNS/O) 79
3.5.3 BET Surface Area and Pore Structure Analysis 79
3.5.4 Scanning Electron Microscopy (SEM) 80
3.5.5 Fourier Transform Infrared Spectroscopy (FTIR) 81
3.5.6 X-Ray Photoelectron Spectroscopy 82
3.5.7 Ultraviolet-Visible Spectroscopy (UV-Vis) 83
3.6 Preparation and Optimization of Amoxicillin (AMX) Adsorption Condition using Box-Behnken Design (BBD) 84
3.6.1 Preparation of AMX Solutions 84
3.6.2 Single Factor Experiments to Prepare PKSAC for AMX Adsorption 85
3.6.3 Optimization and Prediction of AMX Adsorption 86
3.7 AMX Adsorption Kinetic 87
3.8 AMX Adsorption Isotherm 88
3.9 Adsorption Energy by Density Functional Theory (DFT) in the PKSAC-AMX System 90

CHAPTER 4 RESULTS AND DISCUSSION **92**
4.1 Introduction 92
4.2 Structural and Chemical Modification of PKSAC 93
4.2.1 Single Factor Experiments to Prepare PKSAC for AMX Adsorption 93
4.2.2 Characteristic Examination of PKSAC 96
4.2.2.1 Yield and Textural Properties 96
4.2.2.2 Surface Chemistry 100
4.3 Optimization of AMX Adsorption Condition using Response Surface Methodology 104

4.3.1 Statistical Analysis and Regression Model of AMX Adsorption 104
4.3.2 Interaction Effect of Process Variables on the Response 108
4.3.3 Numerical Optimization of AMX Adsorption 111
4.4 Analysis of AMX Adsorption Performance 113
4.4.1 Adsorption Kinetics 113
4.4.2 Adsorption Isotherms and the Effect of Temperature 117
4.4.3 Adsorption Energy in the PKSAC-AMX System 121
4.4.3.1 Electron Density and Molecular Interactions in AMX Adsorption 121
4.4.3.2 Statistical Analysis of Energy Gap and Adsorption Energy 125
4.5 Adsorption Mechanisms 127

CHAPTER 5 CONCLUSION **131**
5.1 Conclusion 131
5.2 Recommendations 132

REFERENCES **134**
APPENDICES **154**
AUTHOR'S PROFILE **157**

LIST OF TABLES

Tables	Title	Page
Table 2.1	The Range of Antibiotics Identified in Water Sources Worldwide	23
Table 2.2	The Occurrence of Pharmaceutical Contaminants Detected in Water Source in Malaysia	25
Table 2.3	Acidic Modification of Biomass-Derived Activated Carbon for Antibiotic Adsorption	39
Table 2.4	Alkaline Modification of Biomass -Derived Activated Carbon for Antibiotic Adsorption	47
Table 2.5	Influence of Biomass Precursors and Activating Agents on the Physiochemical Properties of Activated Carbon	59
Table 3.1	List of All the Chemicals Used in This Study	75
Table 3.2	Actual and Coded Variables with Their Levels for AMX Removal	87
Table 4.1	Characteristics of Biochar and PKSAC	97
Table 4.2	Experimental Design and Response for AMX Removal	105
Table 4.3	Analysis of Variance (ANOVA) for AMX Removal (%) by PKSAC	107
Table 4.4	Surface Charge of the PKSAC and AMX at Various pH Values	109
Table 4.5	Predicted Optimum Operating Condition of AMX Adsorption by PKSAC Obtained Using Desirability Function Approach	112
Table 4.6	PFO and PSO Kinetic Parameters of AMX by PKSAC	116
Table 4.7	Elovich Kinetic Parameter of AMX by PKSAC	117
Table 4.8	Isotherm Model Parameters (Langmuir, Freundlich, and Redlich–Peterson) for AMX Adsorption onto PKSAC at Different Temperatures.	118
Table 4.9	Comparative Analysis of Maximum AMX Adsorption	

	Capacities Across Various Adsorbents.	120
Table 4.10	DFT Analysis of Energy Gap and Adsorption Energy for the Compounds	122
Table 4.11	Summary of Linear Regression Analysis Between Energy Gaps and Adsorption Energy	127
Table 4.12	Summary of Evidence Supporting the Purposed Adsorption Mechanism of AMX onto PKSAC	129

LIST OF FIGURES

Figures	Title	Page
Figure 2.1	Overall Trend of Antibiotics Utilization in Malaysia from 2018 to 2023	19
Figure 2.2	The Occurrence of Antibiotics to the Environment	21
Figure 2.3	The Synthesis Pathways for Activated Carbon from Biomass	37
Figure 2.4	pH Distribution of Antibiotic Adsorption on Different Types of Biomass-Derived Activated Carbon	65
Figure 2.5	Initial Concentration Distribution of Antibiotic Adsorption on Different Types of Biomass-Derived Activated Carbon	67
Figure 2.6	Adsorbent Dosage Distribution of Antibiotic Adsorption on Different Types of Biomass-Derived Activated Carbon	69
Figure 3.1	Operational Framework of This Study	74
Figure 3.2	Chemical Structure of Amoxicillin Trihydrate	75
Figure 4.1	AMX Removal by (a) Different Impregnation Ratio, (b) Different Activation Temperature	94
Figure 4.2	N_2 Adsorption/Desorption Isotherms at 77K for (a) Biochar, (b) PKSAC	98
Figure 4.3	SEM Images of the (a) Biochar and (b) PKSAC	99
Figure 4.4	FTIR Spectra of Biochar and PKSAC Before and After AMX Adsorption	101
Figure 4.5	(a) XPS Survey Spectra of PKSAC and PKSAC+AMX; (b) High-Resolution C 1s Spectra; and (c) High-Resolution O 1s Spectra of PKSAC and PKSAC+AMX	103
Figure 4.6	(a) Normal Probability Plot and (b) Experimental and Actual Removal of AMX (%)	108
Figure 4.7	(a) pH_{PZC} of PKSAC and Contour Plot About the Interaction Between (b) pH and Adsorbent Dosage, (c) Time and Adsorbent Dosage, and (d) Time and pH.	110
Figure 4.8	Desirability Ramp Plot Showing the Predicted Optimum	

	Operating Conditions for AMX Adsorption by PKSAC Obtained from Numerical Optimization	113
Figure 4.9	Adsorption Kinetic of AMX onto PKSAC by PSO, PSO and Elovich Kinetic Model Under (a) 100 ppm, (b) 200 ppm, (c) 300 ppm and (d) 400 ppm	114
Figure 4.10	Langmuir, Freundlich, and Redlich–Peterson Isotherm Plots for AMX Adsorption onto PKSAC at (a) 25 ℃, (b) 35 ℃, (c) 45 ℃, and (d) 55 ℃	119
Figure 4.11	Electron Density of (a) PKSAC and (b) AMX	121
Figure 4.12	Molecular Interactions of (a) PKSAC-OH: AMX-COOH, (b) PKSAC-OH: AMX-NH_2 and (c) PKSAC-OH: AMX-OH	123
Figure 4.13	HOMO/LUMO Orbital Visualizations of the (a) PKSAC-OH: AMX-COOH, (b) PKSAC-OH: AMX-NH_2 and (c) PKSAC-OH: AMX-OH	124
Figure 4.14	Scatter Plot with Linear Regression Showing the Relationship Between Energy Gap and Adsorption Energy	126
Figure 4.15	Proposed Mechanisms Governing AMX Adsorption onto PKSAC.	129

LIST OF PLATES

Plates	Title	Page
Plate 3.1	Photograph of Washed and Dried Raw PKS (Left) and Ground PKS Biochar (Right)	76
Plate 3.2	Photograph of Horizontal Split-Able Tube Furnace	78
Plate 3.3	Photograph of Vario EL III CHNS/O Elemental Analyzer	79
Plate 3.4	Photograph of the BET Surface Area Analyzer	80
Plate 3.5	Photograph of the Scanning Electronic Microscope	81
Plate 3.6	Photograph of the Fourier Infrared Spectroscopy	82
Plate 3.7	Photograph of the X-ray Photoelectron Spectrometer	83
Plate 3.8	Photograph of the UV-Vis Spectrometer	84

LIST OF SYMBOLS

Symbols

C_0	Initial Concentration
C_e	Equilibrium Concentration
K_F	Freundlich Isotherm Constant
K_L	Langmuir Isotherm Constant
K_{RP}	Redlich-Peterson Isotherm Constant
R	Removal Efficiency
R^2	Regression Coefficient
R_L	Langmuir Separation Factor
k_1	Rate Constant for PFO
k_2	Rate Constant for PSO
q_e	Adsorption Capacity at Equilibrium
q_m	Maximum Monolayer Adsorption Capacity of the Adsorbent
q_{max}	Maximum Adsorption Capacity
q_t	Uptake Capacity at Time
V	Volume
b	Constant of the Surface Coverage
g	Exponent
k	Number of Factors Studied

m	Weight
βi	Regression Coefficients for the Linear Terms
βij	Regression Coefficients for the Quadratic Terms
βo	Regression Coefficients for the Intercept
β_0	Intercept
β_1	Slope

LIST OF ABBREVIATIONS

Abbreviations

AC	Activated Carbon
AMP	Ampicillin
AMR	Antimicrobial Resistance
AMX	Amoxicillin
ANNs	Artificial Neural Networks
ANOVA	Analysis of Variance
AOPs	Advanced Oxidation Processes
ARB	Antibiotic-Resistance Bacteria
ARG	Antibiotic-Resistant Genes
BBD	Box-Behnken Design
BC	Biochar
BET	Brunauer-Emmett-Teller
BJH	Barrett-Joyner-Halenda
CCD	Central Composite Design
CPX	Cephalexin
CTC	Chlortetracycline
DFT	Density Functional Theory
DDD	Defined Daily Doses
Eg	Energy Gap

ENX	Enrofloxacin
ESP	Electrostatic Potential
FTIR	Fourier-Transform Infrared Spectroscopy
GAs	Genetic Algorithms
HOMO	Highest Occupied Molecular Orbital
IUPAC	International Union of Pure and Applied Chemistry
LCA	Life Cycle Assessment
LEV	Levofloxacin
LUMO	Lowest Unoccupied Molecular Orbital
MOFs	Metal-Organic Frameworks
MSOM	Malaysian Statistics on Medicines
NF	Nanofiltration
NOM	Natural Organic Matter
OTC	Oxytetracycline
OVAT	One-Variable-At-a-Time
PAC	Powdered Activated Carbon
PFO	Pseudo-First Order
pH_{PZC}	Point of Zero Charge
pKa	Acid Dissociation Constant
PKS	Palm Kernel Shell
PKSAC	PKS-Derived Activated Carbon
POME	Palm Oil Mill Effluent

PSO	Pseudo-Second Order
RO	Reverse Osmosis
RSM	Response Surface Methodology
RSS	Residual Sum of Squares
SE	Standard Error
SEM	Scanning Electron Microscopy
SMX	Sulfamethoxazole
TC	Tetracycline
UF	Ultrafiltration
UV-Vis	Ultraviolet-Visible Spectroscopy
WHO	World Health Organization
XPS	X-ray Photoelectron Spectroscopy

LIST OF NOMENCLATURES

Nomenclatures

C	Carbon
$C_6H_8O_7$	Citric Acid
H_2SO_4	Sulfuric Acid
H_3PO_4	Phosphoric Acid
HCl	Hydrochloric Acid
$KHCO_3$	Potassium Bicarbonate
KOH	Potassium Hydroxide
N_2	Nitrogen
NaOH	Sodium Hydroxide
O	Oxygen

CHAPTER 1
INTRODUCTION

1.1 Research Background

Antibiotics are widely utilized for treating infectious diseases in both humans and animals. However, a considerable amount is not entirely metabolized in the body and is subsequently excreted as active substances into wastewater systems. These substances predominantly enter aquatic ecosystems through domestic sewage and wastewater treatment facilities, which frequently do not eliminate them. Consequently, antibiotic residues have been extensively identified in rivers, lakes, and even sources of drinking water. Research has documented antibiotic concentrations in various surface waters globally, ranging from nanograms per Liter (ng/L) to micrograms per Liter (μg/L), with some extreme instances reaching as high as 16,216 ng/L (Xiong et al., 2015). In Malaysia, both groundwater and surface water have been shown to contain notable levels of pharmaceutical contaminants, including antibiotics, raising concerns regarding their effects on environmental and human health. Studies have reported the occurrence of antibiotics in Malaysian aquatic environments at concentrations ranging from 1.7 to 365 ng/L, depending on the antibiotic compound and sampling location. Sulfamethoxazole, trimethoprim, erythromycin, and ciprofloxacin are among the most frequently detected antibiotics in surface waters, indicating their widespread distribution and persistence in the environment (Mohamad et al., 2022). Furthermore, an examination of drinking water distribution systems in Malaysia identified antibiotic-resistant genes (ARG), highlighting the potential dangers associated with antibiotic pollution (Adzima et al., 2019; Wee et al., 2020).

Amoxicillin (AMX), a broad-spectrum β-lactam antibiotic belonging to the penicillin class, is among the most widely used antibiotics globally and has been frequently identified in aquatic environment (Wee et al., 2020). Its persistence in water bodies raises concern about its impact on microbial communities and potential disruption of aquatic ecosystems (Heard et al., 2021). The use of antibiotics in Malaysia healthcare sector has been on the rise, with studies analyzing antibiotic consumption trends in public and private healthcare facilities from 2018 to 2021 (Rahman et al., 2016). The presence of AMX and other antibiotics in water has also been associated

with the spread of ARGs, complicating the management of bacterial infections (Mohamad et al., 2022). Furthermore, conventional wastewater treatment systems are often ineffective in completely removing antibiotic residues such as amoxicillin, resulting in their continuous discharge into aquatic environments and increasing the risk of contamination in drinking water sources. Recent studies have highlighted that advanced and emerging treatment technologies are still required to effectively eliminate antibiotics from hospital and pharmaceutical wastewater (Mohamad et al., 2022).

Various methods have been utilized to eliminate antibiotics from water, such as adsorption, advanced oxidation processes (AOPs), microwave-assisted degradation, and photocatalytic purification (Cuerda-Correa et al., 2019; Huang et al., 2022). While these methods have proven effective in degrading antibiotic contaminants, they also exhibit specific limitations. AOPs, such as Fenton oxidation and ozonation, can decompose a broad spectrum of antibiotic compounds but are highly energy-intensive and may generate toxic byproducts, including aldehydes, ketones, carboxylic acids, and nitrosamines, which can be harmful to aquatic organisms and human health (Larsson & Flach, 2021). Microwave-assisted degradation is effective, however, it necessitates specialized equipment and incurs high operational costs, which restricts its practical implementation (Zakaria & Dhar, 2022). These constraints emphasize the necessity for a more economical, efficient, and scalable solution, making adsorption as a compelling alternative.

Adsorption has garnered considerable attention due to its simplicity, cost-effectiveness, and high efficiency in removing antibiotics (Ahmed et al., 2015). A significant advantage of adsorption is its capacity to capture antibiotics without altering their chemical structure, thereby preventing the formation of toxic degradation byproducts that are often produced in oxidative and photocatalytic processes (Premarathna et al., 2019). Furthermore, adsorbents can be regenerated and reused multiple times, making them a more sustainable option compared to single-use degradation techniques (Krasucka et al., 2021). Additionally, adsorption systems can be easily scaled up from laboratory studies to industrial applications, making them a practical and flexible option for real-world wastewater treatment applications (Wee et al., 2020). Given these advantages, adsorption stands out as one of the most viable, cost-effective, and environmentally friendly approaches for addressing antibiotic pollution in aquatic environments.

A variety of adsorbent materials have been investigated for the removal of

antibiotics from contaminated water sources, including zeolites, activated carbon, biochar, metal-organic frameworks (MOFs), and nanomaterials. Zeolites, which are microporous aluminosilicate minerals, are widely utilized due to their high surface area, tunable porosity, and cation-exchange capabilities (Tian et al., 2023). However, their effectiveness is limited by a low affinity for non-ionic antibiotics and a reduced adsorption capacity for larger molecules. Furthermore, the regeneration process for zeolites necessitates high temperatures, which can elevate operational costs (Wang et al., 2019).

MOFs are another class of material frequently employed for antibiotic removal, characterized by their ultra-high porosity and tunable chemical functionality, which facilitate selective antibiotic adsorption (Saboor et al., 2022). Despite their promising performance, MOFs exhibit poor stability in aqueous environments, and their complex synthesis processes contribute to their high cost for large-scale applications (Sargazi et al., 2020). Nanomaterials, including carbon nanotubes and graphene oxide, have also been utilized due to their large surface area and rapid adsorption kinetics. However, concerns regarding their high manufacturing costs, potential cytotoxicity, and challenges in recovery from treated water raise questions about their environmental sustainability (Mandal et al., 2020).

Among the various materials explored for antibiotics removal, activated carbon (AC) remains one of the most effective and widely used adsorbent. Commercial activated carbon, commonly produced from non-renewable sources including coal, or petroleum, is known for its high surface area and extensive pore structure that contribute to its strong adsorption performance (Premarathna et al., 2019). However, its high production costs, limited regeneration potential and potential release of previously adsorbed pollutants during desorption pose significant drawback (Mostafapour et al., 2022). Moreover, its reliance on fossil-based precursors raises concerns about sustainability and environmental impact. These limitations have driven the search for alternative adsorbents that offer cost-effectiveness, sustainability and comparable adsorption efficiency.

Biomass-derived carbon adsorbent including AC and biochar (BC) have emerged as promising alternatives due to their renewable nature and environmental sustainability in comparison to other available materials (Kumar et al., 2019). Derived from agricultural residues, wood waste, and other biomass-based materials, these materials exhibit well-developed microporous structure, diverse pore size distribution

and surface functionalized surface groups that contribute to strong adsorption capacities (Anuar et al., 2023). Their production from abundant waste biomass also decreases dependency of fossil precursors, addressing both environmental and resource sustainability concerns.

Compared to conventional commercial activated carbon, biochar can be produced through a simpler and less energy-intensive pyrolysis process without extensive activation treatment (Premarathna et al., 2019). In contrast, activated carbon generally requires additional physical or chemical activation steps to enhance pore development and surface area. Nevertheless, biomass-derived activated carbon combines the sustainability of biomass feedstocks with improved adsorption performance, making both AC and BC promising materials for large-scale environmental applications (Zulfiqar et al., 2024). Additionally, they also demonstrates high stability and resistance to microbial degradation, making it suitable for long-term environmental applications (Li et al., 2022). The presence of oxygenated surface functional groups enhances interactions with antibiotic molecules, contributing to improved adsorption selectivity. Chemical modification further amplifies these properties, allowing BC to achieve adsorption performances comparable to more advanced synthetic adsorbents (Premarathna et al., 2019).

Beyond their structural advantages, biomass-derived adsorbents offer safer and more practical use compared to nanomaterials, which often raise concerns related to cytotoxicity and post-treatment recovery (Krasucka et al., 2021). Their functionalized surfaces facilitate electrostatic and hydrogen-bonding interactions, providing strong affinity toward a broad range of antibiotics. With demonstrated improvements following chemical modification, biomass-derived AC continues to evolve as a competitive and environmentally responsible alternative for wastewater treatment (Premarathna et al., 2019).

Various biomass-derived AC have been successfully applied for antibiotic removal from wastewater due to their high surface area, porosity, and functionalized surface groups. Coconut shell-based activated carbon has demonstrated remarkable adsorption efficiency, exceeding 90% for antibiotics enrofloxacin especially when chemically modified to enhance porosity and functional groups (DasSharma et al., 2020). Similarly, sawdust-based activated carbon, when treated with phosphoric acid (H_3PO_4) has shown high reusability and adsorption capacity, making it a cost-effective solution for wastewater treatment (Wan et al., 2016). Rice husk biochar, known for its

silica-rich composition and oxygenated surface groups, effectively adsorbs tetracycline, leveraging electrostatic interactions to improve removal efficiency (Liu et al., 2012). Other biomass sources, including corn stalks, have also been transformed into highly efficient adsorbents. Corn stalk biochar, particularly when modified with potassium hydroxide (KOH), enhances levofloxacin (LEV) removal by improving ion exchange mechanisms and electrostatic interactions. The versatility of these biomass-based materials offers a sustainable and cost-effective approach for wastewater treatment, reducing reliance on synthetic adsorbents while maintaining high adsorption efficiencies.

Palm kernel shell (PKS) serves as an excellent precursor for biomass-based activated carbon, particularly in the context of antibiotic removal, especially in Malaysia, where it is abundantly produced as a byproduct of the palm oil industry. The high carbon content, abundant availability, and low cost of PKS make it a sustainable precursor for activated carbon production. As PKS is an agricultural waste generated in large quantities by the palm oil industry, its utilization can reduce raw material costs and minimize waste disposal problems (Ahmed et al., 2015). The porous structure and high fixed carbon content of PKS enhance its effectiveness in adsorption applications, allowing it to efficiently remove various pollutants, including antibiotics, from contaminated water sources (Ahmed et al., 2015). Furthermore, the low ash content and high surface area of activated PKS contribute to its strong adsorption capabilities, which are critical for effective environmental remediation.

Recent studies have demonstrated the PKS-derived activated carbon (PKSAC) has been successfully employed in treating palm oil mill effluent (POME), leading to significant reductions in organic pollutants and dyes in both batch and continuous adsorption processes (Huat et al., 2022). Additionally, research has shown that PKSAC is effective in adsorbing heavy metals and carcinogenic hydrocarbons from water sources, achieving substantial pollutant removal in a relatively short contact time (Huat et al., 2022; Rabia & Hussein, 2020). These findings underscore the versatility and efficiency of PKSAC in environmental remediation efforts.

Moreover, the application of PKSAC extends to the adsorption of various antibiotics. For example, a study highlighted the potential of PKSAC to effectively adsorb antibiotics such as tetracycline, ampicillin and amoxicillin demonstrating its capability to address antibiotic contamination in wastewater (Opeoluwa et al., 2023). While PKSAC has been widely investigated for pollutant removal, studies integrating

synthesis optimization, adsorption modelling, surface characterization, and DFT analysis for amoxicillin adsorption remain limited

The effectiveness of PKSAC in adsorption applications is significantly influenced by the activation method used. There are two primary activation techniques: physical activation and chemical activation. Physical activation involves carbonizing the raw material at high temperatures under an inert atmosphere, followed by activation using gases such as steam or carbon dioxide (Liu et al., 2012). This method allows for controlled pore development and enhances the surface area, but it often requires higher energy input and longer processing times, which may limit its efficiency for large-scale applications (Liu et al., 2012). On the other hand, chemical activation involves the use of activating agents such as phosphoric acid, potassium hydroxide, or zinc chloride to modify the carbon structure (Gao et al., 2020). This process enhances porosity, increases adsorption capacity, and requires lower activation temperatures, making it a preferred method for producing highly porous activated carbon in a more efficient manner (Gao et al., 2020).

Most studies on activated carbon focus on increasing the surface area as a key factor in adsorption performance. However, emerging research suggests that surface chemistry plays a crucial role in adsorption efficiency. Chemical modifications, such as the introduction of functional groups containing oxygen, nitrogen, or sulfur, can significantly enhance adsorption selectivity and improve interactions with pollutants (Anuar et al., 2023). Despite these advancements, the underlying mechanisms governing adsorption on chemically modified activated carbon remain insufficiently understood, particularly for antibiotic contaminants such as amoxicillin. While adsorption kinetics are commonly evaluated using pseudo-first order and pseudo-second order models, these models are often used solely to describe adsorption behaviour without linking the observed kinetic trends to the underlying adsorption mechanism at the molecular level (Li et al., 2022). Further research is therefore needed to investigate how chemical activation influences adsorption kinetics, surface interactions, and adsorption selectivity of amoxicillin on activated carbon materials. Integrating kinetic modelling with advanced characterization techniques and computational approaches may provide deeper mechanistic insight into the adsorption process. A comprehensive understanding of these factors is essential for elucidating the adsorption mechanism and optimizing the performance of biomass-derived activated carbon for pharmaceutical wastewater treatment. Such knowledge will contribute to the

development of more efficient and sustainable adsorbents for the removal of emerging contaminants from aquatic environments.

1.2 Problem Statement

Amoxicillin (AMX) is one of the most widely prescribed antibiotics worldwide and is extensively used in both human and veterinary medicine. Due to its incomplete metabolism, a significant fraction of the administered AMX is excreted and subsequently enters domestic sewage, hospital effluents, and other municipal wastewater streams. Conventional wastewater treatment plants primarily employ physical and biological treatment processes, such as primary sedimentation and activated sludge systems. However, these treatment processes are often unable to completely remove AMX, resulting in its release into surface water, groundwater, and other aquatic environments. The continuous discharge of AMX has raised concerns regarding the development of antibiotic-resistant bacteria and the potential adverse effects on aquatic ecosystems and public health.

An effective carbon adsorbent must exhibit a high surface area and a well distributed pore structure that is specifically tailored to target pollutants. To enhance these characteristics, researchers frequently modify biochar using various activation agents. Among these, PKSAC has been subjected to treatment with different chemical activators to improve its adsorption capabilities. Notably, KOH has been identified as a particularly advantageous activator due to its ability to significantly enhance the surface area and pore structure of activated carbon materials. However, the effects of different activation agents can vary widely, influencing the physical and chemical properties of biomass materials, as well as their overall adsorption capacities

Given these variations, it is essential to investigate the specific impact of KOH activation on PKSAC, particularly concerning its structural and chemical characteristics and its efficiency in adsorbing AMX. The adsorption capacity of PKSAC is strongly affected by operational condition including pH, temperature, and contact time, necessitating a comprehensive understanding of these variables to optimize PKSAC as an effective adsorbent for AMX.

Furthermore, understanding the adsorption mechanism is critical for the design of efficient biomass-derived adsorbents. Despite extensive research focused on enhancing surface area, there remains a notable gap in the understanding of the

underlying adsorption mechanisms. While kinetic and isotherm studies have been conducted, they do not provide a comprehensive understanding of the underlying mechanisms of the adsorption processes involved. Previous studies have reported that AMX adsorption on various adsorbents is governed by mechanisms such as hydrogen bonding, electrostatic interactions, pore filling, and π–π interactions. However, these mechanisms have largely been inferred from characterization techniques and adsorption modelling, providing only indirect evidence of the adsorbate–adsorbent interactions. Previous studies in other adsorption systems have indicated that Density Functional Theory (DFT) analysis can yield valuable insights into these mechanisms, facilitating a deeper understanding of the interactions between adsorbates and adsorbents. Nevertheless, due to differences in precursor composition and surface chemistry, the adsorption behaviour of amoxicillin on KOH-modified palm kernel shell activated carbon requires specific mechanistic investigation and cannot be directly extrapolated from other biomass-derived activated carbons.

Recognizing this gap in the literature, the present study aims to address the limitations of current research by investigating the adsorption mechanism of AMX onto KOH-activated PKSAC. This investigation will be complemented by DFT analysis, which will provide a theoretical framework to elucidate the interactions at play, thereby enhancing the understanding of the adsorption process and contributing to the developments of more effective biomass-derived adsorbents.

1.3 Research Objectives

The primary aim of this study was to enhance the adsorption of AMX using KOH-modified PKS activated carbon. To achieve this goal, the specific research objectives are as follows:

a) To evaluate the structural and chemical changes induced by KOH modification of PKSAC and their impact on the adsorption capacity for AMX.
b) To determine the impact of key operational variables including adsorbent dosage, pH solution, and contact time on AMX adsorption efficiency with PKSAC through response surface methodology (RSM).
c) To study the kinetics, isotherms, and adsorption energy of AMX adsorption using DFT

d) To assess the adsorption mechanism and the influence of the surface functionality and pore structure of PKSAC that contributes to adsorption performance.

1.4 Scope and Limitations of the Study

1.4.1 Scope of the Study

To achieve the desired research objectives outlined in sub-chapter 1.3, the scope of the study was defined as follows:

1.4.1.1 Materials and Methods

Biomass source: This study utilized PKS, an abundant agricultural waste product in Malaysia, as the precursor for activated carbon production.

Activation: This study utilized KOH as a chemical activating agent to enhance the surface properties and porosity of activated carbon. KOH was selected due to its effectiveness in promoting pore development and increasing surface area. The KOH-to-PKS impregnation ratios investigated were 1: 0.5, 1:1, 1:2, and 1:3. These values were selected based on previous studies reporting effective pore development within this range (Wu et al., 2021). Ratios below 1:1 may provide insufficient activation, whereas ratios above 1:3 may lead to excessive pore widening, structural collapse, reduced carbon yield, and increased chemical consumption.

AMX Adsorption Study: This study quantitatively assessed the adsorption capacity of PKSAC for the removal of amoxicillin (AMX) using an initial AMX concentration of 20 ppm in a 200 mL aqueous solution. The selected concentration was adopted from previous adsorption studies on antibiotic contaminants and was considered appropriate for evaluating the adsorption performance of activated carbon materials under controlled laboratory condition (DasSharma et al., 2020). The research investigated how KOH activation and surface modifications influenced the performance of PKSAC in adsorbing AMX from aqueous solutions.

1.4.1.2 Characterization Techniques

Structural and Surface Analysis: This study utilized techniques including Brunauer-Emmett-Teller (BET) surface area and scanning electron microscopy (SEM) analysis to evaluate the morphological and structural properties of the synthesized materials. These analyses provided insight into the relationship between physical structure and adsorption efficiency.

Chemical Analysis: Characterization techniques used to determine the chemical composition, and functional groups present on the carbon adsorbent surface area X-ray photoelectron spectroscopy (XPS), Fourier-transform infrared spectroscopy (FTIR) and Ultraviolet-Visible spectroscopy (UV-Vis). These analyses helped elucidate the role of chemical interactions in AMX adsorption.

1.4.1.3 Performance Evaluation

This section integrates experimental finding with computational simulations to achieve a comprehensive understanding of the adsorption mechanism. DFT simulations were used to complement experimental data and provide molecular-level insight into the adsorption process.

Adsorption Energy: The binding energy of AMX onto the PKSAC was evaluated to quantify the feasibility and strength of adsorption interaction. This analysis revealed how surface modifications influenced the affinity of PKSAC for AMX.

Electronic properties: Computational analysis of the energy gap, specifically the difference between the Highest Occupied Molecular Orbital (HOMO) and the Lowest Unoccupied Molecular Orbital (LUMO), was conducted. This analysis provided critical information on the electron density distribution, molecular reactivity and interaction potential of PKSAC and AMX.

Adsorption Mechanism: DFT simulations were used identified dominant interactions mechanism governing adsorption, including hydrogen bonding, π-π stacking, electronic forces and pore filling effects. These interaction pathways are crucial in enhancing adsorption performance and contribute significantly to the effective removal of AMX.

1.4.1.4 Optimization and Prediction Modelling

Response Surface Methodology (RSM): RSM was used as a tool to optimize and predict the optimal condition for maximum AMX removal efficiency by evaluating interactions among key variables (adsorbent dosage, pH and contact time) using Box-Behnken design (BBD).

1.4.2 Limitation of the Study

Despite the comprehensive approach, this study is subject to several limitations that may affect the generalizability and application of its findings. These limitations are as follows:

1.4.2.1 Experimental conditions

The study focused exclusively on the adsorption of AMX under controlled laboratory conditions. It did not consider the presence of competing contaminants, such as other pharmaceuticals, heavy metals, or natural organic matter (NOM), which are typically present in real wastewater. These factors could interfere with the adsorption process and influence the removal efficiency of AMX, potentially limiting the applicability of the results to real-world scenarios.

1.4.2.2 Technical challenges

While the laboratory-scale production of PKSAC showed effective results, its scalability for industrial use remains uncertain. One of the main challenges is maintaining consistent adsorbent properties, as variations in the physicochemical characteristics of PKS feedstock and activation conditions, particularly the KOH impregnation ratio and activation temperature, may significantly affect the surface area, pore structure, and functional group distribution of the final product. To mitigate this issue, strict quality control measures, standardized operating procedures, and optimized activation conditions are required to ensure product consistency and reproducibility during large-scale production. In addition, pilot-scale studies are necessary to evaluate the feasibility of translating laboratory findings to industrial applications.

1.4.2.3 Performance evaluation

Although the kinetic study was conducted, real-world flow systems with non-ideal mixing can impact adsorption rates. Uneven mixing may cause uneven adsorbate and adsorbent distribution, creating stagnant zones with higher adsorbate concentration, which affects overall adsorption kinetics.

1.4.2.4 Modelling limitations

The BBD is a statistical method for optimizing processes by testing conditions in a controlled environment. In this study, it improved AMX adsorption onto PKSAC. However, the static conditions used do not reflect the dynamic flow found in real wastewater treatment systems, affecting effectiveness. This study aims to provide a comprehensive understanding of the synthesis and performance of PKSAC in AMX adsorption while acknowledging the constraints and potential areas for future research.

1.5 Significance of Study

The knowledge gained from this study offers a fundamental understanding to synthesize high performance of activated carbon, particularly using local biomass as a carbon precursor. The specific contributions of this study are as follows:

1.5.1 Society

The research offers an eco-friendly solution for removing pharmaceutical contaminants like AMX from water. This contributes to public health by ensuring access to cleaner, safer water, reducing antibiotics pollution's risk on humans and aquatics ecosystems. Improved water quality also supports socioeconomic development by benefiting communities dependent on agriculture and fisheries.

1.5.2 Knowledge Generation and Human Capital

This work advances understanding of adsorption mechanisms through the integration of experimental techniques with computational tools like DFT. These insights enrich the knowledge base in material science and environmental engineering, fostering innovation in sustainable technologies. The interdisciplinary approach build

capacity in green human capital, equipping future researchers and engineers to address global water and waste challenges.

1.5.3 Government

The study showcases how agricultural waste, like PKS, can be used to create valuable adsorbents, aligning with Malaysia's Green Technology Master Plan 2017–2030. This plan emphasizes "Waste to Wealth," promoting the efficient use of waste to produce value-added products, supporting a circular economy, and reducing environmental impact.

By converting agricultural residues into eco-friendly adsorbents, the research advances waste utilization and meets the goals of the Green Technology Master Plan. Policymakers can apply these findings to develop low-cost, sustainable wastewater treatment systems, cutting reliance on traditional technologies and reducing carbon footprints. This approach also aligns with global sustainability goals including SDG 12 (Responsible Consumption and Production), while strengthening regulatory frameworks for a green and circular economy.

1.5.4 Environment and Sustainability

By valorizing PKS and reducing antibiotic contaminants, this study supports sustainable waste management practices. It minimizes reliance on non-renewable resources for adsorbent production, reducing carbon footprints. The optimized biochar-based adsorbent offers a sustainable pathway to combat water pollution, contributing to the UN Sustainable Development Goals (SDG 6: Clean Water and Sanitation).

1.6 Thesis Organization

This thesis is structured into five chapters. Chapter 1 (Introduction) presents an overview of the study, including the general background, problem statement, objectives, scope and limitations, and significance of the study. Chapter 2 (Literature Review) provides a comprehensive review of antibiotics removal from biomass-based carbon adsorbent, covering the significance of antibiotics in the environment, removal method of antibiotics from wastewater, activated carbon synthesis, factors influencing the adsorption process and activated carbon for AMX removal at molecular level. Chapter 3 (Research Methodology) provides a detailed explanation of the methodology, including the reactor description, materials used, analytical instruments and operational protocols. Chapter 4 (Results and Discussion) offers an in-depth analysis of finding aligned with the research objectives. This includes the synthesis and characterization of activated carbon produced from varying KOH ratios, activation temperature, and optimization of AMX adsorption under different parameters. The chapter further examines the adsorption mechanisms by integrating kinetics, isotherm and adsorption energy with DFT which provides a molecular-level understanding of AMX adsorption by simulating interactions between the activated carbon's functional groups and AMX molecules. Finally, Chapter 5 presents conclusions and offers a prospective view and recommendations for future research.

CHAPTER 2
LITERATURE REVIEW

2.1 Introduction to Antibiotics

Antibiotics are compound produced naturally by microorganisms or synthesized artificially to eliminate bacteria and other pathogenic microorganisms. They play a critical role in the treatment of bacterial infections and have greatly reduced illness and death associated with infectious diseases. The term "antibiotic" was first introduced by Selman Waksman in 1942, emphasizing substances derived from living organisms that are antagonistic to the growth of other microorganisms (Muteeb et al., 2023).

The discovery and utilization of antibiotics have revolutionized medical practices, enabling the effective treatment of previously fatal infections. Beyond human medicine, antibiotics play crucial roles in veterinary practices and agriculture, contributing to animal health and food production. However, extensive use of antibiotics has contribute to the development of antibiotic resistance, posing significant challenges to public health worldwide (Dhingra et al., 2020).

2.1.1 History and Development of Antibiotics

The historical trajectory of antibiotics is marked by pivotal discoveries and developments that have shaped modern medicine. The discovery of penicillin by Alexander Fleming in 1928 marked the beginning of the antibiotic era. Fleming observed that the *Penicillium notatum* release a compound that was able to suppress the growth of *Staphylococcus aureus*. This groundbreaking finding remained underutilized until the late 1930s and early 1940s when Howard Florey and Ernst Boris Chain developed methods for the mass production and purification of penicillin, facilitating its widespread use during World War II to treat infections among soldiers and civilians (Gaynes, 2017).

Following the success of penicillin, the mid-20th century witnessed the "Golden Age" of antibiotic discovery, characterized by the identification of various antibiotic classes through systematic screening of soil microorganisms (Muteeb et al., 2023). Notable discoveries during this period include streptomycin, chloramphenicol,

tetracyclines, and erythromycin, each contributing significantly to the treatment of diverse bacterial infections. However, the extensive use of antibiotics led to the emergence of antimicrobial resistance (AMR), necessitating ongoing research and development of novel antibiotics and alternative therapies (Nicolaou & Rigol, 2018).

2.1.2 Functions of Antibiotics in Human, Animal, and Plant Health

Antibiotics are pivotal agents in combating bacterial infections across various domains, including human medicine, veterinary practice, and agriculture. Their primary function involves either killing bacteria (bactericidal action) or inhibiting their growth (bacteriostatic action), thereby facilitating the resolution of infections. The application and impact of antibiotics in these sectors are multifaceted and warrant a comprehensive examination (Mahtab et al., 2021).

In human medicine, antibiotics have revolutionized the treatment of bacterial infections since their widespread introduction in the mid-20th century. They are employed to address a load of conditions, ranging from minor ailments like strep throat to severe diseases such as bacterial meningitis and sepsis (Mahtab et al., 2021). By targeting specific bacterial structures or functions including a cell wall synthesis, protein synthesis, nucleic acid synthesis, or metabolic pathways, antibiotics effectively eradicate pathogens or impede their proliferation. This targeted action aids the immune system in overcoming infections and has significantly reduced morbidity and mortality associated with bacterial diseases (Muteeb et al., 2023).

Nevertheless, the inappropriate and excessive use of antibiotics in human healthcare has contributed to the development of antibiotic-resistant bacterial strains, creating a significant public health concern. Resistance mechanisms, such as enzyme-mediated antibiotic degradation, alterations in bacterial targets, and efflux systems that remove antibiotics from bacterial cells, have made certain treatments ineffective. This necessitates the development of novel antibiotics and the implementation of stringent antibiotic stewardship programs to preserve the efficacy of existing drugs (Belay et al., 2024; Salam et al., 2023).

In veterinary medicine, antibiotics serve dual purposes: therapeutic and prophylactic. Therapeutically, they are administered to treat bacterial infections in animals, ensuring their health and welfare (Nicolaou & Rigol, 2018). Prophylactically, antibiotics have been used to prevent disease outbreaks, especially in intensive farming

systems where animals are at increased risk due to close confinement. Additionally, sub-therapeutic doses of certain antibiotics have historically been employed as growth promoters in livestock, enhancing feed efficiency and weight gain (Cuong et al., 2021). The application of antibiotics in animals, particularly for growth enhancement and disease control, has raised concerns regarding the emergence of antibiotic-resistant bacteria that can be transferred to humans through direct exposure or the consumption of animal-derived products (Mahtab et al., 2021). This has prompted regulatory measures in various countries to restrict or ban the non-therapeutic use of antibiotics in agriculture. For instance, the European Union has prohibited the use of antibiotics as growth promoters since 2006, advocating for responsible use to mitigate resistance development (Lean et al., 2021).

Antibiotics are occasionally applied in agriculture to manage bacterial infections in plants (Batuman et al., 2024). They are applied to control diseases such as fire blight in apple and pear trees, caused by *Erwinia amylovora*, and bacterial spots in peaches and nectarines, caused by *Xanthomonas* species. The use of antibiotics in crop production is intended to minimize yield losses and sustain agricultural productivity (Batuman et al., 2024).

However, the use of antibiotics in plant health is controversial due to potential environmental impacts and the risk of promoting antibiotic resistance in soil microbiota. Antibiotics introduced into the environment can affect non-target microorganisms, potentially disrupting soil microbial communities essential for nutrient cycling and plant health. Consequently, there is a growing emphasis on integrated disease management strategies that combine cultural practices, resistant plant varieties, and biological control methods to reduce reliance on chemical treatments (Polianciuc et al., 2020).

2.1.3 Types of Antibiotics and Usage Statistics in Asia and Malaysia

Antibiotics are essential for managing bacterial infections and are categorized according to their mechanism of action and range of antimicrobial activity. The World Health Organization (WHO) categorizes antibiotics into three groups: Access, Watch, and Reserve, to guide their rational use and manage AMR (Belay et al., 2024; Salam et al., 2023). In both Asia and Malaysia, the most used antibiotics fall under the Access and Watch categories (Lim et al., 2024).

Penicillin, particularly AMX, are among the most frequently prescribed due to their effectiveness and affordability. Other widely used antibiotics include cephalosporins such as cefuroxime and cephalexin, macrolides like erythromycin and azithromycin, and fluoroquinolones including ciprofloxacin and levofloxacin. These agents are employed to treat a wide range of infections, notably respiratory and urinary tract infections (Lim et al., 2024; Shamsuddin et al., 2016).

In the broader Asian context, antibiotic consumption is characterized by high variability across countries, influenced by disparities in healthcare infrastructure, regulation, and public awareness (Polianciuc et al., 2020). Southeast Asia has been reported to have some of the highest rates of antibiotic consumption globally. Inadequate diagnostic practices contribute considerably to this trend, with amoxicillin, azithromycin, and ciprofloxacin among the most commonly administered antibiotics in outpatient settings (Lim et al., 2024). These consumption patterns reflect both accessibility and frequent misuse, especially in areas with limited regulatory oversight and poor public health education.

Malaysia is a notable example in Southeast Asia, providing extensive data on antibiotic consumption through the Malaysian Statistics on Medicines. (MSOM). Data from 2018 to 2021 show that national antibiotic usage peaked at 6.56 defined daily doses (DDD) per 1000 inhabitants per day in 2019, followed by a marked decline to 4.17 DDD in 2021. This drop is largely attributed to reduced healthcare access and utilization during the COVID-19 pandemic (Lim et al., 2023). A closer examination of sector-specific data reveals stark contrasts between public and private healthcare settings. The public healthcare sector mainly utilized antibiotics classified under the Access category antibiotics, with amoxicillin accounting for approximately 81% of overall antibiotic consumption. Conversely, the private sector showed a broader and more diverse consumption pattern, with higher utilization of Watch category antibiotics, such as cephalosporins (15–41%) and macrolides, and overall antibiotic use nearly ten times greater than in the public sector by 2021 (Lim et al., 2024).

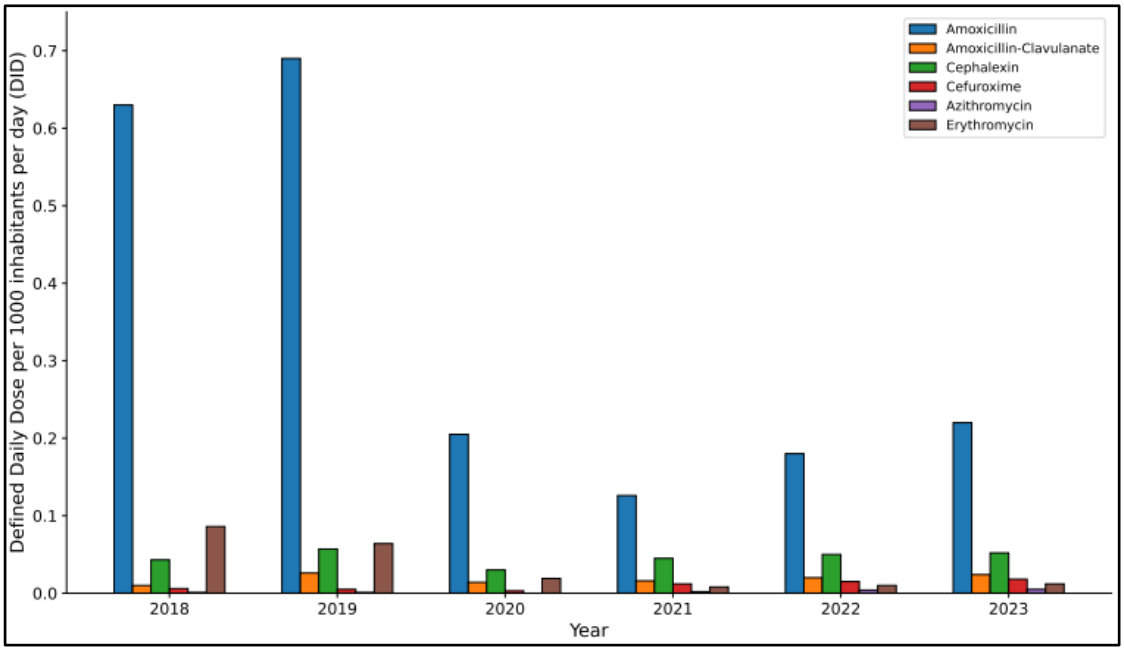

Figure 2.1 Overall Trend of Antibiotics Utilization in Malaysia from 2018 to 2023.

Detailed breakdowns of individual antibiotics in public and private sector usage are further illustrated in Figure 2.1. Amoxicillin remained the most frequently utilized antibiotic throughout the study period, with a utilization rate of 0.629 DDD in 2018, increasing to 0.691 DDD in 2019 before declining to 0.126 DDD in 2021. A gradual increase was subsequently observed, reaching 0.180 DDD in 2022 and 0.220 DDD in 2023. Cephalexin exhibited relatively stable utilization, fluctuating between 0.030 and 0.057 DDD over the study period (Lim et al., 2023, 2024; Shamsuddin et al., 2016). Other antibiotics, including amoxicillin-clavulanate, cefuroxime, azithromycin, and erythromycin, showed comparatively lower utilization rates but continued to contribute to the overall antibiotic burden. These trends demonstrate changes in antibiotic prescribing practices over time and highlight the influence of healthcare policies, prescribing guidelines, and accessibility of healthcare services on antibiotic consumption patterns (Mangala Praveena et al., 2019).

2.2 Antibiotics Pollution

The widespread presence of antibiotics, which are essential for combating bacterial infections in humans and animals, has inadvertently led to their emergence as environmental pollutants. These pharmaceuticals are released into ecosystems through wastewater discharge, agricultural runoff, and pharmaceutical manufacturing activities

(Mangala Praveena et al., 2019). In agricultural systems, antibiotics can enter the environment through the application of livestock manure, animal waste, and biosolids containing unmetabolized antibiotic residues. During rainfall or irrigation events, these residues can be transported from agricultural land into nearby rivers, lakes, and groundwater through surface runoff and leaching processes. Even at low concentrations, antibiotics can disrupt ecological balance by affecting microbial communities that are vital for nutrient cycling and other ecosystem functions (Polianciuc et al., 2020). Their environmental presence also contributes to the emergence of antibiotic-resistant bacteria (ARB), posing a significant threat to public health through contaminated water and food sources (Mangala Praveena et al., 2019).

Conventional wastewater treatment plants are often unable to effectively remove these compounds, resulting in their persistence in the environment, chronic exposure to aquatic organisms, and eventual entry into the food chain (Mackuľak et al., 2019). When bacteria encounter sublethal levels of antibiotics, they develop resistance mechanisms that intensify the challenge and ultimately compromise the efficacy of treatments that were once effective. Addressing these challenges requires a multi-faceted approach. Responsible antibiotic stewardship in human and veterinary medicine can reduce environmental contamination, and advanced wastewater treatment technologies capable of removing diverse micropollutants are essential to mitigate this burden (Collignon & McEwen, 2019; Serwecińska, 2020).

2.2.1 Sources and Occurrence of Antibiotics Pollution

These pharmaceutical compounds are introduced into ecosystems through wastewater from urban and industrial sources, agricultural runoff containing manure or fertilizer, and direct discharge from pharmaceutical manufacturing facilities and lead to significant environmental contamination (Figure 2.2). Antibiotics persist in the environment because of their chemical stability and accumulation in water bodies, soils, and sediments. Studies have documented their presence in diverse settings, including municipal wastewater, rivers, and drinking water, raising concerns regarding ecotoxicological risks (Kraemer et al., 2019).

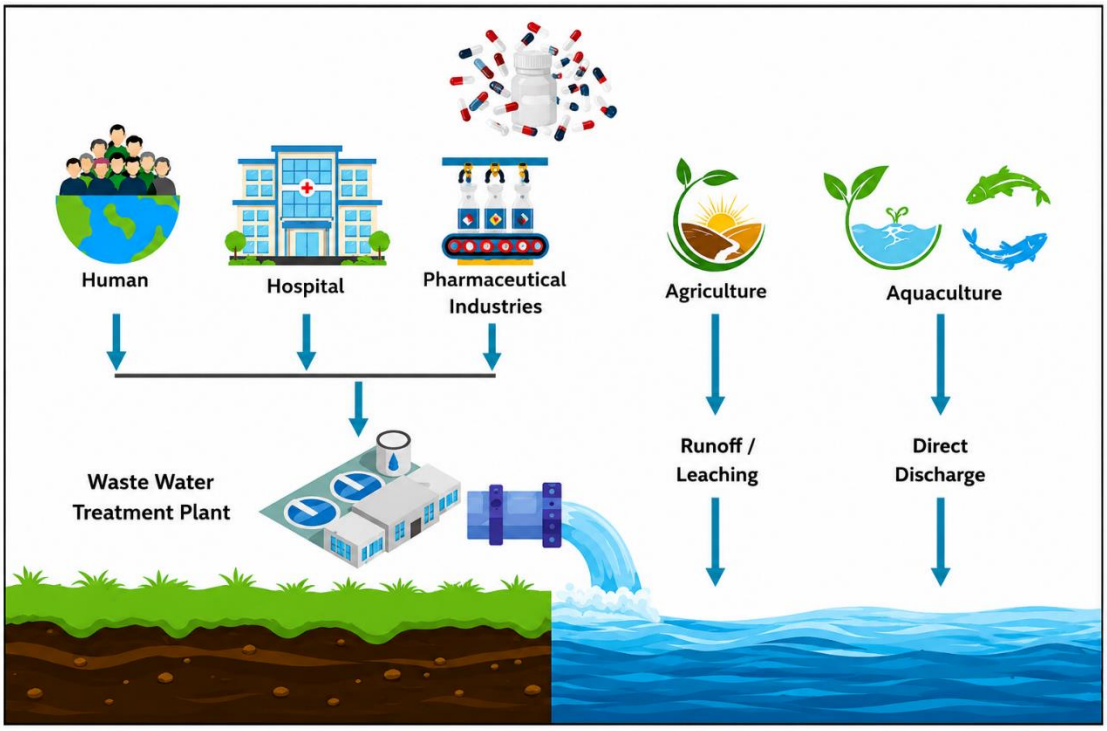

Figure 2.2 The Occurrence of Antibiotics to the Environment (Source: Figure been created by author)

Antibiotics have a profound impact on microbial communities, disrupting natural diversity by suppressing susceptible species while fostering the proliferation of resistant strains. This imbalance affects microbes vital for nutrient cycling, organic matter decomposition, and energy flow, potentially altering ecosystem functionality (Grenni et al., 2018). Additionally, sublethal antibiotic concentrations in the environment exert selective pressure that accelerates the emergence of ARGs. These genes, frequently transmitted between bacteria populations through horizontal gene transfer, are widely detected in soil, water systems, and even drinking water, underscoring their pervasive spread and the difficulty of containment (Polianciuc et al., 2020).

The increasing presence of antibiotic-resistance bacteria (ARB) due to environmental contamination poses a serious public health threat, undermining the efficacy of medical treatments and raising the risk of untreatable infections. Bacteria utilize various resistance mechanisms including reduced permeability, active efflux, target modification, and enzymatic degradation to survive antibiotic exposure (Bobate et al., 2023). The transmission of ARB and ARGs occurs through interconnected pathways, including contaminated water sources, soil, and food chains, amplifying risks

to human and animal health. Addressing the origins and movement of these contaminants is essential to mitigating their global impact (Grenni et al., 2018).

2.2.2 Global and Regional Statistic on Antibiotics Pollution

Antibiotic contamination of aquatic environments has become a pressing environmental and public health issue, particularly in East and Southeast Asia. A review encompassing over 150 studies conducted between 2006 and 2020 identified widespread detection of antibiotic residues in surface waters such as rivers, lakes, and coastal zones (Kraemer et al., 2019). High contamination levels were especially prevalent in urban and industrial regions, reflecting significant anthropogenic pressure. More recent studies published up to 2025 continue to report the persistent occurrence of antibiotics in aquatic environments, highlighting wastewater treatment plant effluents, aquaculture activities, livestock production, and untreated sewage as major sources of contamination (Batuman et al., 2024). The continued detection of antibiotic residues and antibiotic resistance determinants in aquatic systems indicates that antibiotic pollution remains an ongoing environmental challenge requiring effective mitigation and treatment strategies (Kraemer et al., 2019). Table 2.1 demonstrates that antibiotic contamination is a widespread environmental issue affecting aquatic systems across Asia, Europe, and North America. Various classes of antibiotics, including sulfonamides, quinolones, macrolides, tetracyclines, and β-lactam antibiotics, have been detected in rivers, lakes, estuaries, and groundwater at concentrations ranging from a few ng/L to several 10^3 ng/L. The occurrence and concentration levels of these antibiotics vary depending on the degree of urbanization, industrial activities, wastewater management practices, and agricultural intensity within each region (Kovalakova et al., 2020).

Table 2.1
The Range of Antibiotics Identified in Water Sources Worldwide

Region/Country	Water Source	Antibiotic	Concentration Range (ng/L)	Reference
China	Rivers, lakes, groundwater	Sulfamethoxazole	12 – 10,600	(Haiyang Chen et al., 2018)
		Norfloxacin	8 – 8,540	
		Erythromycin	15 – 6,230	
Vietnam	Rivers and canals	Sulfamethoxazole	4.8 – 1,420	(Ngo et al., 2021)
		Ciprofloxacin	3.2 – 890	
Thailand	Rivers and estuaries	Norfloxacin	5 – 1,350	(Sinthuchai et al., 2016)
		Tetracycline	8 – 780	
		Sulfadiazine	4 – 540	
Malaysia	Rivers	Amoxicillin	100 – 1,000	(Low et al., 2021)
		Tetracycline	80 – 760	
		Erythromycin	45 – 420	
Europe (Spain, UK, Romania)	Rivers and estuaries	Sulfamethoxazole	1.9 – 203	(Manyi-Loh et al., 2018)
		Ciprofloxacin	ND – 203	
		Trimethoprim	5 – 150	(Ahmad et al., 2021)
North America (USA, Canada)	Rivers and estuaries	Sulfamethoxazole	15 – 145	(Amarasiri et al., 2020)
		Erythromycin	10 – 120	
		Trimethoprim	8 – 98	(Sosa-Hernandez et al., 2021)

Among the countries surveyed, China reported some of the highest antibiotic concentrations, with sulfamethoxazole, norfloxacin, and erythromycin reaching concentrations exceeding 10,000 ng/L in certain water bodies (Chen et al., 2018). These elevated concentrations have been attributed to intensive population density, pharmaceutical manufacturing activities, and the discharge of municipal and industrial wastewater (Chen et al., 2018). In Southeast Asia, antibiotics such as sulfamethoxazole, ciprofloxacin, tetracycline, norfloxacin, and amoxicillin were frequently detected in rivers, canals, and estuarine environments, indicating significant contributions from

domestic wastewater, aquaculture activities, livestock farming, and agricultural runoff (Low et al., 2021; Ngo et al., 2021; Sinthuchai et al., 2016).

Similar contamination trends have also been reported in Europe, and North America, where antibiotics including sulfamethoxazole, ciprofloxacin, trimethoprim, erythromycin, and amoxicillin were detected in various aquatic environments (Amarasiri et al., 2020; Manyi-Loh et al., 2018; Sosa-Hernandez et al., 2021). Although the reported concentrations in these regions were generally lower than those observed in some Asian countries, their widespread occurrence demonstrates the persistence of antibiotic residues despite the implementation of advanced wastewater treatment technologies. These findings suggest that conventional treatment systems are often insufficient for the complete removal of pharmaceutical contaminants, allowing their continuous release into the environment (Hazra & Durso, 2022).

In the Malaysian context, recent studies provide valuable insights into the occurrence, distribution, and sources of antibiotics and other pharmaceutical contaminants in aquatic environments. As summarized in Table 2.2, antibiotics such as amoxicillin, ciprofloxacin, chloramphenicol, and sulfamethoxazole, together with other pharmaceutical compounds including diclofenac, caffeine, dexamethasone, and triclosan, have been detected in various Malaysian water bodies (Mangala Praveena et al., 2018). River systems, including Sungai Lui, Sungai Gombak, Sungai Selangor, and Sungai Langat in Selangor, have been identified as important receptors of pharmaceutical contamination, with maximum reported concentrations reaching 267.20 ng/L in Sungai Gombak (Mangala Praveena et al., 2018; Subari et al., 2017). Additionally, traces of antibiotics have been detected in drinking water sources in Putrajaya and Kajang, suggesting that conventional water treatment processes may not eliminate pharmaceutical contaminants and raising concerns regarding long-term human exposure, even at low concentrations (Adzima et al., 2019; Mangala Praveena et al., 2019). Previous environmental risk assessment studies have reported predicted no-effect concentration (PNEC) values for amoxicillin ranging from approximately 7.8 to 78 ng/L. These values are commonly used as ecotoxicological thresholds for assessing the potential environmental risks of amoxicillin in aquatic ecosystems (Sosa-Hernandez et al., 2021). Concentrations exceeding the PNEC may pose ecological risks to aquatic organisms and contribute to the development of antibiotic resistance (Amarasiri et al., 2020).

Table 2.2

The Occurrence of Pharmaceutical Contaminants Detected in Water Sources in Malaysia

Water Source	**Sampling Location / Study Area**	**Pharmaceutical Contaminants Detected**	**Maximum Reported Concentration (ng/L)**	**Reference**
River Water	Sungai Lui, Selangor	Amoxicillin, Caffeine, Chloramphenicol, Ciprofloxacin, Dexamethasone, Diclofenac, Nitrofurazone, Sulfamethoxazole, Triclosan	112.40	(Mangala Praveena et al., 2018)
	Sungai Gombak, Selangor	Amoxicillin, Caffeine, Chloramphenicol, Ciprofloxacin, Dexamethasone, Diclofenac, Nitrofurazone, Sulfamethoxazole, Triclosan	267.20	
	Sungai Selangor, Selangor	Amoxicillin, Caffeine, Chloramphenicol, Ciprofloxacin, Dexamethasone, Diclofenac, Nitrofurazone, Sulfamethoxazole, Triclosan	198.91	
	Sungai Langat, Selangor	Furosemide	109.00	(Subari et al., 2017)

Tap / Drinking Water	Putrajaya, Federal Territory	Amoxicillin, Caffeine, Chloramphenicol, Ciprofloxacin, Dexamethasone, Diclofenac, Nitrofurazone, Sulfamethoxazole, Triclosan	0.38	(Mangala Praveena et al., 2019)
Tap / Drinking Water	Kajang, Selangor	Ciprofloxacin	0.0667	(Adzima et al., 2019)
Aquaculture Farm Effluent	Perak, Pahang, Johor, Kelantan and Penang	Tetracyclines, Sulfonamides, Quinolones, Macrolides, Trimethoprim and Lincomycin	1.099×10^6	(Lean et al., 2021)
Hospital Effluent	Nilai and Seremban, Negeri Sembilan	Theophylline	3314.00	(Al-Qaim et al., 2018)
Domestic Wastewater	Residential Areas, Selangor	Amoxicillin, Ciprofloxacin and Sulfamethoxazole	1280.00	(Amarasiri et al., 2020)
Pharmaceutical Industry Effluent	Industrial Areas, Selangor	Amoxicillin, Erythromycin and Tetracycline	5430.00	(Ripanda et al., 2025)
Agricultural Runoff	Agricultural Areas, Kedah	Sulfonamides, Tetracycline and Trimethoprim	2150.00	(Sosa-Hernandez et al., 2021)

Note: Values reported represent the maximum concentrations detected in the respective studies. The pharmaceutical contaminants listed include antibiotics and other commonly detected pharmaceutical compounds reported in Malaysian aquatic environments.

The occurrence of pharmaceutical contaminants in Malaysia originates from multiple anthropogenic sources. Hospital effluents, particularly those reported in Nilai and Seremban, Negeri Sembilan, have been identified as important contributors of pharmaceutical residues due to the intensive use of medications in healthcare facilities (Al-Qaim et al., 2018). Similarly, aquaculture activities in Perak, Pahang, Johor, Kelantan, and Penang have been associated with the presence of various antibiotic classes, including tetracyclines, sulfonamides, quinolones, macrolides, trimethoprim, and lincomycin, with concentrations reaching as high as 1.099×10^6 ng/L (Lean et al., 2021). Additional sources include domestic wastewater from residential areas, pharmaceutical industry effluents from industrial zones, and agricultural runoff associated with livestock farming and fertilizer application. These activities contribute to the continuous release of pharmaceutical contaminants into rivers, drainage systems, and groundwater through wastewater discharge, surface runoff, and leaching processes (Amarasiri et al., 2020).

The widespread occurrence of pharmaceutical contaminants across both urban and rural environments highlights the influence of healthcare practices, pharmaceutical consumption, veterinary applications, aquaculture activities, and agricultural intensification on environmental pollution (Amarasiri et al., 2020). These challenges are further exacerbated by rapid urbanization, increasing demand for pharmaceuticals, and limitations in wastewater treatment and waste management infrastructure (Ahmad et al., 2021; Manyi-Loh et al., 2018). Consequently, effective mitigation strategies are required to minimize the environmental dissemination of pharmaceutical contaminants and reduce the risk of antimicrobial resistance development. Such strategies should include the implementation of advanced wastewater treatment technologies, strengthened antibiotic stewardship programmes, continuous environmental monitoring, and the establishment of comprehensive regulatory frameworks. Through these integrated efforts, the release of pharmaceutical contaminants into the environment can be better controlled, thereby protecting aquatic ecosystems and public health (Ahmad et al., 2021; Clara et al., 2025).

2.2.3 Environmental and Human Health Impact of Antibiotics Pollution

The pollution of ecosystems by antibiotics represents a critical intersection between environmental degradation and public health risk, largely driven by anthropogenic activities such as pharmaceutical manufacturing, healthcare practices, livestock farming, and aquaculture (Amarasiri et al., 2020). These practices contribute to the dissemination of antibiotic residues into natural environments, primarily through wastewater discharges and agricultural runoff. Once introduced, these compounds exert selective pressure on microbial communities, fostering the proliferation of ARB and ARGs, with implications that traverse ecological and human health domains (Kraemer et al., 2019).

From an environmental perspective, antibiotics disrupt microbial community structures and reduce biodiversity across both aquatic and terrestrial ecosystems (Manyi-Loh et al., 2018). In water bodies, antibiotics persist in sediments and the water column, altering microbial dynamics essential for biogeochemical cycles and ecosystem services (Al-Qaim et al., 2018) . Similarly, in soil, antibiotic contamination impairs microbial diversity and function, affecting soil fertility and plant health. These ecological disturbances can have cascading effects on food webs and the resilience of natural systems (Polianciuc et al., 2020).

The human health implications are profound. Environmental reservoirs of ARBs and ARGs act as conduits for the spread of AMR, undermining the efficacy of life-saving antibiotics (Ripanda et al., 2025). Humans are exposed to these resistant organisms through multiple pathways, including consumption of contaminated water and food and direct contact with polluted environments (Amarasiri et al., 2020). This led to infections that are more difficult to cure, raising healthcare expenses, lengthening hospital stays, and increasing mortality rates. The World Health Organization has recognized AMR as one of the most urgent global health challenges, largely fuelled by such environmental pathways (Amarasiri et al., 2020).

The confluence of environmental and health risks associated with antibiotic pollution necessitates integrated mitigation strategies. These include the development of advanced wastewater treatment technologies, stricter regulations on antibiotic use, and the promotion of sustainable agricultural practices (García-ávila et al., 2024; Kamalesh et al., 2024). Embracing the “One Health” perspectives, acknowledging the interdependence of human, animal, and environmental health, is imperative for

addressing the root causes and systemic impacts of antibiotic pollution (Ripanda et al., 2025).

2.3 Removal Methods for Antibiotics in Water Systems

The increasing presence of antibiotics in aquatic environments has necessitated the development and optimization of diverse removal strategies, each aiming to address the persistence, toxicity, and resistance-inducing potential of these compounds (Sosa-Hernandez et al., 2021). Conventional biological treatments, such as the activated sludge process, remain prevalent due to their integration into existing municipal wastewater treatment frameworks (Yin et al., 2024). These systems rely on microbial communities to degrade organic matter, including some antibiotics. However, their performance is often inconsistent, particularly for structurally complex or recalcitrant compounds (Hazra & Durso, 2022). To enhance treatment efficiency, advanced biological processes such as fixed-film bioreactors and membrane bioreactors (MBRs) have been developed (García-ávila et al., 2024; Kamalesh et al., 2024). Fixed-film bioreactors provide a larger surface area for microbial attachment, improving biomass retention and biodegradation efficiency, while MBRs combine biological treatment with membrane filtration, enabling more effective removal of suspended solids and selected pharmaceutical contaminants (Singh et al., 2023). Despite these advantages, the removal efficiency of antibiotics remains highly dependent on the physicochemical properties of the compounds and operating conditions. Certain antibiotics exhibit resistance to biodegradation and may inhibit microbial activity, thereby reducing treatment efficiency. Furthermore, MBR systems are associated with higher operational costs and membrane fouling issues, whereas fixed-film systems may experience biofilm overgrowth and clogging during long-term operation. Consequently, although advanced biological treatments can improve antibiotic removal compared to conventional activated sludge systems, complete elimination of antibiotic residues remains challenging (Yin et al., 2024).

In response to these limitations, physical and chemical techniques have been extensively researched and implemented. Among physical approaches, membrane filtration technologies, including reverse osmosis (RO), nanofiltration (NF), and ultrafiltration (UF), stand out due to their ability to achieve high rejection rates of antibiotics through size exclusion and charge repulsion mechanisms. For instance, RO

has demonstrated removal efficiencies exceeding 90% for numerous antibiotic classes, although operational issues like membrane fouling, high energy consumption, and concentrate disposal remain significant drawbacks (García-ávila et al., 2024; Kamalesh et al., 2024).

Chemical treatments, particularly AOPs, represent a powerful alternative for antibiotic degradation. These include ozonation, Fenton and photo-Fenton reactions, and photocatalysis, which generate reactive species capable of oxidizing antibiotic molecules into less harmful products (Wang & Zhuan, 2020). Ozonation has demonstrated high efficacy in degrading a broad spectrum of antibiotic compounds. However, if not properly controlled, the process may result in the formation of transformation products with potential ecotoxicological effects, thereby posing additional risks to environmental and public health (Wang & Zhuan, 2020). Similarly, the photo-Fenton process has proven efficient under controlled pH and catalyst conditions. The photocatalytic degradation using semiconductors like titanium dioxide under ultraviolet light has also gained attention for its potential to achieve complete mineralization, though scalability and energy requirements pose challenges (Khader et al., 2024).

Adsorption methods offer another robust and adaptable solution, particularly useful for polishing steps in treatment chains. Activated carbon, in both powdered and granular forms, remains the most established adsorbent due to its high surface area and affinity for various antibiotic molecules (Sharma et al., 2024). Recent advancements have explored the efficacy of novel materials such as biochar, carbon nanotubes, and metal-organic frameworks, which exhibit enhanced adsorption capacities and regeneration potential (Sharma et al., 2024). Nevertheless, the sustainability of these materials and the fate of spent adsorbents continue to be actively investigated (Gusti, 2025).

Furthermore, the integration of multiple removal techniques into hybrid systems is emerging as a promising avenue. By combining the strengths of individual methods, including coupling biological treatment with adsorption or integrating membrane processes with AOPs these systems aim to overcome the limitations of single technologies and enhance overall treatment efficacy (Alardhi et al., 2024; Ejraei et al., 2019). Constructed wetlands, though less technologically intensive, offer an eco-friendly and cost-effective option for decentralized antibiotic removal, leveraging plant uptake and microbial action to reduce contaminant loads (Lv et al., 2022).

The effective removal of antibiotics from aquatic environments necessitates a comprehensive strategy that synergistically combines technological advancements, environmental stewardship, and economic viability (Singh et al., 2023). Although a generally applicable solution has yet to be realized, ongoing improvements in the integration of biological, chemical, and physical treatment approaches offer a promising direction for reducing the ecological and public health hazards caused by antibiotic residues (Haque et al., 2024).

2.4 Adsorption as a Prominent Removal Method: Advantages and Challenges

Adsorption is widely recognized as a simple, economical, and scalable treatment technology for large-scale wastewater treatment applications (Anuar et al., 2023). However, the scalability of biomass-derived activated carbons may be influenced by factors such as feedstock availability, activation procedures, production costs, and the ability to maintain consistent adsorbent properties during large-scale manufacturing. Therefore, further studies are required to evaluate the practical feasibility of translating laboratory-scale findings into industrial-scale applications (Anuar et al., 2023; Sharma et al., 2024). Activated carbon is preferred as an adsorbent due to its porous structure, wide surface area, and variable surface chemistry, which enables efficient capture of antibiotic compounds. Several operational parameters play a significant role in determining the adsorption performance of activated carbon, including pH solution, initial antibiotics concentration, contact duration, and temperature (Gusti, 2025).

Among these variables, solution pH is particularly important because it alters both the ionization behaviour of antibiotic molecules and the surface charge characteristics of activated carbon (Sharma et al., 2024). Depending on the antibiotic type, adsorption behaviour can vary considerably across acidic, neutral, and alkaline conditions, typically within the pH range of 3.0 to 11.0. Changes in pH influence electrostatic interactions, hydrogen bonding, and other adsorption mechanisms, thereby affecting the overall adsorption efficiency (Luo et al., 2021). Similarly, increasing the initial pollutant concentration generally enhances the adsorption driving force and increases the adsorption rate. However, excessive pollutant concentrations may eventually lead to saturation of the available adsorption sites, thereby reducing the overall removal efficiency over prolonged adsorption periods (Putra et al., 2009). Despite its advantages, its effectiveness is constrained by adsorbent saturation, which

requires periodic regeneration or replacement. Techniques such as thermal or chemical reactivation can recover the adsorbent capacity, although these processes can increase operational costs (Putra et al., 2009).

Recent advancements in adsorption technology have focused on the development of advanced materials to enhance their efficiency and sustainability for antibiotic removal. Graphene-based composites, biochar, and magnetically activated carbon have shown exceptional promise due to their high adsorption capacities and tunable surface properties (Singh et al., 2023). For instance, graphene oxide and reduced graphene oxide offer enhanced adsorption performance because of their large specific surface areas and abundant functional groups (Huang et al., 2021). Biochar produced from agricultural residues provides a low-cost and sustainable adsorbent option, whereas magnetic activated carbon simplifies the separation of adsorbents from treated water. Furthermore, hybrid systems combining adsorption with AOPs or biological treatments have demonstrated enhanced removal efficiencies by leveraging the strengths of multiple methods (Huang et al., 2021). For example, coupling adsorption with ozonation can simultaneously degrade and capture antibiotics, whereas integrating adsorption with microbial biodegradation improves the biodegradability of residual contaminants (Lee et al., 2020). These hybrid approaches offer a balanced solution to the challenges of single-method systems, particularly addressing the limitations of adsorbent saturation.

Thus, adsorption using activated carbon remains the cornerstone of antibiotic removal technologies, owing to its simplicity, scalability, and effectiveness (Anuar et al., 2023). By addressing current challenges, such as adsorbent regeneration and by-product management, and integrating advanced materials and hybrid systems, adsorption can further enhance wastewater treatment processes (Bagotia, 2025). Future research should focus on optimizing adsorbent properties, scaling up innovative technologies, and evaluating their long-term performance under real-world conditions. Such efforts are essential to mitigate the ecological and public health risks posed by antibiotic contamination in wastewater and to contribute to sustainable environmental management (Hussain et al., 2025).

2.5 Adsorption Materials for Antibiotics Removal

2.5.1 Conventional and Emerging Adsorbents for Antibiotics

Conventional adsorbents, particularly AC, have been extensively applied for the removal of a wide range of antibiotics, including tetracyclines, sulfonamides, and fluoroquinolones (Anuar et al., 2023). Activated carbon's high surface area, well-developed porosity, and diverse surface functional groups enable effective interactions with antibiotic molecules through mechanisms such as hydrogen bonding, π-π interactions, and electrostatic forces (Phoon et al., 2020). Both powdered and granular forms are used, with powdered activated carbon (PAC) generally offering faster kinetics and higher removal efficiency due to its finer particle size (Wahyu et al., 2025)

Emerging adsorbents have evolved to address limitations associated with conventional materials such as regeneration difficulties and high cost. These include carbon-based nanomaterials (e.g., carbon nanotubes, graphene oxide), MOFs, and magnetic composites (Ahmad et al., 2024). Carbon nanotubes and graphene derivatives exhibit exceptional adsorption capacities owing to their unique surface chemistry and high aspect ratios, facilitating enhanced molecular interactions with various antibiotics (Phoon et al., 2020). Similarly, MOFs are notable for their tunable porosity and chemical functionality, although their environmental safety and scalability remain under investigation (Ajala et al., 2023).

In addition, biosorbents derived from agricultural and industrial wastes, including sawdust, coconut shells, and fruit peels, are gaining popularity due to their low cost and sustainability (Ahmad et al., 2024). These materials are often chemically modified to improve their surface characteristics and increase their affinity for antibiotics. Despite their growing success in lab-scale studies, the application of many emerging adsorbents at the industrial scale is still limited, emphasizing the need for further research on regeneration, cost-efficiency, and environmental safety (Anuar et al., 2023).

2.5.2 Biomass-derived Activated Carbon: Advantages and Challenges

Biomass-derived AC has emerged as a highly promising material for antibiotic removal due to its environmental friendliness, cost-effectiveness, and competitive adsorption performance (Ajala et al., 2023). Produced through the pyrolysis and activation of lignocellulosic materials such as agricultural residues, this material offers high surface area, abundant active sites, and diverse functional groups, enabling efficient removal of various antibiotics from water (Ahmad et al., 2024). Various types of biomass have been investigated to produce biochar and activated carbon due to their abundance, renewable nature, and favorable carbon content. The commonly reported biomass precursors and their applications in pollutant removal are summarized in Table 2.3.

One of the most significant advantages of biomass-derived AC is its sustainability. Using renewable resources such as coconut shells, rice husks, and forestry residues not only provides a value-added route for waste utilization but also reduces dependence on fossil-derived precursors (Ullah et al., 2024). Additionally, the properties of biomass-derived AC can be fine-tuned through activation methods (physical or chemical) and surface modification, which enhances its adsorption capacity and selectivity toward specific antibiotics (Tiryaki et al., 2014).

However, several challenges must be addressed before large-scale implementation. These include variability in biomass feedstock composition, which affects the consistency and quality of the final adsorbent (Wahyu et al., 2025). Moreover, although biomass-derived AC generally shows high initial adsorption efficiency, its regeneration and reuse potential may be limited due to pore blockage, loss of active surface functional groups, structural degradation during repeated regeneration cycles, and incomplete desorption of adsorbed contaminants (Lee et al., 2020). These factors can gradually reduce adsorption performance and undermine the economic and environmental benefits associated with adsorbent reuse. The risk of leaching potentially hazardous substances during use and regeneration processes also warrants careful evaluation, particularly for biochar or ACs derived from waste materials (Bagotia, 2025). Furthermore, performance under real wastewater conditions characterized by complex matrices and competing ions often differs from idealized laboratory settings. As such, pilot-scale and field applications are critical to assess long-term efficacy, operational feasibility, and environmental impacts (Sharma et al., 2024).

2.6 Synthesis of Activated Carbon for Antibiotics Adsorption

2.6.1 Preparation Techniques for Biomass-derived Activated Carbon

Generally, any precursors with a high carbon proportion are useful for synthesizing carbon-based adsorbents. Biomass and biochar possess high carbon content, making them ideal precursors to produce carbon-based adsorbents. Many studies utilized biomass from agricultural wastes for the synthesis of carbon materials, including rice straw (Chen et al., 2021), corn straw (Yang et al., 2020), corncob (Huiqin Li et al., 2020), and coconut shell (DasSharma et al., 2020). In some studies, other resources were also used in the carbon-adsorbent production, such as municipal sludge (Ma et al., 2021), algae (Wu et al., 2021), forest processing residue (Aghababaei et al., 2017), and sawdust (Zhou et al., 2017).

Among these biomass precursors, PKS is particularly advantageous due to its favourable lignocellulosic composition, high fixed carbon content, low ash content, and well-developed pore structure after activation (Huat et al., 2022). PKS typically contains approximately 20–30% cellulose, 20–25% hemicellulose, and 45–55% lignin. The relatively high lignin content promotes greater char formation during pyrolysis, resulting in higher carbon yield and improved suitability for activated carbon production (Pamidimukkala & Soni, 2018). Furthermore, the unique physicochemical properties of PKSAC, including its high surface area and tunable porosity, enhance its adsorption capacity for organic pollutants such as antibiotics (Huat et al., 2022). Additionally, PKSAC has been shown to exhibit excellent thermal stability and mechanical strength, which further supports its use in water treatment applications (Rabia & Hussein, 2020).

Numerous studies have investigated the conversion of palm kernel shell (PKS) into activated carbon using various physical and chemical modification techniques (Opeoluwa et al., 2023). Physical activation methods, such as steam activation and microwave-assisted activation, have been reported to improve pore development and surface area, whereas chemical activation using agents such as KOH, H_3PO_4, and $ZnCl_2$ further enhances porosity and surface functionality (Ahmed et al., 2015). These modified PKSAC materials have demonstrated promising performance for the removal of heavy metals, dyes, phenolic compounds, and other organic contaminants from wastewater (Huat et al., 2022). However, most previous studies primarily focused on adsorbent preparation, physicochemical characterization, and adsorption performance

evaluation. Limited attention has been given to the removal of emerging contaminants such as antibiotics, particularly AMX. In addition, adsorption mechanisms are frequently interpreted based on adsorption kinetics and equilibrium models, which may not fully explain the interactions between adsorbents and adsorbates (Opeoluwa et al., 2023). Therefore, further investigation is required to achieve a more comprehensive understanding of the adsorption behaviour of modified PKSAC for antibiotic removal.

Well-developed porosity, hydrophobic surfaces, and oxygen-surface groups play a pivotal role in antibiotic adsorption. These factors improve electrostatic attraction, resulting in increased efficiency of the adsorption capacity of the contaminants on the activated carbon (Pego et al., 2019). However, the performance of biomass and biochar is commonly restricted by their moderate to low surface area, and the limited number of surface functional groups present. Accordingly, adjustments have been proposed to enhance biomass and biochar's adsorption capacities by enhancing their porosity (Pamidimukkala & Soni, 2018). The adjustments involve additional pre-activation and activation steps which lead to the production of activated carbon with better intrinsic adsorbent properties (Sultana et al., 2022).

The pre-activation process requires the biomass materials to be cleaned with deionized water to remove any dirt or other contaminants before drying at temperatures of 65-105 °C. This is followed by milling the biomass materials to minimize the particle size, permitting uniform and rapid carbonization by minimizing the heat gradient (Yahya et al., 2018). The carbonization process is the next step in biochar formation (Figure 2.3). Biochar with high porosity properties can be produced through physical and chemical activations. In recent years, energy- and chemical-saving procedures such as microwave heating (Ahmed & Theydan, 2012) and hydrothermal carbonization treatment (Jais et al., 2021) have also been proposed as alternative pathways to synthesize biochar and activated charcoal. Two primary factors, including synthesis conditions and the biomass composition feedstock, significantly impact on the porosity, surface chemistry, and yields of the carbon-based adsorbent. Subsequently, the chemical activation method is carried out on the pretreated biochar materials through infusion and permeation of the activation agent solution. A dehydrating chemical is frequently used as an activation agent, given the ability to inhibit the development of tar and the evolution of semi-solid volatile compounds (DasSharma et al., 2020).

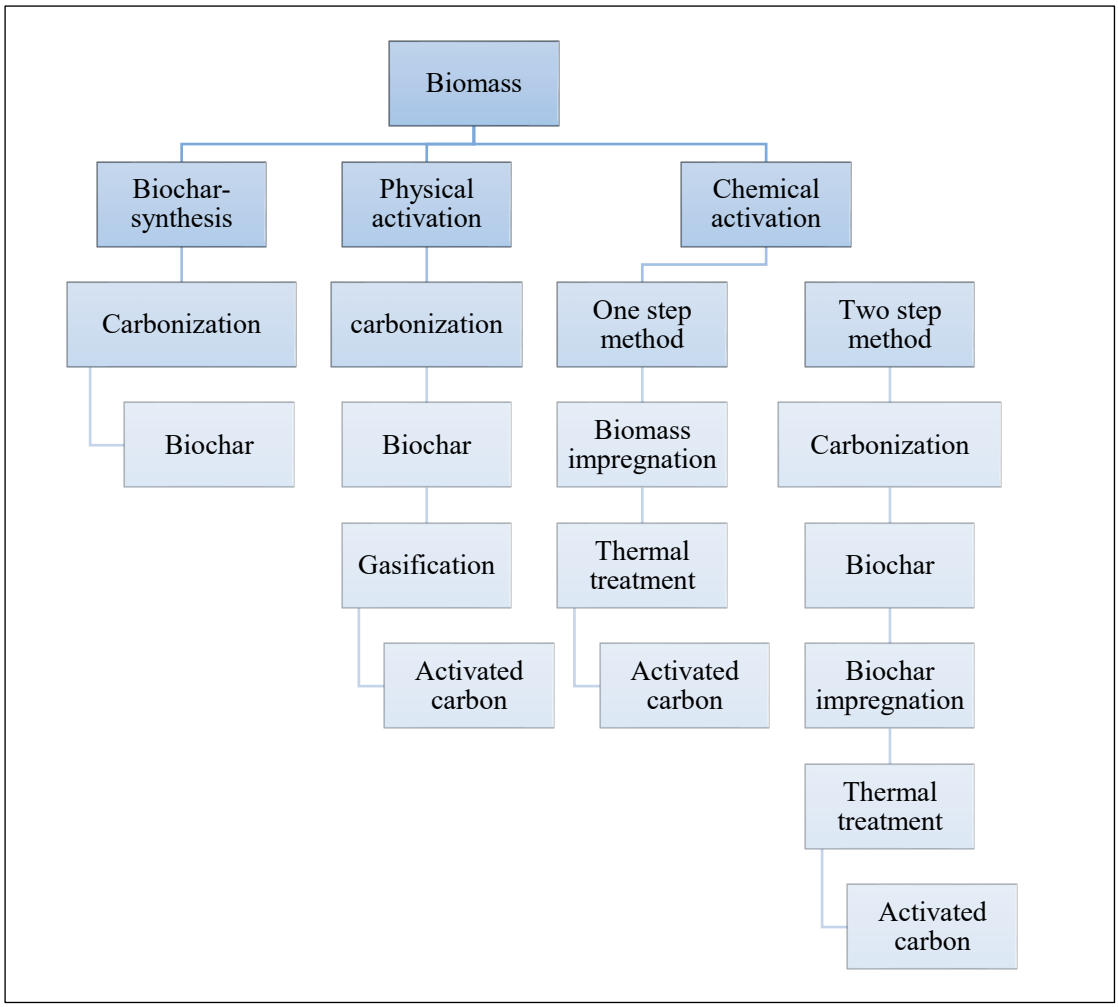

Figure 2.3 The Synthesis Pathways for Activated Carbon from Biomass.

The carbonization process requires an inert environment with temperatures between 500 °C and 800 °C. Temperature is the primary determinant of porosity. A low carbonization temperature (<400 °C) causes no significant porous development, probably due to the incomplete removal of volatile matter (Pego et al., 2019). In contrast, the application of temperatures between 400 °C and 900 °C increases the porosity secondary to the release of most of the volatile matter, resulting in a significant increase in the surface area (Aghababaei et al., 2017). For instance, lignocellulosic materials need a temperature range of 400–800 °C for chemical activation, which is lower than the typical temperature for the physical activation process (Ahmed & Theydan, 2012).

Biochar can be transformed into activated carbon through one-step or two-step processes. The latter involves an additional step of impregnating biochar with activating agents before the thermal treatment (Zhou et al., 2017). Other than the pre-carbonization

process, another chemical activation step can be conducted before the thermal treatment step (Pego et al., 2019). The reaction outcomes between activating agents and biomass precursors vary depending on structures and activation conditions (Pego et al., 2019).

Acids are activating agents with the capability to remove impurities, such as metals, and introduce the acid functional groups on the surface of carbon adsorbent (Jais et al., 2021). According to Table 2.3, the common acids include hydrochloric acid (HCl), sulfuric acid (H_2SO_4), phosphoric acid (H_3PO_4) and citric acid ($C_6H_8O_7$) (Premarathna et al., 2019).

H3PO4 modification could enhance the surface area of activated carbon produced from rice straw (372.2 m^2/g) and swine manure (319 m^2/g). Moreover, rice straw and swine manure-derived activated carbon had a maximum adsorption capacity of 552 and 365.4 mg/g, respectively, even though there was no significant improvement on functional groups of raw adsorbent on a qualitative level (Chen et al., 2018). However, according to other research, H_3PO_4 can develop cross-links across the surface of the Prosopis juliflora wood, resulting in diverse acidic functional groups like carbonyl (-CO), carboxyl (-COOH), lactones (-(C=O)-O-), phenols (C_6H_5OH) and quinones ($C_6H_4O_2$) [111]. At the same time, these functional groups enhanced porosity, which could be responsible for the surface heterogeneity caused by the acid treatment, resulting in maximum adsorption removal of 250 mg/g for ciprofloxacin and 714.29 mg/g for amoxicillin, respectively (Chandrasekaran et al., 2020). However, acid modification can also change the surface area of the activated carbon and the effect of the surface varies with the type and the concentration of the acid (Xia et al., 2013). For example, the surface area of forest residue-derived activated carbon slightly decreased from 421 m^2/g to 354 m^2/g after the concentration of H_3PO_4 was increased from 1 M to 5 M (Aghababaei et al., 2017). Weak acids such as boric acid also improved the surface area of the activated carbon obtained from hickory sawdust (from 766.60 m^2/g to 1190.61 m^2/g) but slightly declined from 1190.61 m^2/g to 1137.61 m^2/g with further increase in the boric acid ratio from 1:1 to 1:2. This action could be linked to the eventual collapse of some pore walls in the core of the adsorbent (Aghababaei et al., 2017). Therefore, many factors can affect the surface area of the adsorbent, including the concentration and types of acids, feedstock, and preparation conditions.

Table 2.3

Acidic Modification of Biomass-Derived Activated Carbon for Antibiotic Adsorption.

Biomass	**Antibiotic**	**Carbonization method**	**Chemical agent**	**Modification method**	**Modification condition**	**Surface area (m^2/g)**	**Adsorption condition**	**Removing Capacity (mg/g)**	**Ref.**
Sugarcane bagasse	Tetracycline	HTC	HCl	One - step method	N/A	9.3	Initial antibiotic concentration: 50 mg/L pH: 5 Adsorbent dosage: 1 g/L Contact time: 24 h	68.2	(Jais et al., 2021)
Coffee bean waste	Levofloxacin	Pyrolysis (muffle furnace)	H_3PO_4	Two-step method	Carbonization temperature: 350-550 °C, 120 min (N_2 gas) Chemical ratio: - Impregnation time: 120 min Impregnation temperature: 80 °C	429.19	Initial antibiotic concentration: 40 mg/L pH: 6 Adsorbent dosage: 0.8 g/L Contact time: 180 min	110.70	(Maged et al., 2021)

					Activation temperature: 550 °C, 30 min				
Walnut shell	Sulphonamide	Pyrolysis (tube furnace)	HNO_3	One-step method	Carbonization temperature: 500 °C, 2 h (Ar gas) Chemical ratio: - Impregnation time: 12 h Impregnation temperature: 60,80, 100 °C Oven dried (60 °C, 24 h)	N/A	Initial antibiotic concentration: 20 mg/L pH: 6 Adsorbent dosage: 0.002 g Contact time: 48 h	46	(Geng et al., 2021)
Eucalyptus sawdust	Metronidazole (MTZ) Dimetridazole (DTZ)	Pyrolysis (muffle furnace)	H_3PO_4	One-step method	Chemical ratio: 0.5, 0.75, 1 Impregnation time: 2 h Impregnation temperature: - Activation temperature: 350,450,550 °C, (90,120, 150 min –	882.04	Initial antibiotic concentration: 20 mg/L pH: - Adsorbent dosage: 0.2 g Contact time: 120 min	MTZ:167.5 DTZ : 200	(Wan et al., 2016)

					0.3 L/min N_2 flow)				
Prosopis juliflora wood	Ciprofloxacin (CIP) Amoxicillin (AMX)	Pyrolysis (muffle furnace)	H_3PO_4	One-step method	Chemical ratio: 2.5 Impregnation time: - Impregnation temperature: - Activation temperature: 600 °C, 2 h	946.06	Initial antibiotic concentration: 100 mg/L pH: 7 (AMX), 4 (CIP) Adsorbent dosage: 1 mg/mL Contact time: 24 h	CIP :250 AMX:714.2	(Chandrasekaran et al., 2020)
Corn straw	Tetracycline	Pyrolysis (muffle furnace)	H_3PO_4	One-step method	Chemical ratio: 0.5,1,2,3 Impregnation time: 30 min Impregnation temperature: - Activation temperature: 300 °C, 2 h (N_2 gas)	463.89	Initial antibiotic concentration: 50 mg/L pH: 4 Adsorbent dosage: 1 g/L Contact time: 120 min	227.3	(Yang et al., 2020)
Cotton shell	Sulfadiazine	Pyrolysis (tube furnace)	H_3PO_4	Two-step method	Carbonization temperature: 350 °C, 2 h Chemical ratio:	1225.58	Initial antibiotic concentration: 10-100 mg/L pH: 4	86.98	(Meng et al., 2020)

					2.25,2.5,2.75 Impregnation time: 6,12,24 h Impregnation temperature: room temperature Activation temperature: 350 °C, 2 h (N_2 gas)		Adsorbent dosage: 1 g/L Contact time: 12 h		
Forest-processing residue	Oxytetracycline	Pyrolysis (horizontal furnace)	H_3PO_4	One-step method	Chemical ratio: - Impregnation time: 24 h Impregnation temperature: room temperature Activation temperature: 400,600 °C, 1 h (N_2 gas)	354.02	Initial antibiotic concentration: - pH:4 Adsorbent dosage: 5 mg Contact time: 72 h	263.8	(Aghababaei et al., 2017)
Sour cherry stalk	Ciprofloxacin	Pyrolysis (tube furnace)	H_3PO_4	One-step method	Carbonization temperature: - Chemical ratio: 1,2,3,4 Impregnation time: - Impregnation	1556	Initial antibiotic concentration: 100 mg/L pH: 6.3 Adsorbent dosage: 15 mg	410.06	(Sayin et al., 2021)

					temperature: - Activation temperature: 300, 400, 500 °C, 2 h (N_2 gas)		Contact time: 60 min		
Bamboo	Sulfathiazole (STZ) Sulfamethoxazole (SMX) Sulfamethazine (SMT)	Pyrolysis (fixed bed reactor)	H_3PO_4	Two-step method	Carbonization temperature: 380 °C, 2 h (2.5 psi N_2) Chemical ratio: - Impregnation time: 3 h Impregnation temperature: 50 °C Activation temperature: 600 °C, 2 h (2.5 psi N_2)	1.12	Initial antibiotic concentration: - pH: 3.5 Adsorbent dosage: - Contact time: 24 h	STZ: 40.11 SMX:34.01 SMT: 25.11	(Ahmed et al., 2017)
Hickory sawdust	Sulfamethoxazole	Pyrolysis (muffle furnace)	H_3BO_3	One-step method	Chemical ratio: 0.1, 0.25, 0.5, 1,2 Impregnation time:10 min Impregnation temperature: -	1191.62	Initial antibiotic concentration: 50 mg/L pH: 3 Adsorbent dosage:0.5 g/L Contact time:	96	(Zhang et al., 2022)

					Activation temperature: 700 °C, 2 h		240 min		
Rice straw	Tetracycline	Pyrolysis (muffle furnace)	H_3PO_4	One-step method	Carbonization temperature: 700 °C, 2 h Chemical ratio: - Impregnation time: 24 h Impregnation temperature: room temperature Activation temperature: oven dried	372.2	Initial antibiotic concentration: 30-200 mg/L pH: 9 Adsorbent dosage: 5-10 mg Contact time: 216 h	552	(Chen et al., 2018)
Rice straw	Tetracycline	Pyrolysis (muffle furnace)	$C_{76}H_{52}O_{46}$	One-step method	Carbonization temperature: 700 °C, 2 h Chemical ratio: 1-10% Impregnation time: 24 h Impregnation temperature: -	61.1	Initial antibiotic concentration: 100 mg/L pH: 4 Adsorbent dosage:30 mg Contact time: 48 h	308	(Chen et al., 2021)

					Activation temperature: freeze dried				
Cherry kernel	Sulfamethoxazole	Pyrolysis (muffle furnace)	H_3PO_4	One-step method	Chemical ratio: - Impregnation time: - Impregnation temperature: - Activation temperature: 500 °C, 1 h	657.1	Initial antibiotic concentration: 1-50 mg/L pH: 6 Adsorbent dosage: 4 g/L Contact time: 5- 300 min	19.181	(Turk Sekulic et al., 2019)
Wood sawdust	Tetracycline	Pyrolysis	H_3BO_3	One-step method	Chemical ratio: - 1 Impregnation time: - Impregnation temperature: - Activation temperature: 400, 600 °C, 2 h	305.5	Initial antibiotic concentration: 1-300 mg/L pH: 6 Adsorbent dosage: 15 mg Contact time: 60 min	173.9	(Yuan et al., 2021)

Nitrogen (N_2); Argon (Ar)

Meanwhile, the main aim of alkaline modification is to increase the surface area and the oxygen-containing functional groups. Table 2.4 shows common alkaline used includes potassium hydroxide (KOH), sodium hydroxide (NaOH), and potassium bicarbonate ($KHCO_3$). The performance of adsorption can be significantly impacted by the activation temperature and impregnation ratio. This can be seen from the result of willow branched-derived activated carbon (WBAC) produced with an activation mass ratio from 1:1 to 4:1 (KOH: WBC) and the activation temperature of 750, 800 and 850 °C (Yang et al., 2019). When the activation mass ratio was settled at 4, the adsorption capacities of WBAC750-4 (2906 m^2/g), WBAC800-4 (3212 m^2/g), and WBAC850-4 (3342 m^2/g) were 987, 1026 and 1182 mg/g, respectively (Yang et al., 2019). There was a positive linear correlation for relationship between the adsorption ability and the porosity properties of the activated carbon (Yang et al., 2019). However, in some cases, the high addition of KOH may result in the collapse of the developed pore structure and decrease the adsorption capability (Ahmed & Theydan, 2012). Enteromorpha prolifera (algae) -derived activated carbon modified with KOH shows a satisfactorily high specific surface area with 2172.08 m^2/g for 0.5:1 mass ratio, but the surface area suddenly declined to 930.85 m^2/g, 1161.75 m^2/g and 1832.98 m^2/g when the mass ratio was increased from 1:1 to 2:1 and 3:1, respectively (Wu et al., 2021).

Additionally, the preparation method also influenced the effect of alkaline modification on the surface area of the adsorbent. For example, Albizia lebbeck seed pod-derived activated carbon produced using the microwave method (1824 m^2/g) (Ahmed & Theydan, 2012). Compared to conventional heating, the microwave method of activation has different heating mechanisms and additional benefits, including uniform volumetric heating, regulation of the heating process, a high heating rate and ensuring that the sample has indirect contact with the heat source (Hoseinzadeh et al., 2013).

Table 2.4

Alkaline Modification of Biomass -Derived Activated Carbon for Antibiotic Adsorption

Biomass	**Antibiotic**	**Carbonization method**	**Chemical agent**	**Modification method**	**Modification condition**	**Surface area (m^2/g)**	**Adsorption condition**	**Removing Capacity (mg/g)**	**Ref.**
Coffee ground	Sulphonamide	Pyrolysis (furnace)	KOH NH_3H_2O	One-step method	Carbonization temperature: Pre-treated with KOH 700 °C, 1 h (N_2 gas) Chemical ratio: 3 Impregnation time: 9 h Impregnation temperature: 50 °C Activation temperature: oven dried	2039	Initial antibiotic concentration: 10 mg/L pH: 3 Adsorbent dosage: 5 mg Contact time: -	96.6	(Wang et al., 2021)
Spent coffee ground	Tetracycline	Pyrolysis (horizontal tube furnace)	NaOH	One-step method	Chemical ratio: 1 Impregnation time: 2 h Impregnation temperature: 25 °C	116.59	Initial antibiotic concentration: 10 mg/L pH: 7.5 Adsorbent	113.64	(Nguyen et al., 2021)

					Activation temperature: 600 °C, 2 h (100 cc/min N_2 gas)		dosage: 100 mg Contact time: 24 h		
Enteromorpha prolifera (algae)	Sulfamethoxazole	Pyrolysis (muffle furnace)	KOH	Two-step method	Carbonization temperature: 500 °C, 2 h (400 ml/min N_2 gas) Chemical ratio: 0, 0.5, 1,2,3 Impregnation time: - Impregnation temperature: - Activation temperature: 800 °C, 2 h (200 ml/min N_2 gas)	2172	Initial antibiotic concentration: 0-80 mg/L pH: 5 Adsorbent dosage: 2mg Contact time: 24 h	744	(Wu et al., 2021)
Anthriscus sylvestris	Cephalexin	Pyrolysis (muffle furnace)	NaOH	Two-step method	Carbonization temperature: 300 °C, 15 min (1 L/min N_2 gas) Chemical ratio: - Impregnation time:	N/A	Initial antibiotic concentration: 10-100mg/L pH: 4 Adsorbent dosage: 0.25 g/L	724.54	(Shirani et al., 2020)

					2 h Impregnation temperature: - Activation temperature: 600 °C, 2 h (2 L/min N_2 gas)		Contact time: 0-500 min		
Corncob	Levofloxacin (LEV) Amoxicillin (AMX) Tetracycline (TC)	Pyrolysis (tube furnace)	KOH	One-step furnace	Chemical ratio: - Impregnation time: - Impregnation temperature: - Activation temperature: 700 °C, 1 h (Ar gas)	2368	Initial antibiotic concentration: - pH: - Adsorbent dosage: 0.2 g/L Contact time: 60 min	LEV:482 AMX:371 TC:439.70	(Li et al., 2020; Huiqin Li et al., 2020)
Date stone	Levofloxacin	Pyrolysis (furnace) Microwave	KOH	Two-step method	Carbonization temperature: 500 °C, 1 h Chemical ratio: - Impregnation time: 24 h Impregnation temperature: room temperature	817	Initial antibiotic concentration: 50 mg/L pH: 9 Adsorbent dosage: 0.15 g/L Contact time: 90 min	100.38	(Darweesh & Ahmed, 2017)

					Activation temperature: 620 W, 8 min				
Albizia lebbeck seed pod	Cephalexin	Microwave	KOH K_2CO_3	One-step method	Chemical ratio: - 3 Impregnation time: 24 h Impregnation temperature: room temperature Activation temperature: 620 W, 8 min	1824.88	Initial antibiotic concentration: 20-100 mg/L pH: 7 Adsorbent dosage:0.5 g/L Contact time: 1.5 h	137.02	(Ahmed & Theydan, 2012)
Tea waste	Tetracycline	HTC Pyrolysis (muffle furnace)	$KHCO_3$	Two-step method	Hydrothermal temperature: 200 °C, 10 h (N_2 gas) Chemical ratio: 6 Impregnation time: - Impregnation temperature: - Activation temperature: 700 °C (N_2 gas)	1350.11	Initial antibiotic concentration: 10-200 mg/L pH: 3 Adsorbent dosage: 0.01 g Contact time: 24 h	451.49	(Li et al., 2021)
Coconut shell	Enrofloxacin	Pyrolysis (muffle furnace)	KOH	One-step method	Carbonization temperature: 650	1005.76	Initial antibiotic concentration:	12.347	(DasSharma, et al., 2020)

					°C, 1 h Chemical ratio: 1 Impregnation time: 24 h Impregnation temperature: - Activation temperature: oven dried		10 mg/L pH: 6 Adsorbent dosage: 3 g/L Contact time: 9 h		
Pinewood	Chlortetracycline	Pyrolysis (horizontal furnace)	NaOH	Two-step method	Carbonization temperature: 525 °C Chemical ratio: - Impregnation time: 2 h Impregnation temperature: - Activation temperature: 800 °C, 2 h	852.95	Initial antibiotic concentration: 0.2-150 ppm pH: 1 Adsorbent dosage: 0.001g Contact time: 72 h	434.8	(Taheran et al., 2016)
Willow branches	Tetracycline	Pyrolysis (horizontal tube furnace)	KOH	Two-step method	Carbonization temperature: 500 °C, 2 h (N_2 gas) Chemical ratio:	3342	Initial antibiotic concentration: 100-400 mg/L pH: 3	1300	(Yang et al., 2019)

					1,2,3,4 Impregnation time: - Impregnation temperature: - Activation temperature: 750,800,850 °C, 2 h (50 ml/min N_2 gas)		Adsorbent dosage: - Contact time: 24 h		
Waste cassia bakeriana seed pod	Ciprofloxacin	Pyrolysis (muffle furnace)	KOH	One-step method	Chemical ratio: 1 Impregnation time: 24 h Impregnation temperature: room temperature Activation temperature: 700 °C, 1 h (200 ml/min N_2 gas)	283.4	Initial antibiotic concentration: 25-250 mg/L pH: - Adsorbent dosage: - Contact time: 24 h	600	(Theamwong et al., 2021)
Corn stover	Tetracycline	Pyrolysis	KOH	Two-step method	Carbonization temperature: 290 °C (N_2 gas) Chemical ratio: 10 Impregnation time: -	494	Initial antibiotic concentration: 10-100 mg/L pH: 7.4 Adsorbent	132.9	(Haghighat et al., 2020)

					Impregnation temperature: - Activation temperature: 790 °C (0.5 L/min N_2 gas)		dosage: 0.1-1 g/L Contact time: 5-60 min		
Sugarcane bagasse	Sulfamethoxazole	HTC	NaOH	One-step method	Chemical ratio: - Impregnation time: 4 h Impregnation temperature: 70 °C Activation temperature: 200 °C, 18- 20 h	1099	Initial antibiotic concentration: 5-50 mg/L pH: 5.4 Adsorbent dosage: 0.1 g/L Contact time: 150 min	400	(Prasannamedha et al., 2021)
Rice husk	Tetracycline	Pyrolysis	KOH	One-step method	Carbonization temperature: 450, 500 °C Chemical ratio: - Reaction time: 1 h Reaction temperature: 60 °C Activation temperature: oven dried (80 °C, 12 h)	117.8	Initial antibiotic concentration: - pH: 7 Adsorbent dosage: - Contact time: 24 h	58.8	(Liu et al., 2012)

Pinus taeda	Tetracycline	Pyrolysis (quartz tube furnace)	NaOH	Two-step method	Carbonization temperature: 300 °C, 15 min (1 L/min N_2 gas) Chemical ratio: - Impregnation time: 2 h Impregnation temperature: room temperature Activation temperature: 800 °C, 2 h (2 L/min N_2 gas)	959.9	Initial antibiotic concentration: 10-100 mg/L pH: 6 Adsorbent dosage: 0.01 g Contact time: 7 days	274.8	(Jang et al., 2018)
Pomelo peel	Tetracycline Oxytetracycline Chlortetracycline	Pyrolysis (muffle furnace)	KOH	Two-step method	Carbonization temperature: 400, 600 °C, 2 h Chemical ratio: 4 Impregnation time: - Impregnation temperature: -	2457.36	Initial antibiotic concentration: 5-50 mg/L pH: 8.5 Adsorbent dosage: 10 mg Contact time: 75	TC:476.19 OTC:407.5 CTC:555.5	(Cheng et al., 2020)

					Activation temperature: 600 °C, 2 h		h		
Enteromorpha clathrate (algae)	Tetracycline	Pyrolysis (fixed bed reactor)	NaOH	Two-step method	Carbonization temperature: 500 °C, 1 h (150 cm^3/min N_2 gas) Chemical ratio: 0.25, 0.5, 0.75, 1, 2 Impregnation time: 2 h Impregnation temperature: - Activation temperature: 800 °C, 90 min (150 cm^3/min N_2 gas)	1238.49	Initial antibiotic concentration: 50 – 500mg/L pH: 5 Adsorbent dosage: - Contact time: 960 min	381.584	(Wei et al., 2022)
Tea waste	Tetracycline	Pyrolysis (tubular furnace)	$KHCO_3$	Two-step method	Carbonization temperature:700 °C, 2 h Chemical ratio: 6	1981	Initial antibiotic concentration: 10-200 mg/L pH: 3	293.46	(Li et al., 2021)

	Impregnation time: - Impregnation temperature: - Activation temperature: 700 °C, 2 h	Adsorbent dosage: 0.01 g Contact time: 24h

2.6.2 Influence of Activated Carbon Structure, Surface Chemistry, and Pore Characteristics on Antibiotics Adsorption

The adsorption performance of activated carbon is strongly influenced by its precursor source, activation method, activating agent, and resulting physicochemical properties (Sayin et al., 2021). Different biomass feedstocks possess distinct lignocellulosic compositions, mineral contents, and carbon yields, which affect pore development and surface chemistry during activation (Xia et al., 2013). Consequently, activated carbons derived from different biomass sources often exhibit substantial variations in surface area, pore size distribution, functional groups, and adsorption behaviour towards antibiotic contaminants.

The type of biomass precursor plays a significant role in determining the structural characteristics of activated carbon (Sayin et al., 2021). Biomass materials with high lignin content, such as palm kernel shell and coconut shell, generally produce activated carbons with higher fixed carbon content, greater thermal stability, and well-developed microporous structures (Huat et al., 2022). In contrast, agricultural residues such as sugarcane bagasse, rice husk, and corncob often contain higher proportions of cellulose and hemicellulose, resulting in activated carbons with more oxygen-containing surface functional groups and relatively larger pore structures (Sayin et al., 2021). These differences influence the adsorption performance of activated carbon by affecting both the accessibility of adsorption sites and the nature of adsorbate–adsorbent interactions (Xia et al., 2013).

The activation process further determines the physicochemical properties of activated carbon. Various activating agents, including KOH, NaOH, H_3PO_4, $ZnCl_2$, and HCl, have been employed to enhance pore development and surface functionality (Anuar et al., 2023). Among these activating agents, KOH is widely recognised as one of the most effective chemical activators due to its ability to promote extensive micropore formation and produce activated carbons with exceptionally high surface areas (Ahmed & Theydan, 2012). During activation, KOH reacts with the carbon matrix, generating metallic potassium and gaseous products that enlarge existing pores and create new microporous structures (Ahmed & Theydan, 2012). Consequently, KOH-activated carbons frequently exhibit surface areas exceeding 1000 m^2/g (Nguyen et al., 2021). In contrast, phosphoric acid activation promotes mesopore development

and introduces acidic oxygen-containing functional groups, while $ZnCl_2$ facilitates dehydration reactions and pore generation during carbonization (Anuar et al., 2023). The amount of activating agent is equally important, as insufficient activator loading may result in limited pore development, whereas excessive activator usage may cause pore widening, structural collapse, and reduced mechanical stability (Chen et al., 2018).

The pore structure of activated carbon is a critical factor governing adsorption performance. According to the International Union of Pure and Applied Chemistry (IUPAC) classification, pores are categorised into micropores (<2 nm), mesopores (2–50 nm), and macropores (>50 nm) (Sing et al., 1985). Micropores contribute predominantly to adsorption capacity due to their large internal surface area, whereas mesopores facilitate mass transfer and improve accessibility of adsorbate molecules to internal adsorption sites (Sing et al., 1985). Macropores primarily function as transport channels. For antibiotic adsorption, a hierarchical pore structure containing both micropores and mesopores is generally desirable because antibiotic molecules vary in molecular size and may experience diffusion limitations within exclusively microporous materials (Hafizuddin et al., 2021). Therefore, activated carbons possessing a balanced pore size distribution often demonstrate superior adsorption performance.

Besides pore structure, surface chemistry plays an equally important role in determining adsorption behaviour (Jais et al., 2021). Activated carbon surfaces commonly contain oxygen-containing functional groups such as hydroxyl (-OH), carboxyl (-COOH), carbonyl (C=O), and ether groups (Sultana et al., 2022). These functional groups facilitate adsorption through hydrogen bonding, electrostatic attraction, Lewis acid-base interactions, and surface complexation (Sultana et al., 2022). For example, hydroxyl and carboxyl groups can act as hydrogen bond donors or acceptors, strengthening interactions with polar antibiotic molecules (Xia et al., 2013). Furthermore, the ionization state of both the adsorbent surface and antibiotic molecules is highly dependent on solution pH, making electrostatic interactions an important adsorption mechanism (Maged et al., 2021). Table 2.5 summarizes the effects of biomass precursor type and activating agent on the development of pore structure, surface chemistry, and physicochemical properties of activated carbon, which ultimately govern its adsorption performance.

Table 2.5
Influence of Biomass Precursors and Activating Agents on the Physicochemical Properties of Activated Carbon

Biomass Source	**Activating Agent**	**Surface Area (m^2/g)**	**Dominant Pore Type**	**Average Pore Size (nm)**	**Main Functional Groups**	**Key Characteristics**	**Ref.**
Palm Kernel Shell	KOH	798–2000	Microporous	1–3	–OH, –COOH, C=O	High carbon yield, extensive microporosity	(Opeoluwa et al., 2023)
Coconut Shell	KOH	1000–2500	Microporous	1–2	–OH, –COOH	High surface area and thermal stability	
Corncob	H_3PO_4	500–1500	Mesoporous	2–10	–OH, phosphate groups	Enhanced pore accessibility	(Liu et al., 2022)
Rice Husk	NaOH	400–1200	Mixed micro/mesoporous	2–8	Si–O, –OH	Silica-rich surface	(Liu et al., 2012)
Sugarcane Bagasse	HCl / H_3PO_4	9–800	Mesoporous	3–20	–OH, –COOH	Abundant oxygen-containing groups	(Prasannamedha et al., 2021)

The aromatic structure of activated carbon also contributes significantly to adsorption performance (Luo et al., 2021). Many antibiotics, including fluoroquinolones, sulfonamides, and tetracyclines, contain aromatic rings that can interact with graphitic domains on the activated carbon surface through π–π electron donor–acceptor interactions (Huang et al., 2021). Activated carbons produced at higher carbonization temperatures or through KOH activation generally possess higher aromaticity, which enhances these interactions (Jais et al., 2021). In addition, hydrophobic interactions may contribute to the adsorption of relatively non-polar antibiotic molecules, particularly under neutral and alkaline conditions where electrostatic interactions become less dominant (Jais et al., 2021).

Although high surface area is often regarded as the primary factor governing adsorption performance, numerous studies have demonstrated that surface chemistry can be equally important (Maged et al., 2021). Activated carbons with moderate surface areas but abundant oxygen-containing functional groups have occasionally exhibited superior adsorption capacities compared with materials possessing significantly larger surface areas (Li et al., 2020). Therefore, adsorption performance should be viewed as a combined function of pore structure, surface chemistry, surface charge, and adsorbate properties rather than being solely dependent on surface area (Sultana et al., 2022). Understanding the relationship between these factors is essential for the rational design of activated carbon adsorbents for antibiotic removal from aqueous environments.

2.7 Optimization Tools for Antibiotics Adsorption Efficiency

The increasing presence of antibiotics in aquatic environments, stemming from pharmaceutical, agricultural, and domestic sources, has necessitated the development of highly efficient remediation strategies. Among these, adsorption has gained significant traction due to its operational simplicity, economic viability, and effectiveness across a broad range of pollutants (Anuar et al., 2023). However, the heterogeneity of antibiotic structures and wastewater compositions requires tailored optimization strategies to enhance the performance of adsorption systems (Wen et al., 2023).

Optimization techniques serve as vital tools to systematically investigate the influence of multiple process variables, such as initial contaminant concentration, pH, adsorbent dose, contact time, and temperature, on adsorption capacity. These techniques

aim not only to enhance performance but also to reduce operational costs and environmental impacts (Wahyu et al., 2025). Traditional one-variable-at-a-time (OVAT) approaches, while simple, fail to capture interactive effects between variables. Hence, advanced statistical and computational methods like factorial design, RSM, and artificial intelligence-based models such as artificial neural networks (ANNs) and genetic algorithms (GAs) are increasingly being adopted (Hussain et al., 2025).

The selection of a specific optimization tool depends on the nature of the system and the complexity of variable interactions. Statistical tools are generally preferred for preliminary screening and response modelling, while machine learning algorithms are better suited for nonlinear and dynamic systems (Wei et al., 2022). Combining these tools provides a comprehensive understanding of system performance and enable real-time process optimization, which is crucial for large-scale implementation in wastewater treatment plants (Hussain et al., 2025).

2.7.1 Response Surface Methodology (RSM) for Process Optimization

RSM is a combination of statistical and mathematical techniques designed to model and optimize processes where multiple variables influence a response of interest. RSM provides empirical models that capture the relationships between factors and responses through a minimal number of experiments, making it exceptionally valuable for adsorption studies (Jawad & Surip, 2022).

RSM is typically implemented using design matrices such as Central Composite Design (CCD), Box-Behnken Design (BBD), and Doehlert Matrix. These matrices enable the identification of significant factors, exploration of quadratic effects, and evaluation of variable interactions (Wei et al., 2022). In antibiotic adsorption, RSM has been widely employed to optimize conditions for maximum removal efficiency and adsorbent capacity (Ajebli et al., 2022). Variables such as pH, adsorbent dose, temperature, and initial concentration are modelled to determine the optimal conditions (Wei et al., 2022).

For example, in optimizing the adsorption of ciprofloxacin, RSM has proven effective in modelling the synergistic effects of operational parameters (Wajid et al., 2022). The generated response surfaces and contour plots allow for visualization of interaction effects, while the analysis of variance (ANOVA) helps in determining the statistical significance of the model and individual variables (Jawad & Surip, 2022).

Furthermore, RSM facilitates sensitivity analysis, which helps prioritize the most critical process parameters affecting adsorption performance (Wajid et al., 2022).

Recent advancements have seen RSM integrated with desirability function approaches for multi-response optimization, allowing simultaneous consideration of multiple objectives such as adsorption capacity and regeneration efficiency (Jawad & Surip, 2022). This makes RSM particularly suitable for scaling up adsorption processes in real-world wastewater treatment applications (Nguyen et al., 2017).

2.7.2 Density Functional Theory (DFT) in Adsorption Studies

DFT is a first-principles computational method that provides atomistic insights into adsorption mechanisms by solving the quantum mechanical behavior of electrons in molecular systems (Wei et al., 2022). In the context of antibiotic adsorption, DFT is instrumental in evaluating the electronic interactions between the adsorbent surface and antibiotic molecules (Ajebli et al., 2022).

DFT can predict adsorption energies, charge transfer behavior, density of states, molecular orbitals, and electrostatic potential maps. These parameters are crucial in understanding how surface chemistry, functional groups, and material morphology influence adsorption performance (Liu et al., 2022). For instance, DFT has revealed that hydrogen bonding, π-π interactions, and electrostatic forces are the dominant mechanisms for tetracycline and ciprofloxacin binding onto functionalized carbon-based adsorbents (Kumar et al., 2022).

One significant advantage of DFT is its ability to screen and design new adsorbent materials before experimental synthesis. This reduces trial-and-error approaches and accelerates the development of high-performance materials (Bedia et al., 2018). For example, DFT analysis has been applied to simulate the adsorption of antibiotics on doped graphene, MOFs, and biomass-derived activated carbons, leading to the identification of key adsorption sites and energy profiles (Zhang et al., 2024).

DFT also complements spectroscopic studies such as FTIR and XPS by offering a theoretical interpretation of bonding interactions observed experimentally. This dual approach strengthens the reliability of conclusions drawn about adsorption mechanisms and enables fine-tuning of material design parameters (Wei et al., 2022). With advancements in computational power and the availability of software such as VASP, Gaussian, and Quantum ESPRESSO, DFT is now a cornerstone in the field of

adsorption science (Bedia et al., 2018).

2.8 Adsorption Mechanism of Antibiotics Removal

Adsorption isotherms describe how a solute interacts with an adsorbent at a constant temperature and are essential for understanding adsorption capacity and interaction characteristics (Ouyang et al., 2024). Among the commonly applied models, the Langmuir model assumes monolayer adsorption onto a homogenous surface with a finite number of identical binding sites, often interpreted as being associated with chemisorption-related characteristic. Conversely, the Freundlich isotherm accounts for heterogeneous surface energies and multilayer adsorption, indicating physical adsorption processes (Wang & Guo, 2020).

To assess the adsorption rate characteristics, kinetic models are frequently employed (Jang et al., 2018). The pseudo-first-order model assumes that the adsorption rate is directly proportional to the number of unoccupied sites, often suitable for early adsorption stages. In contrast, the pseudo-second-order model assumes that the rate-limiting steps involves interactions related to valence forces and if often been associated with chemisorption-type process in the literature (Wei et al., 2022). For antibiotics such as amoxicillin, the pseudo-second-order model has frequently been reported to provide a better fit to experimental data,suggesting the involvement of strong adsorbate-adsorbent interactions (Spaltro et al., 2021).

Additional models like the intraparticle diffusion model offer insights into the rate-limiting steps. A multilinear plot of adsorption capacity vs. the square root of time indicates whether the diffusion process occurs in stages (external surface adsorption followed by intraparticle diffusion) (Mangla et al., 2022). Often, multiple rate-limiting steps are involved, including film diffusion and pore diffusion, as observed in the adsorption of tetracycline and ciprofloxacin onto carbonaceous materials (Wang & Guo, 2020).

2.9 Influence of Process Condition on Adsorption Performance

The adsorption performance of biomass-derived activated carbon is strongly influenced by operating conditions, including solution pH, initial antibiotic concentration, and adsorbent dosage. These parameters affect the surface characteristics of the adsorbent, the speciation of antibiotic molecules, and the availability of adsorption sites, ultimately determining adsorption capacity and removal efficiency.

2.9.1 Influence of pH on Adsorption Performance

Solution pH is one of the most important parameters influencing antibiotic adsorption because it affects both the surface charge characteristics of activated carbon and the ionization behaviour of antibiotic molecules (Li et al., 2020). Consequently, pH directly governs the electrostatic interactions between adsorbents and adsorbates, thereby influencing adsorption efficiency and capacity. In addition, the adsorption behaviour is strongly dependent on the point of zero charge (pH_{PZC}) of the activated carbon and the acid dissociation constant (pKa) of the antibiotic (Li et al., 2021). Generally, activated carbon surfaces are positively charged at pH values below the pH_{PZC} and negatively charged at pH values above the pH_{PZC}. Similarly, many antibiotics may exist as cationic, zwitterionic, or anionic species depending on the solution pH (Sayin et al., 2021). The optimum pH values reported for antibiotic adsorption using biomass-derived activated carbons are summarized in Figure 2.4. Most studies reported optimum adsorption performance within a pH range of approximately 5.0 to 7.5 (Anuar et al., 2023). For example, Yang (2020) investigated tetracycline adsorption using H_3PO_4 activated corn straw-derived activated carbon and reported a pH_{PZC} value of 4.15. Tetracycline possesses three dissociation constants (pKa = 3.4, 7.6, and 9.7), causing the molecule to exist in different ionic forms depending on the solution pH. The authors observed that adsorption performance was highly dependent on electrostatic interactions between the activated carbon surface and tetracycline species, with favourable adsorption occurring within the pH range of 5.0 to 7.0 (Yang et al., 2020).

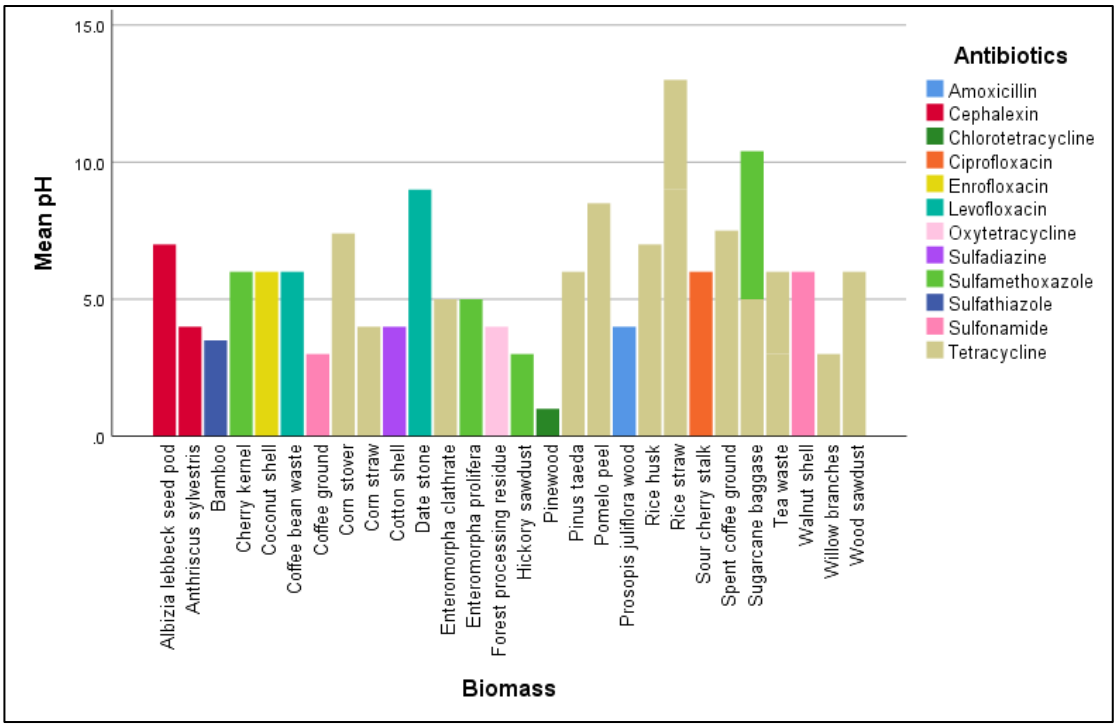

Figure 2.4 pH Distribution of Antibiotic Adsorption on Different Types of Biomass-Derived Activated Carbon.

Similarly, Sayin (2021) reported that the optimum adsorption of cephalexin onto sour cherry stalk-derived activated carbon occurred at pH 6.3. The activated carbon exhibited a pH_{PZC} value of approximately 1.2, whereas cephalexin possesses two pKa values of 6.1 and 8.7. Under these conditions, cephalexin predominantly exists as cationic and zwitterionic species, facilitating adsorption through a combination of electrostatic attraction and hydrophobic interactions. As a result, the highest adsorption performance was achieved at pH 6.3 (Sayin et al., 2021).

Prasannamedha (2021) investigated sulfamethoxazole adsorption using sugarcane bagasse-derived activated carbon with a pH_{PZC} of approximately 6.5. The study reported optimum adsorption within the pH range of 5 to 7.5 (Prasannamedha et al., 2021). At lower pH values, protonation of the activated carbon surface reduced adsorption performance due to electrostatic repulsion between positively charged surface sites and protonated sulfamethoxazole molecules (Bedia et al., 2020). As the pH approached neutral conditions, adsorption performance improved due to more favourable electrostatic interactions and enhanced accessibility of adsorption sites (Zhang et al., 2024).

Overall, the findings indicate that pH significantly influences antibiotic adsorption by controlling the surface charge of activated carbon and the speciation of antibiotic molecules (Bedia et al., 2020). Most biomass-derived activated carbons exhibit optimum adsorption performance under mildly acidic to neutral conditions, where favourable electrostatic interactions, hydrogen bonding, and surface complexation mechanisms can occur simultaneously (Mangla et al., 2022).

2.9.2 Influence of Initial Antibiotic Concentration on Adsorption Performance

The initial antibiotic concentration is an important operational parameter that influences the adsorption performance of biomass-derived activated carbon (Spaltro et al., 2021). It determines the concentration gradient between the aqueous phase and the adsorbent surface, which serves as the driving force for mass transfer during adsorption. Consequently, variations in the initial antibiotic concentration can significantly affect both adsorption capacity and removal efficiency (Cela-Dablanca et al., 2022).

The distribution of initial antibiotic concentrations reported in previous studies is presented in Figure 2.5. Most adsorption studies employed initial antibiotic concentrations ranging from 5 to 100 mg/L, although higher concentrations have also been investigated to evaluate adsorption capacity under more challenging conditions. Generally, adsorption capacity increases with increasing initial antibiotic concentration due to the greater driving force for mass transfer (Mangla et al., 2022). However, adsorption efficiency often decreases at excessively high concentrations because the available adsorption sites become saturated (Anuar et al., 2023).

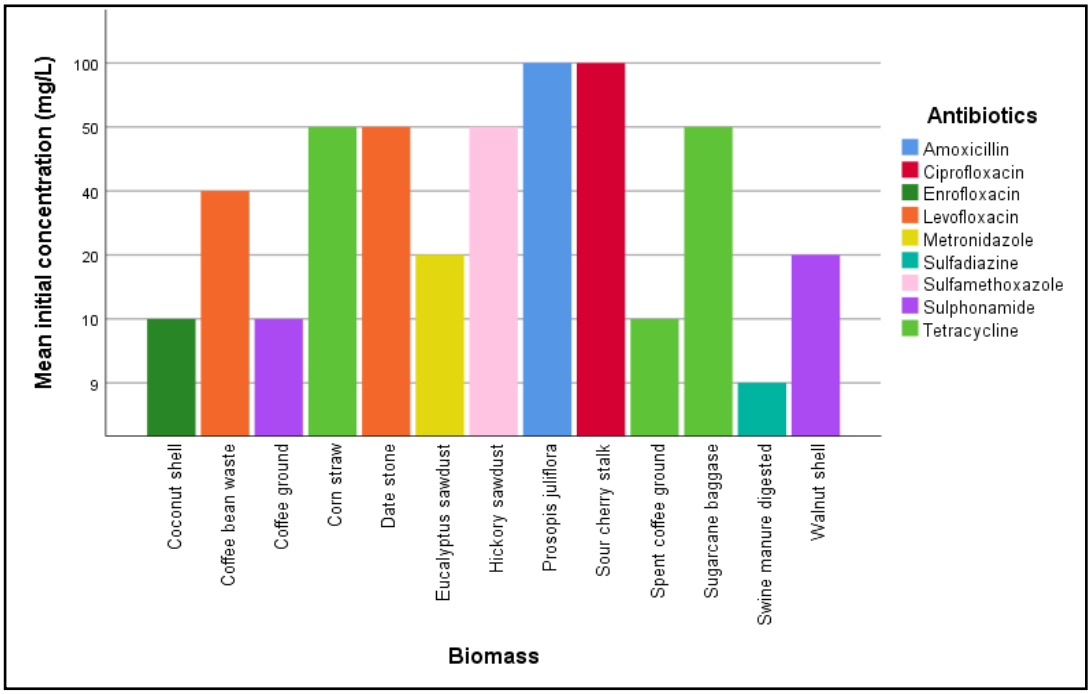

Figure 2.5 Initial Concentration Distribution of Antibiotic Adsorption on Different Types of Biomass-Derived Activated Carbon.

For example, Darweesh (2017) investigated the adsorption of levofloxacin (LEV) using date stone-derived activated carbon and reported that the highest removal efficiency of 97.01% was achieved at an initial concentration of 50 mg/L. However, when the concentration increased from 50 to 250 mg/L, the removal efficiency decreased substantially from 97.01% to 41.40% (Darweesh & Ahmed, 2017). This behaviour was attributed to the limited number of available adsorption sites relative to the increasing number of antibiotic molecules present in the solution (Anastopoulos et al., 2020).

Similarly, Dassharma (2020) studied the adsorption of enrofloxacin (ENX) using activated carbon derived from coconut shell. The authors observed that increasing the initial ENX concentration from 5 to 10 mg/L enhanced the removal efficiency to approximately 80.38%. The improvement was attributed to the increased concentration gradient between the solution and adsorbent surface, which facilitated mass transfer (DasSharma et al., 2020). However, further increases in concentration resulted in a decline in adsorption efficiency due to progressive saturation of the available active sites (Wei et al., 2022).

In general, lower initial antibiotic concentrations favour higher removal efficiencies because the number of adsorption sites exceeds the number of adsorbate

molecules (Ouyang et al., 2024). In contrast, higher concentrations increase competition among antibiotic molecules for the limited adsorption sites available on the activated carbon surface (Spaltro et al., 2021). As adsorption proceeds, the adsorbent gradually approaches saturation, reducing the percentage removal despite the increased availability of antibiotic molecules in solutions (Limousy et al., 2016).

Therefore, the initial antibiotic concentration significantly affects adsorption performance by influencing the mass transfer driving force and the degree of adsorbent site saturation. While moderate increases in concentration may enhance adsorption capacity, excessively high concentrations often result in reduced removal efficiency due to limitations in the number of available adsorption sites (Spaltro et al., 2021).

2.9.3 Influence of Adsorbent Dosage on Adsorption Performance

Adsorbent dosage is another critical operational parameter affecting the adsorption performance of biomass-derived activated carbon. The dosage determines the total number of available adsorption sites and the overall surface area accessible for antibiotic uptake (Ouyang et al., 2024). Consequently, variations in adsorbent dosage can significantly influence both adsorption efficiency and adsorption capacity during the treatment process (Mangla et al., 2022).

The distribution of adsorbent dosages reported for antibiotic adsorption using biomass-derived activated carbons is presented in Figure 2.6. Most studies employed adsorbent dosages ranging from 0.05 to 4.0 g/L, depending on the type of antibiotic, adsorbent characteristics, and experimental conditions. In general, increasing the adsorbent dosage enhances the removal efficiency because more adsorption sites and active functional groups become available for antibiotic uptake (Limousy et al., 2016).

For example, Darweesh (2017) investigated the adsorption of levofloxacin (LEV) using date stone-derived activated carbon and reported that increasing the adsorbent dosage from 0.05 to 0.15 g/L significantly improved the removal efficiency from 45.54% to 99.51% (Darweesh & Ahmed, 2017). The enhancement was attributed to the greater number of available adsorption sites and the increased surface area provided by the higher adsorbent dosage (Anastopoulos et al., 2020).

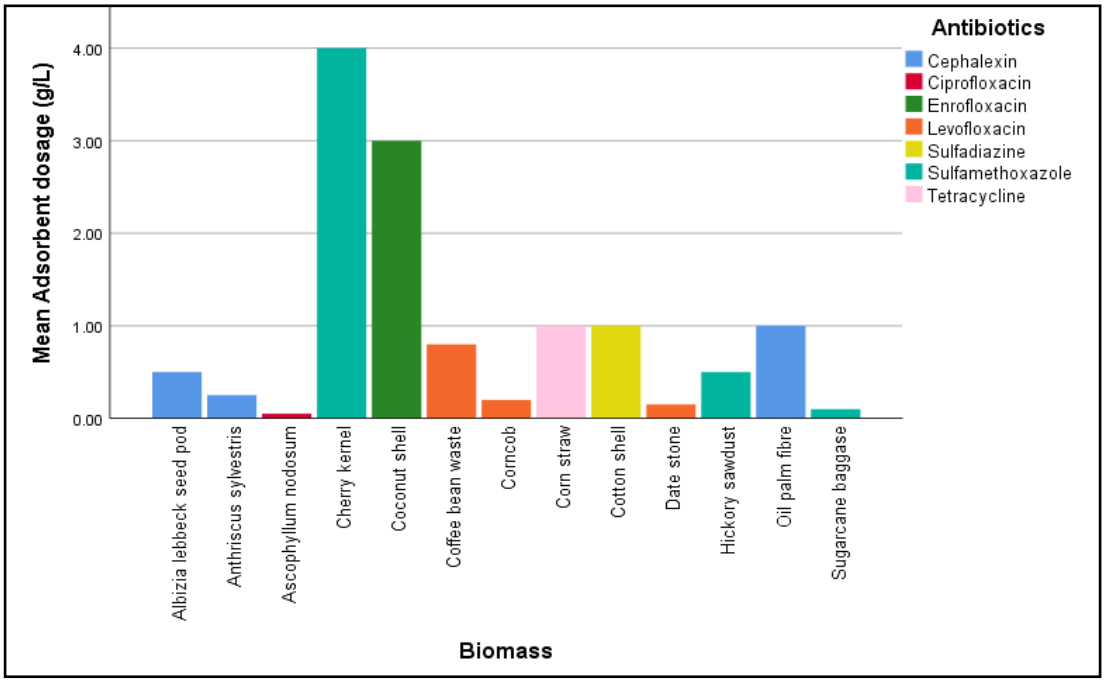

Figure 2.6 Adsorbent Dosage Distribution of Antibiotic Adsorption on Different Types of Biomass-Derived Activated Carbon.

Similarly, Shirani (2020) evaluated cephalexin adsorption using activated carbon derived from Anthriscus sylvestris and observed a positive correlation between adsorbent dosage and removal efficiency. The authors reported that increasing the dosage resulted in improved adsorption performance due to the increased availability of active sites and enhanced interaction between the antibiotic molecules and the adsorbent surface (Shirani et al., 2020).

Although increasing adsorbent dosage generally improves adsorption efficiency, excessive dosage does not always lead to proportional improvements in performance (Sharafinia et al., 2023). At sufficiently high dosages, particle aggregation may occur, reducing the effective surface area available for adsorption. In addition, the presence of surplus adsorption sites relative to the number of antibiotic molecules can lead to underutilization of the adsorbent, resulting in lower adsorption capacity expressed on a mass basis (mg/g) (Huang et al., 2017).

Overall, adsorbent dosage significantly influences adsorption performance by controlling the availability of adsorption sites and accessible surface area. Increasing dosage generally enhances antibiotic removal efficiency. However, an optimum dosage

should be identified to balance adsorption performance and adsorbent utilization efficiency (Thongpat et al., 2021).

2.10 Interaction Mechanism between Amoxicillin (AMX) and Activated Carbon

AMX, a β-lactam antibiotic, possesses a complex molecular structure characterized by multiple ionizable functional groups, including an amine ($-NH_2$), a carboxylic acid (-COOH), and a phenolic moiety (Thongpat et al., 2021). These functional groups facilitate interactions with adsorbent surfaces through various mechanisms such as electrostatic attractions, hydrogen bonding, π–π interactions, which have often been interpreted in the literature as involving chemisorption related interaction (Limousy et al., 2016).

Solution pH is a key factor that controls the ionization states of AMX and the protonation – deprotonation behavior of functional group on the adsorbent surfaces, thereby affecting the nature and strength of adsorption interactions (Antonelli et al., 2021). Under acidic conditions, AMX predominantly exists in protonated or zwiterrionic forms, which can enhance electrostatic attractions toward negatively charged or partially deprotonanted adsorbent surfaces depending on the surface chemistry. Conversely, under alkaline conditions, AMX predominantly adopts an anionic form due to deprotonation of acidic functional groups, which may lead to electrostatic repulsion when the adsorbent surface also carries negative charge (Cela-Dablanca et al., 2022). However, this repulsion can be mitigated by the presence of multivalent cations or polar functional groups on the adsorbent that facilitate complexation or other specific interactions (Sharafinia et al., 2023).

Hydrogen bonding is widely reported as an important mechanism in the adsorption of AMX onto activated carbon (Chayid & Ahmed, 2015). Surface functional groups such as hydroxyl and carboxyl on activated carbon can act as hydrogen bond donors or acceptors, enabling favorable interactions with corresponding functional groups on the AMX molecule (Jang et al., 2018). Additionally, the aromatic rings present in both AMX and carbon-based adsorbents facilitated π–π stacking or electron donor–acceptor interactions, which can further stabilize the adsorbed species and enhance adsorbed performance (Anastopoulos et al., 2020).

Recent studies employing DFT calculations have provided theoretical support for the proposed adsorption mechanism. DFT analyses reveal that the electronic

properties of AMX and modified activated carbon surface, including favorable frontier orbital alignment and charge distribution complementary, play important roles in governing adsorption behavior (Zhang et al., 2024). These theoretical insights are consistent with experimental observations indicating that surface oxidation of activated carbon enhances adsorption capacity by introducing additional polar functional groups, thereby increasing the strength and number of hydrogen bonding and electrostatic interactions (Wei et al., 2022).

2.11 Summary

This chapter offers an in-depth review of antibiotic contamination and the strategic use of biomass-derived activated carbon for its remediation from aqueous systems. It begins by outlining the history, function, and usage patterns of antibiotics, particular emphasis on Asia and Malaysia, thereby establishing the context for their widespread environmental presence. The major sources and impacts of antibiotic pollution on ecosystems and human health are highlighted, emphasizing the urgent need for effective removal technologies. Among various treatment methods, adsorption is identified as a leading approach due to its operational simplicity and high efficiency.

The chapter further examines various adsorbents, with particular focus on biomass-derived activated carbon, exploring its synthesis techniques and how these influence porosity and surface chemistry. Adsorption kinetics, isotherm modelling, and process optimization techniques, including RSM are discussed, along with DFT simulations that provide molecular-level insight into adsorption interaction. Special attention is given to the adsorption of AMX, considering its molecular structure, polarity and interaction with activated carbon surfaces. Despite significant progress in this field, several critical gaps remain unaddressed, particularly concerning the use of PKSAC for AMX removal, setting the stage for identifying key research gaps that need to be addressed as outlined below:

a) Existing studies have primarily focused on coconut shells, rice husks, and other agricultural residues as precursors for AC, while palm kernel biomass remains underexplored despite its high carbon content and abundant availability. The surface properties, porosity, and functional group compositions of PKSAC need

further investigation to determine its suitability for AMX adsorption in comparison to other biomass sources.

b) The choice of activation methods including physical and chemical activation plays a crucial role in determining the adsorption efficiency of biomass-derived AC. While some studies have explored the activation of other biomass types, systematic investigations into the effect of different activation agents on PKSAC adsorption capacity for AMX are lacking. Optimization of activation conditions such as temperature, time, and impregnation ratio could further enhance PKSAC properties.

c) Although adsorption kinetics and isotherm models have been widely applied to describe antibiotics adsorption onto activated carbon, limited studies have been integrated these models with molecular level analysis to elucidate the underlying adsorption mechanism of AMX on PKSAC.

d) DFT has been increasingly employed to provide molecular level insights into antibiotic adsorption on activated carbon. However, there is limited DFT modeling for PKSAC, leaving uncertainties regarding how functional groups (-OH, -COOH, $-NH_2$) contribute to AMX adsorption in PKSAC specifically. Further computational studies are needed to elucidate these interactions.

The findings presented in this thesis provide valuable insights into the development of biomass-derived activated carbon for antibiotic adsorption, specifically focusing on the influence of precursor selection, activation techniques, and surface modifications on adsorption efficiency. This study also examines the adsorption kinetics and isotherm models that govern the interaction between AMX and activated carbon, supported by DFT analysis to better understand molecular-level interactions.

CHAPTER 3
RESEARCH METHODOLOGY

3.1 Introduction

This section describes the materials, apparatus, and experimental workflow employed throughout the study. The research was systematically structured around four primary objectives, each addressing a specific aspect of AMX adsorption using KOH-modified PKSAC. The experimental phases were organized into six sequential steps: (1) raw material preparation and activated carbon synthesis, (2) surface characterization and functionality analysis, (3) adsorption experiments and process optimization using RSM, (4) adsorption kinetics, isotherm, and energy modelling, (5) mechanistic interpretation of adsorption related to surface and pore properties, and (6) data analysis and conclusion. The complete operational framework reflecting these interconnected phases and objectives is illustrated in Figure 3.1.

3.2 Operational Framework

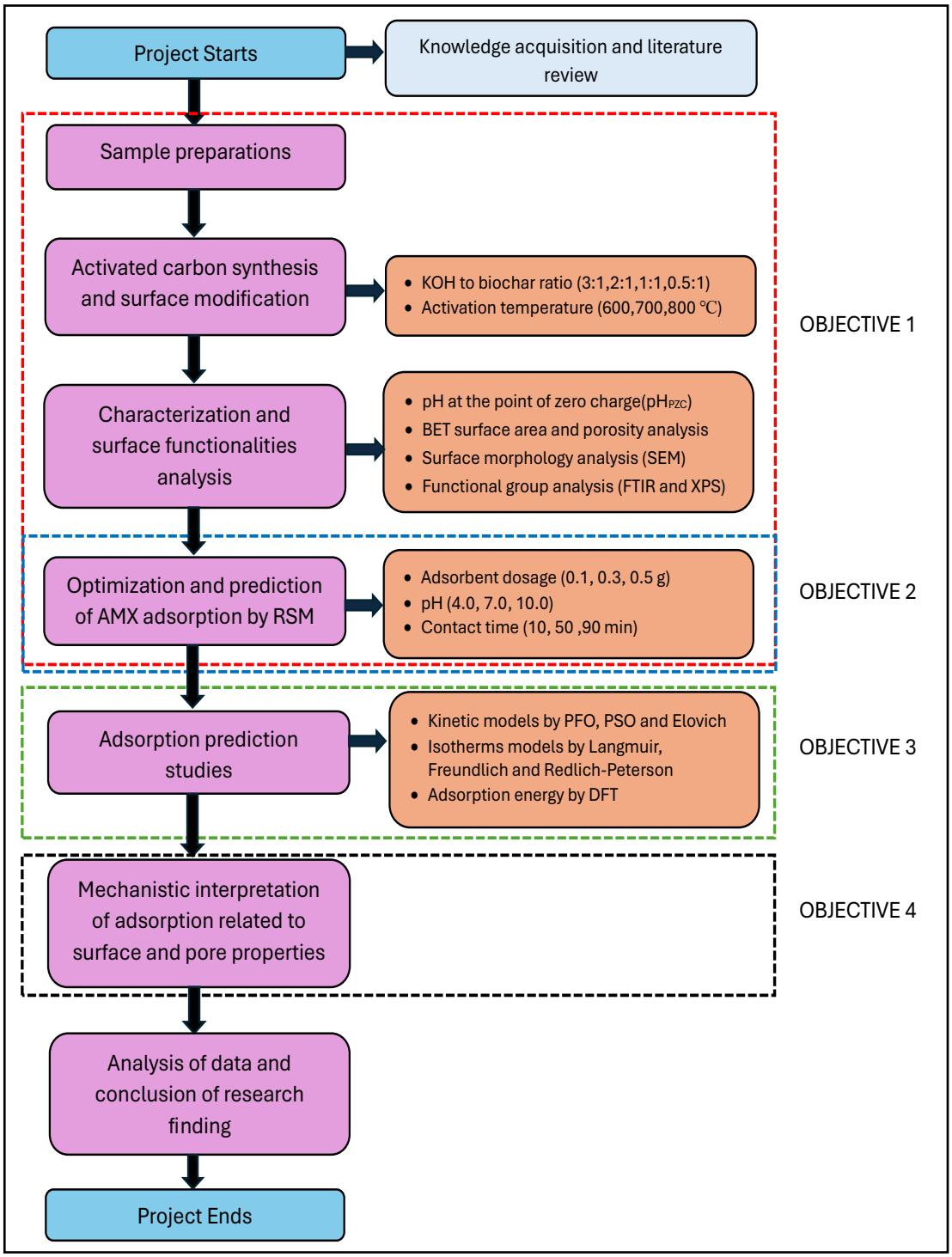

Figure 3.1 Operational Framework of this Study

3.3 Materials

Several chemicals were used in this study. Details of these chemicals are listed in Table 3.1. Amoxicillin trihydrate or Amoxicillin (AMX) was selected as the model antibiotic in this study due to its widespread use and frequent detection in aquatic environments. The chemical structure of AMX is presented in Figure 3.2 (Limousy et al., 2016).

.

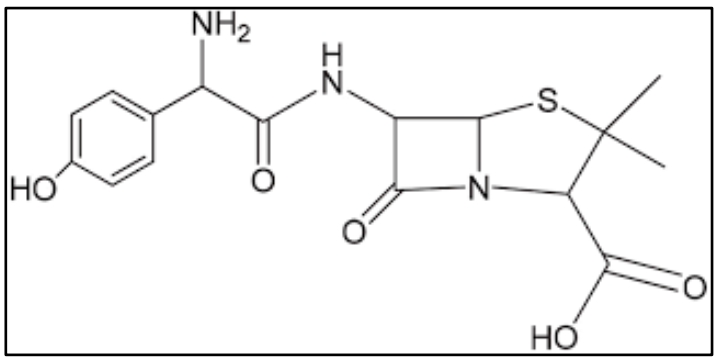

Figure 3.2 Chemical Structure of Amoxicillin Trihydrate

Table 3.1
List of all the chemicals used in this study

Chemical	Range/Amount	Supplier	Remark
Amoxicillin Trihydrate 500mg (Pharmaceutical grade)	500 – 2000mg (1 to 4 capsules)	Idaman Pharma Manufacturing	Adsorbate
Hydrochloric Acid	0.5 M	Fisher Chemical	pH control
Sodium Hydroxide	0.5 M	Sigma-Aldrich	pH control
Sodium Chloride	0.01 M	R&M Chemicals	Inert electrolyte
Potassium Hydroxide	200 g	R&M Chemicals	Chemical agent

3.4 Synthesis of Activated Carbon

Oil palm kernel shell (PKS) was used as activated carbon precursor in this study. PKS were obtained from an Oil Palm Mill in Banting, Malaysia. PKS samples were washed with distilled water to eliminate dust and contaminants. The washed samples were subsequently dried in an oven at 110℃ for 24 hours to remove residual moisture. After drying, the sample was ground and sieved to obtain particle sizes of 0.5 – 1.0 mm.

Biochar was produced through a pyrolysis process using a tube furnace (OTF-1200X Series). The pyrolysis conditions were selected based on previous studies reporting that temperatures around 600 °C are effective for converting biomass into biochar with enhanced carbon content and well-developed pore structures while maintaining adequate char yield (Rabia & Hussein, 2020). In each experiment, two ceramic boats, each containing approximately 5 g of PKS, were placed in the center of a quartz tube with an inner diameter of 96.5 mm and length of 1000 mm. The PKS was heated to 600 °C at a heating rate of 10 °C/min under N_2 flow (2 L/min) and maintained at 600 °C for 90 minutes. After cooling to room temperature, the biochar was removed, washed with hot distilled water, dried at 110 °C for 24 hours, and stored for further use. Plate 3.1 shows the washed and dried raw PKS (left) and the ground PKS biochar (right) used in the subsequent preparation process. The biochar yield was calculated as the ratio of the dry weight of biochar obtained after pyrolysis to the initial dry weight of raw PKS, as shown in Equation 3.1:



Plate 3.1 Photograph of Washed and Dried Raw PKS (Left) and Ground PKS Biochar (Right).

$$PKS\ Biochar\ Yield\ (\%) = \frac{Weight\ of\ biochar\ obtained}{Initial\ weight\ of\ raw\ PKS} \times 100 \quad (3.1)$$

PKS biochar was chemically activated using KOH at impregnation ratios of 1:0.5, 1:1, 1:2, and 1:3 (biochar:KOH, w:w). The selected impregnation ratios were adopted based on previous studies, which reported that ratios within this range are effective for promoting pore development while minimizing excessive pore widening and structural collapse of the carbon framework (Wu et al., 2021). Specifically, the required amount of KOH pellets corresponding to each impregnation ratio was first dissolved in 200 mL of distilled water. Subsequently, 50 g of biochar was added to the KOH solution, and the mixture was heated and stirred at 85 °C for 3 hours using a hot plate magnetic stirrer to ensure uniform impregnation of the activating agent throughout the biochar structure. The resulting mixture was separated by vacuum filtration using Whatman No. 1 filter paper (11 μm pore size). The recovered impregnated biochar was then dried in an oven at 110 °C for 24 hours prior to thermal activation.

Thereafter, the impregnated biochar underwent heat treatment in a tube furnace at a heating rate of 10 °C/min under N_2 flow (2 L/min). The activation temperatures of 600, 700, and 800 °C were selected based on previous studies reporting that this temperature range is effective for promoting pore development, increasing surface area, and enhancing the adsorption properties of biomass-derived activated carbons while maintaining structural stability (Gao et al., 2020). Temperatures below 600 °C may result in incomplete pore development and insufficient removal of volatile compounds, whereas excessively high temperatures may cause pore widening, pore collapse, and reduced adsorption performance (Yahya et al., 2018). The samples were maintained at the target temperature for 90 minutes. After cooling to room temperature, the activated carbon was washed with hot distilled water to remove residual impurities and subsequently dried at 110 °C for 24 hours before further characterization and adsorption experiments.



Plate 3.2 Photograph of Horizontal Split-Able Tube Furnace

3.5 Characterization Method

3.5.1 pH at the Point of Zero Charge

The pH at the point of zero charge (pH_{PZC}) for PKSAC samples was determined using a previously described method (Jang et al., 2018; Xu et al., 2020). Briefly, 50 mL of 0.01 M NaCl solution was prepared in a 250 mL conical flask, and the pH was adjusted to values ranging from 2.0 to 10.0 using 0.5 M HCl or 0.5 M NaOH solution. The initial pH of each solution was recorded immediately after pH adjustment and prior to the addition of PKSAC. Subsequently, 0.1 g of PKSAC was added to the solution, which was then purged with N_2 gas to minimize the interference of atmospheric CO_2. This step was necessary because dissolved CO_2 can form carbonic acid (H_2CO_3), resulting in pH changes that may affect the accuracy of pH_{PZC} determination (Jais et al., 2021). The suspensions were then sealed and shaken for 48 hours at room temperature to allow equilibrium to be reached. After equilibration, the final pH of the solution was measured. The pH_{PZC} was determined from the plot of ΔpH against the initial pH, where ΔpH is defined as the difference between the final pH and the initial pH. The pH_{PZC} corresponds to the point at which ΔpH = 0. All experiments were performed in duplicate to verify the consistency and reproducibility of the measurements (Chandrasekaran et al., 2020).

3.5.2 Elemental Analysis (CHNS/O)

Elemental analysis was conducted to determine the carbon (C), hydrogen (H), nitrogen (N), sulfur (S), and oxygen (O) contents of the biochar and activated carbon samples. The analysis was performed using a Vario EL III CHNS/O Elemental Analyzer (Elementar Analysensysteme GmbH, Langenselbold, Germany). Prior to analysis, the samples were dried at 110 °C for 24 hours and finely ground to ensure sample homogeneity. The obtained elemental composition was used to evaluate the changes in chemical composition resulting from carbonization and KOH activation. An image of the CHNS/O instrument is shown in Plate 3.3.



Plate 3.3 Photograph of the Vario EL III CHNS/O Elemental Analyzer

3.5.3 BET Surface Area and Pore Structure Analysis

A Quantachrome Autosorb Automated Gas Adsorption System was employed to determine the surface area, total pore volume, micropore volume, and pore size distribution. The sample underwent degassing at 300 °C for 6 hours in vacuum conditions before analysis. At 77K, the nitrogen adsorption isotherm was established across a relative pressure range (P/Po) of 0.01 to 0.99. The BET method was utilized to calculate the specific surface area. By measuring the amount of vapor adsorbed at a relative pressure of 0.99, the total pore volume was ascertained. The t-Plot micropore volume method yielded the micropore volume. The mesopore volume was derived by deducting the micropore volume from the total pore volume. The Barret-Joyner-

Halenda (BJH) method was applied to determine the pore size distribution of the AC samples. An image of the BET surface area analyzer is displayed in Plate 3.4.



Plate 3.4 Photograph of the BET Surface Area Analyzer

3.5.4 Scanning Electron Microscopy (SEM)

Scanning Electron Microscopy (SEM) enables the examination of activated carbon surface morphology and pore structure at high magnifications. In this study, a SU3500 Scanning Electron Microscope (Hitachi High-Tech Corporation, Japan) was employed to investigate the surface characteristics of the prepared activated carbon. Prior to analysis, the samples were mounted onto aluminium stubs using conductive carbon tape. SEM images were acquired at an accelerating voltage of 15 kV and a magnification of 1000×. An image of the SEM instrument is shown in Plate 3.5.

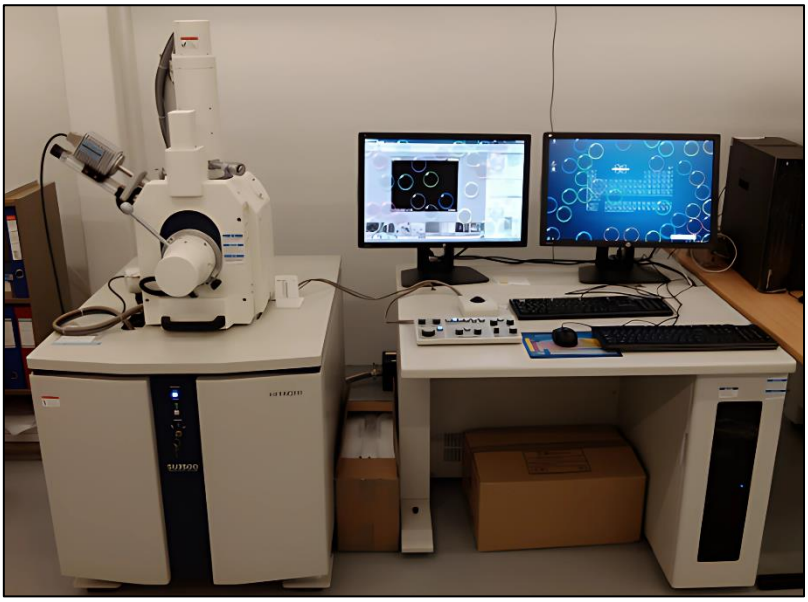

Plate 3.5 Photograph of the Scanning Electronic Microscope

3.5.5 Fourier Transform Infrared Spectroscopy (FTIR)

A Spectrum One Fourier Transform Infrared Spectrometer (PerkinElmer Inc., USA) was employed to identify the functional groups present on the samples. Prior to analysis, the activated carbon samples were finely ground and mixed with spectroscopic-grade potassium bromide (KBr) powder (Sayin et al., 2021). The mixture was then compressed into a pellet prior to FTIR analysis. The spectra were recorded over a wavenumber range of 4000–400 cm^{-1} to identify the functional groups present on the activated carbon before and after AMX adsorption. An image of the FTIR instrument is displayed in Plate 3.6.



Plate 3.6 Photograph of the Fourier Infrared Spectroscopy

3.5.6 X-ray Photoelectron Spectroscopy

X-ray Photoelectron Spectroscopy (XPS) is a surface-sensitive analytical technique used to determine the elemental composition, chemical states, and electronic states of elements present on a material surface. In this study, an XPS system (Kratos Analytical Ltd., United Kingdom) was employed to investigate the effects of KOH activation and amoxicillin adsorption on the surface chemistry of PKSAC. Prior to analysis, the powdered samples were dried and uniformly spread onto the sample holder to ensure adequate surface coverage. The analysis was conducted under high-vacuum conditions, and the spectra were collected from the outermost surface layers of the samples. The XPS measurements were performed at the Centre for Research and Instrumentation Management (CRIM), Universiti Kebangsaan Malaysia, Bangi. An image of the XPS instrument is shown in Plate 3.7.



Plate 3.7 Photograph of the X-ray Photoelectron Spectrometer

3.5.7 Ultraviolet-Visible Spectroscopy (UV-Vis)

Ultraviolet–Visible Spectroscopy (UV–Vis) is a widely used analytical technique for determining the concentration of organic compounds in aqueous solutions based on their light absorption characteristics. In this study, a Cary 60 UV–Vis spectrophotometer (Agilent Technologies, USA) was employed to determine the concentration of amoxicillin (AMX) before and after adsorption experiments. UV–Vis spectroscopy was selected because AMX contains chromophoric functional groups, including aromatic and carbonyl-containing structures, which absorb ultraviolet radiation and enable accurate concentration determination. The concentration of AMX was determined using a calibration curve developed at its maximum absorption wavelength (λmax) of approximately 272 nm. This absorption is primarily associated with $\pi \rightarrow \pi^*$ electronic transitions within the aromatic ring structure of AMX. The absorbance values obtained were subsequently used to calculate the residual concentration of AMX after adsorption. An image of the UV–Vis instrument is shown in Plate 3.8.

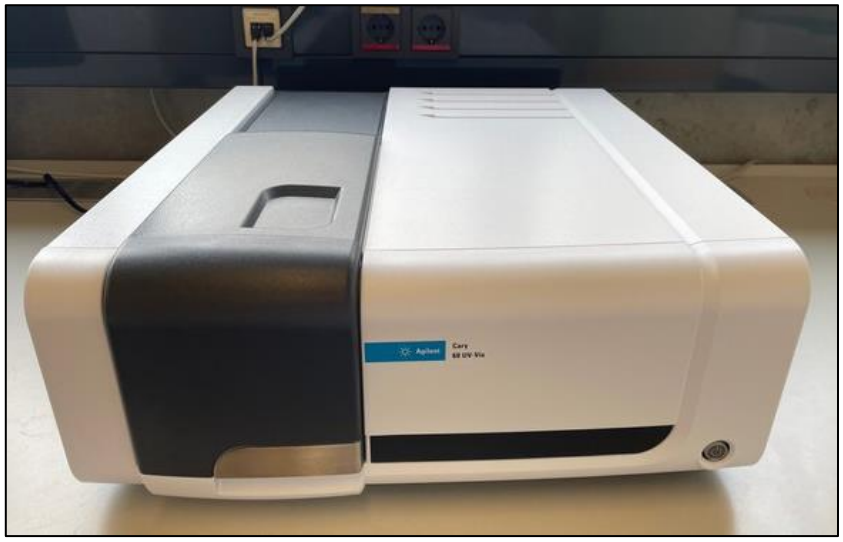

Plate 3.8 Photograph of the UV-Vis Spectrometer

3.6 Preparation and Optimization of Amoxicillin (AMX) Adsorption Condition using Box-Behnken Design (BBD)

3.6.1 Preparation of AMX Solutions

A stock solution of AMX at 500 ppm was prepared by dissolving 0.5 g of AMX in 1000 mL of distilled water. The AMX used in this study was sourced from capsules, each containing 500 mg of AMX. A fresh stock solution was prepared for each experimental batch and used immediately after preparation to minimize potential degradation of AMX in aqueous solution and ensure concentration stability throughout the adsorption experiments (Chayid & Ahmed, 2015). Serial dilutions of the stock solution were performed to construct a calibration curve, analyzed using a UV-visible spectrophotometer (Cary 60, Agilent Technologies) at a wavelength of 272 nm (Chayid & Ahmed, 2015). This stock solution was then diluted to the desired concentrations, with the pH adjusted by 0.5 M of HCl and NaOH as needed for the adsorption experiments.

3.6.2 Single Factor Experiments to Prepare PKSAC for AMX Adsorption

Single-factor experiments were conducted to establish suitable preparation and adsorption conditions prior to the optimization study. The impregnation ratios (1:0.5, 1:1, 1:2, and 1:3) were selected to achieve effective pore development and surface area enhancement while minimizing excessive pore widening and structural collapse of the carbon framework (Chayid & Ahmed, 2015; Huang et al., 2017). Activation temperatures of 600, 700, and 800 °C were chosen due to their effectiveness in improving the textural properties and adsorption performance of biomass-derived activated carbons (Huang et al., 2017). An initial AMX concentration of 20 mg/L was employed to ensure reliable adsorption evaluation and facilitate comparison with reported adsorption studies (Jafari et al., 2023). The adsorbent dosage was fixed at 0.3 g following screening experiments that demonstrated efficient antibiotic removal while maintaining effective adsorbent utilization. The adsorption experiments were conducted at pH 4.0, as the screening results indicated enhanced adsorption performance under acidic conditions.

The effect of activation process parameters, specifically impregnation ratio and activation temperature, on AMX adsorption by PKSAC was evaluated using OVAT experimental approaches. For each experiment, 200 mL of 20 ppm AMX solution was placed in a 250 mL conical flask, followed by addition of 0.3 g of PKSAC prepared using different impregnation ratios (1:0.5, 1:1, 1:2, and 1:3) at a constant activation temperature (600℃). The sample was subjected to rotary shaking at 120 rpm for 90 minutes under room temperature conditions (25 ± 2℃). The pH of the solution was adjusted using 0.1 M NaOH and 0.1 M of HCL to achieve the desired pH for each experiment. To assess the effect of the activation temperature, the same procedure was repeated using PKSAC prepared with a 1:3 impregnation ratio, but with activation temperatures of 600, 700 and 800 ℃.

Following adsorption, the AMX-loaded PKSAC was removed from the solution using a vacuum filtration apparatus equipped with 3 μm filter paper. The remaining AMX concentration was quantified using a UV-visible spectrophotometric analysis at 272 nm (Chayid & Ahmed, 2015). The adsorption performance was evaluated using Equations 3.2 and 3.3 (Xu et al., 2020):

$$R = \frac{C_o - C_e}{C_o} \times 100\% \quad (3.2)$$

where R refers to the AMX removal efficiency, whereas C_0 and C_e represent initial and equilibrium concentrations of AMX (ppm), respectively.

The adsorption capacity q_e (mg/g) was defined based on following equation:

$$q_e = \frac{(C_o - C_e)V}{m} \quad (3.3)$$

Co and Ce represent the initial and equilibrium concentrations of AMX (ppm), respectively. V indicates the volume of the AMX solution (L), whereas m correspond to the dosage of the PKSAC (g).

3.6.3 Optimization and Prediction of AMX Adsorption

AMX removal experiments were conducted using PKSAC prepared with an impregnation ratio of 1:3 and activated at 700°C. In each experiment, 200 mL of AMX solution at a concentration of 20 ppm was measured and placed into a 250 mL conical flask (Jafari et al., 2023). The experimental design and optimization of adsorption conditions were carried out using Design Expert® software (version 13.0; Stat-Ease, Minneapolis, USA). A Box-Behnken Design (BBD) within Response Surface Methodology (RSM) was implemented to determine the effect of critical operational factors on AMX removal performance. Three independent operational variables were selected including adsorbent dosage (A; 0.1–0.5 g), solution pH (B; 4.0–10.0), and adsorption contact time (C; 10–90 minutes). The experimental matrix included both actual and coded variable levels, which each factor evaluated at three designated levels (-1, 0, and +1), as illustrated in Table 3.2. Based on the BBD design, 17 experiments were executed, consisting of 12 unique treatment combinations and five centre-point replicates, to assess experimental error. The functional relationship between the selected independent variables and the response variable (AMX removal efficiency) was represented by a quadratic polynomial equation, as indicated in Equation 3.4 (Jawad & Surip, 2022):

$$Y = \beta o + \sum_{i=1}^{k} \beta i Xi + \sum_{i=1}^{k} \beta i Xi^2 + \sum_{1 \le i \le j}^{k} \beta ij XiXj \quad (3.4)$$

Here, $\beta o, \beta i,$ and βij refer to the regression coefficients associated with the intercept, linear terms, and quadratic interaction terms, respectively. The coded independent variables are represented by Xi and Xj ($i\ and\ j = 1\ to\ 3$), while Y denotes the response variable corresponding to AMX removal efficiency. The symbol k indicates the total number of variables examined. The statistical significance of interaction effects among the independent parameters was evaluated using an analysis of variance (ANOVA).

Table 3.2

Actual and Coded Factor Levels Used for AMX Removal.

Factors name	**Factors code**	**Level of factors**		
		-1	0	+1
Adsorbent dosage (g)	A	0.1	0.3	0.5
pH	B	4	7	10
Time (min)	C	10	50	90

3.7 AMX Adsorption Kinetic

The adsorption kinetic study was conducted separately from the optimization study because its primary objective was to investigate the adsorption rate and interaction mechanism of AMX adsorption onto PKSAC rather than to determine optimum removal conditions. Higher initial AMX concentrations (100–400 mg/L) were employed to provide sufficient concentration gradients and adsorption capacities for kinetic modelling (Jafari et al., 2023). The PKSAC dosage was fixed at 0.5 g, while the solution pH was maintained at pH 4, corresponding to the optimum pH identified during the optimization study. All experiments were conducted at room temperature (25 ± 2 °C).

Adsorption kinetics were conducted by adding 0.5 g of PKSAC into 300 mL of AMX solution at concentrations ranging from 100 to 400 ppm. The suspensions were stirred at 120 rpm, and samples were collected at predetermined intervals over an adsorption period of 7 hours. Preliminary observations showed that the adsorption system approached equilibrium within this period, and therefore the collected data were

used for subsequent kinetic modelling. The adsorption rate and interaction mechanism were evaluated using pseudo-first order (PFO), pseudo-second order (PSO), and Elovich kinetic models, with their nonlinear forms presented in Equations 3.5, 3.6, and 3.7, respectively (Cheng et al., 2020):

$$q_t = q_e\,(1 - exp^{-k_1 t}) \tag{3.5}$$

$$q_t = \frac{{q_e}^2\, k_2\, t}{1 + q_e\, k_2\, t} \tag{3.6}$$

$$\frac{dq_t}{dt} = a \exp(-b q_t) \tag{3.7}$$

In the above equations q_t and q_e correspond to the adsorption capacity of PKSAC at time t and equilibrium (mg/g), respectively. The constants k_1 and k_2 correspond to the PFO and PSO rate constants. Meanwhile, a indicates the chemisorption rate constant, and b represent the surface coverage parameter.

The PFO kinetic model assumes that adsorption rate is controlled by the difference between equilibrium solute concentration and the adsorbed amount, which is typically associated with physisorption driven by weak van der Waals forces. Meanwhile. The PSO model assumes that adsorption rate is proportional to the square of the number of vacant adsorption sites, often indicating chemisorption involving stronger chemical interactions such as valence bonding or electron sharing (Wei et al., 2022). The Elovich model is commonly used to describe adsorption occurring on heterogeneous surfaces or complex systems, where adsorption rate declines due to progressive reduction of available active sites or surface deactivation (Largitte & Pasquier, 2016). Comparison between experimental data and these kinetic model enables determination of dominant adsorption mechanism and evaluation of PKSAC efficiency for AMX removal.

3.8 AMX Adsorption Isotherm

The adsorption isotherm study was conducted to evaluate the equilibrium adsorption behaviour of AMX on PKSAC. An AMX concentration range of 20–400 mg/L was employed to generate sufficient equilibrium data for isotherm modelling across a wide concentration range (Jafari et al., 2023). The solution pH was maintained at 4.0, corresponding to the optimum adsorption condition identified in this study. The

adsorbent dosage was fixed at the optimized value, while temperature was varied to assess its effect on adsorption equilibrium.

Adsorption isotherms were evaluated by mixing 0.5 g of PKSAC with 100 mL of AMX solution maintained at pH 4.0, with initial concentrations ranging from 20 to 400 ppm. The experiments were performed at 25, 35, 45, and 55 °C, and the suspensions were continuously agitated at 120 rpm for 48 hours to ensure equilibrium was reached. Subsequently, the residual AMX concentration was determined, and the adsorption capacity of PKSAC was calculated using Equation 3.2. The equilibrium data were fitted to Langmuir, Freundlich, and Redlich-Peterson isotherm models to evaluate the adsorption behaviour of AMX on PKSAC.

The Langmuir isotherm model explain adsorption as a formation of a single molecular layer on an adsorbent surface consisting of a limited number of adsorption sites with same energy (Largitte & Pasquier, 2016). It assumes that adsorption reaches its maximum capacity when the adsorbent surface is fully covered by a monolayer, with no migration of adsorbed molecules along the surface. The nonlinear Langmuir equation is expressed in Equation 3.8 (J. Wang & Guo, 2020).

$$q_e = \frac{q_m \times K_L \times C_e}{1 + K_L \times C_e} \tag{3.8}$$

In Equation 3.7, q_m represents the maximum monolayer adsorption capacity (mg/g) whilst q_e denotes the adsorption capacity at equilibrium (mg/g). the equilibrium concentration of adsorbate is expressed as C_e (mol/L), while K_L stands for the Langmuir constant associated with the adsorption free energy (L/mol). The adsorption feasibility was evaluated using Langmuir separation factor (R_L), where adsorption is favourable when $0 < R_L < 1$, unfavorable when $R_L > 1$, irreversible when $R_L = 0$ or linear when $R_L = 1$. The value of R_L was calculated using Equation 3.9 (Xu et al., 2020).

$$R_L = \frac{1}{1 + K_L C_0} \tag{3.9}$$

The Freundlich model illustrates multilayer adsorption on heterogeneous surfaces with varying binding energies amongst adsorbent surface sites, accounting for interactions between adsorbed molecules. The non-linear form of the Freundlich model is expressed in an Equation 3.10 (J. Wang & Guo, 2020).

$$q_e = K_F \times C_e^{1/n} \quad (3.10)$$

In Equation 3.9, K_F corresponds to the Freundlich constant (mol/L) -1/n, and n represents a dimensionless parameter describing adsorption intensity.

Meanwhile, the Redlich-Peterson model integrates Langmuir and Freundlich isotherm characteristics, resulting in a hybrid adsorption mechanism that allows for both multilayer and monolayer adsorption. Equation 3.11 can be used to explain adsorption equilibrium over a wide range of adsorbate concentrations (Wang & Guo, 2020).

$$q_e = \frac{K_{RP} C_e}{1 + a_{RP} C_e^{g}} \quad (3.11)$$

Here, K_{RP}(L.g^{-1}) and a_{RP}(Lg.mg^{-g}) correspond to the Redlich-Peterson constant, while g is an exponent parameter with values between 0 and 1. The model simplifies to the Langmuir isotherm when g equals to 1 and tends towards a linear adsorption behavior when g approaches or reaches 0. Furthermore, when C_e approaches to infinity, the relationship can be expressed as $q_e \approx \left(\frac{K_{RP}}{a_{RP}}\right) C_e^{(1-g)}$ (Wang & Guo, 2020).

3.9 Adsorption Energy by Density Functional Theory (DFT) in the PKSAC-AMX System

To explore the mechanism, Gaussian 09 software was used to perform DFT and quantum chemistry calculations to simulate and analyze the adsorption process. DFT calculation using the B3LYP functional and 6-311G basis set were applied to optimize the molecular geometry. The density of states for the AMX molecules adsorbed on PKSAC was calculated (Zhang et al., 2024). Linear regression was used to analyze the relationship between the energy gap (eV) and adsorption energy (kJ/mol) for the three molecular fragments (PKSAC-OH: AMX-COOH, PKSAC-OH: AMX-OH, and PKSAC-OH: AMX-NH_2). The data obtained from the computational simulations were organized into a Pandas® DataFrame and analyzed using the statsmodels library in Python 3.9.19 .

The energy of highest occupied molecular orbital (HOMO (E_H)) represent the electron-donating capability of the molecule, while the energy of the lowest unoccupied molecular orbital (LUMO (E_L)) describes its electron acceptability of the molecule. The

energy gap (Eg) can be determined using Equation 3.12 (Antonelli et al., 2021).

$$E_{g=} E_H - E_L \tag{3.12}$$

It is noteworthy that the E_g value provides important information into the characteristics of the adsorption process. This process can be possible to be influenced by irreversible interaction when E_g less than 7.34 eV or by reversible interaction when E_g exceeds 7.34 (Spessato et al., 2019). On the other hand, the adsorption of energy is the energy change when a molecule adsorbs onto a surface. This reflects the strength of the interaction between the adsorbate (molecule) and the surface of the adsorbent. The adsorption energy can be expressed as follows (Wei et al., 2022).

$$E_{Adsorption} = E_{Total} - (E_{PKSAC} + E_{AMX}) \tag{3.13}$$

The energy related to physical adsorption is approximately 40 kJ/mol, while chemical adsorption usually entails more significant energy levels, ranging from 84 to 417 kJ/mol, as per the findings of other researchers (Wei et al., 2022). Using Python-based tools, non-parametric techniques, Bayesian inference, and linear regression analysis, this study sought to explore the relationship between these variables and extract valuable insights into the adsorption properties of molecular fragments. A linear regression model was used to predict adsorption energy based on the energy gap. The regression equation obtained was as follows:

$$Adsorption\ Energy\ \left(\frac{kJ}{mol}\right) = (\beta_0 + \beta_1) \times Energy\ Gap\ (eV) \tag{3.14}$$

where, β_0 is the intercept and β_1 is the slope, respectively.

CHAPTER 4
RESULTS AND DISCUSSION

4.1 Introduction

This chapter presents the findings of the experimental work and is structured into four parts; each aligned with the study's objectives. The first part provides a comparative analysis of how different activation process parameters, specifically the KOH impregnation ratio and activation temperature, influence AMX adsorption by carbon material derived from PKS. This section includes an evaluation of BET surface area and AMX removal efficiency (%). The optimal activation parameters identified in this phase were subsequently applied to produce PKSAC for use in the next research objective.

The second part focuses on optimizing adsorption conditions for AMX removal. Variables including adsorbent dosage, solution pH, and contact time were systematically investigated. The optimal conditions that resulted in the highest AMX removal efficiency were identified using RSM. In addition, this section includes a predictive analysis of AMX adsorption performance and evaluates the characterization and adsorption efficiency of the optimized PKSAC material.

The third section presents a detailed analysis of AMX adsorption behavior using kinetic models and isotherm fitting evaluations. DFT simulations were employed to calculate adsorption energies and elucidate the electronic interactions at the molecular level. These combined approaches provide a comprehensive understanding of the adsorption dynamics and mechanisms governing AMX interaction with PKSAC.

The final part delves into the adsorption mechanism, highlighting how surface functional groups and pore structure influence AMX uptake. Combined experimental and theoretical findings elucidate the synergistic effects of chemical functionalities and surface porosity on enhancing adsorption efficiency, providing comprehensive mechanistic insights.

4.2 Structural and Chemical Modification of PKSAC

4.2.1 Single Factor Experiments to Prepare PKSAC for AMX Adsorption.

The effect of activation process parameters, specifically impregnation ratio and activation temperature, on the adsorption performance of PKSAC was evaluated using the one-variable-at-a-time (OVAT) approach (Figure 4.1). At a fixed activation temperature of 600 °C, increasing the impregnation ratio from 1:0.5 to 1:3 increased AMX removal from 52.26% to 68.53%, while the lowest AMX removal efficiency was observed for the biochar (29.49%). Simultaneously, the BET surface area increased from approximately 100 m^2/g for the biochar to approximately 550 m^2/g at an impregnation ratio of 1:3. This result demonstrates the importance of KOH activation in enhancing pore development and increasing the availability of adsorption sites (Wu et al., 2021).

The increase in adsorption performance can be attributed to the reaction between KOH and the carbon matrix during activation. KOH activation promotes dehydration, oxidation-reduction reactions, and the intercalation of potassium-containing species into the carbon structure, resulting in the formation of new pores and the enlargement of existing pores (Yang et al., 2019). Consequently, the accessible surface area and pore volume increase, facilitating the diffusion of AMX molecules into the porous structure of PKSAC. Huang et al. (Huang et al., 2017b) reported that an increase in surface area generally enhances the adsorption of organic contaminants. Similarly, Cheng (2020) observed that improved pore development enhanced tetracycline adsorption by facilitating the diffusion of antibiotic molecules into the pore network of biochar (Cheng et al., 2020). Therefore, a similar pore-enhancement mechanism may have contributed to the improved AMX adsorption observed in the present study.

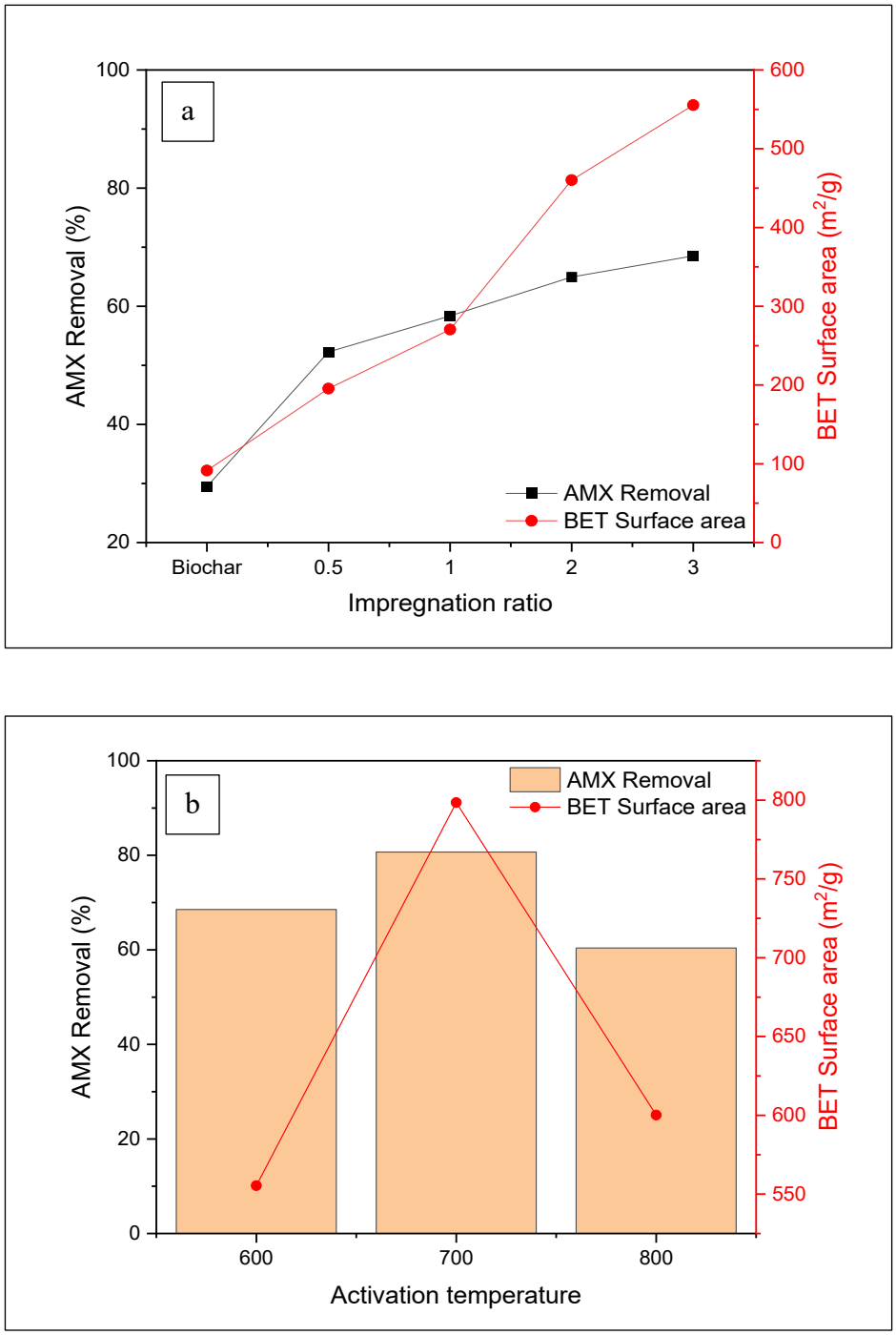

Figure 4.1 AMX Removal by (a) Different Impregnation Ratio, (b) Different Activation Temperature.

As shown in Figure 4.1a, the increase in BET surface area was considerably greater than the increase in AMX removal efficiency. For example, the BET surface area increased by more than five-fold from biochar to PKSAC prepared at a 1:3 impregnation ratio, whereas AMX removal increased from 29.49% to 68.53%. This observation suggests that adsorption performance is governed not only by surface area

but also by pore accessibility, pore size distribution, and surface chemistry. The availability of oxygen-containing functional groups and the accessibility of adsorption sites are equally important for effective AMX adsorption (Limousy et al., 2016). Therefore, increases in surface area do not necessarily result in proportional increases in adsorption performance (Chayid & Ahmed, 2015).

Although the trend indicates that higher impregnation ratios may further increase surface area, excessive KOH loading may lead to over-activation of the carbon matrix (Huang et al., 2017). Under such conditions, excessive pore widening, pore wall thinning, and structural deterioration may occur, reducing the stability of the pore network (Limousy et al., 2016). Furthermore, severe activation may reduce the abundance of oxygen-containing functional groups such as hydroxyl (-OH) and carboxyl (-COOH) groups, which contribute to AMX adsorption through hydrogen bonding and electrostatic interactions (Acosta et al., 2016). Consequently, while the surface area may continue to increase beyond an impregnation ratio of 1:3, the AMX removal efficiency may eventually plateau or decrease due to the loss of effective adsorption sites and favourable surface functionalities. Based on these findings, an impregnation ratio of 1:3 was selected for subsequent investigations.

The effect of activation temperature was subsequently evaluated using the selected impregnation ratio of 1:3. As shown in Figure 4.1b, increasing the activation temperature from 600 to 700 °C improved AMX removal from 68.53% to 80.69%. A similar trend was observed for the BET surface area. The improvement can be attributed to the enhanced reaction between KOH and the carbon matrix at elevated temperatures, which promoted the removal of residual volatile components and non-carbon elements from the biochar structure, thereby facilitating pore development and increasing the accessible surface area (Thongpat et al., 2021). The higher activation temperature also increased the effectiveness of KOH in creating new pores and enlarging existing pores, resulting in a more developed porous structure suitable for AMX adsorption (Thongpat et al., 2021).

However, further increasing the activation temperature from 700 to 800 °C reduced AMX removal from 80.69% to 60.38%. This decline may be attributed to excessive gasification of the carbon matrix during activation, resulting in over-development of the pore structure (Wu et al., 2021). Excessive activation can enlarge micropores into larger pores and partially damage pore walls, reducing the number of

effective adsorption sites available for AMX adsorption (Limousy et al., 2016). In addition, elevated activation temperatures may reduce the abundance of oxygen-containing functional groups such as hydroxyl (-OH) and carboxyl (-COOH) groups through thermal decomposition. These functional groups play an important role in AMX adsorption through hydrogen bonding and electrostatic interactions (Acosta et al., 2016). Therefore, their reduction may negatively affect adsorption performance despite the development of porosity (Thongpat et al., 2021). Based on the combined evaluation of BET surface area and AMX removal efficiency, an activation temperature of 700 °C and an impregnation ratio of 1:3 were selected as the optimum preparation conditions for PKSAC.

4.2.2 Characteristic Examination of PKSAC

4.2.2.1 Yield and Textural Properties

Table 4.1 compares the characteristics of the biochar and PKSAC, focusing on yield, elemental composition determined by CHNS/O elemental analysis, and pore properties. Unless otherwise stated, all characterization results presented in this section correspond to the optimized PKSAC prepared at an impregnation ratio of 1:3 and activation temperature of 700 °C. The yield of biochar, expressed as a percentage of the initial weight of PKS, was 30.18%. Following activation, the yield decreased to 26.54%, while the carbon content decreased from 79.55 to 76.80 wt%. This reduction in yield is attributed to the reaction between KOH and the carbon matrix during activation, which promotes the removal of carbon atoms from the carbon structure and facilitates pore development (Wu et al., 2021). Although the activation process was conducted under an N_2 atmosphere, gaseous products such as CO and CO_2 can still be generated through reactions between KOH and carbon during thermal activation (Jang et al., 2018). The removal of carbon atoms contributes to the formation of new pores and increases the accessible surface area of the activated carbon (Limousy et al., 2016).

Consequently, the BET surface area increased substantially from 91.38 to 798.35 m^2/g, while the total pore volume increased from 0.05 to 0.25 cm^3/g. However, the average pore diameter decreased from 2.83 to 1.80 nm, indicating extensive micropore development and restructuring within the carbon matrix (Nguyen et al., 2021). The significant increase in surface area and pore volume confirms the

effectiveness of KOH activation in enhancing the textural properties of PKSAC. The elemental composition was determined using CHNS/O elemental analysis. The oxygen content increased slightly after KOH activation, indicating the incorporation of oxygen-containing surface functionalities onto the activated carbon surface (Jang et al., 2018). It should be noted that the oxygen content reported in Table 4.1 refers to elemental oxygen chemically bound within the carbon structure and should not be confused with molecular oxygen (O_2) involved in combustion processes. The increase in oxygen content suggests the formation of oxygen-containing functional groups such as hydroxyl (-OH), carbonyl (C=O), and carboxyl (-COOH) groups during activation (Nguyen et al., 2021). These functional groups are beneficial for AMX adsorption as they can participate in hydrogen bonding and electrostatic interactions with AMX molecules (Cheng et al., 2020). Similar observations were reported by Acosta (2016) during the preparation of KOH-activated tire-derived activated carbon (Acosta et al., 2016).

In this study, the discussion emphasizes carbon and oxygen contents, as these elements are directly associated with the pore development and surface functionalization in KOH-activated carbons, which govern adsorption performance. Surface functional group relevant to AMX adsorption were further examined using FTIR and XPS analyses.

Table 4.1
Characteristics of Biochar and PKSAC.

Sample	**C (wt%)**	**O (wt%)**	**Yield (%)**	**BET Surface area (m^2/g)**	**Total pore volume (cm^3/g)**	**Average pore diameter (nm)**
Biochar	79.55	16.34	30.18	91.38 ± 1.12	0.05 ± 0.01	2.83
PKSAC	76.80	20.20	26.54	798.35 ± 5.27	0.25 ± 0.02	1.8

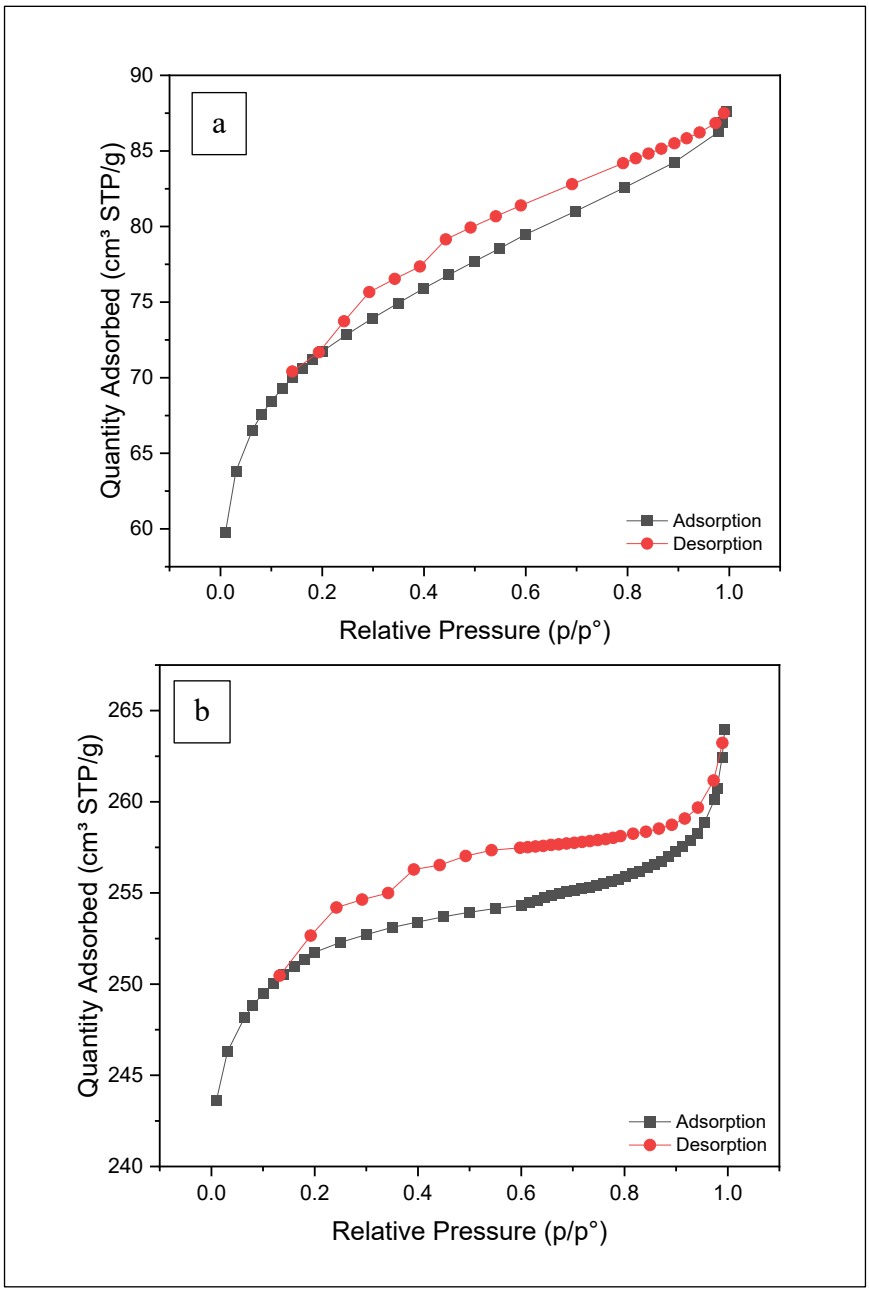

Figure 4.2 N_2 Adsorption/Desorption Isotherms at 77K for (a) Biochar, (b) PKSAC.

International Union of Pure and Applied Chemistry (IUPAC) classifies activated carbon with pore diameters smaller than 2 nm as microporous material (Sing et al., 1985). PKSAC exhibits an average pore diameter of 1.8 nm, suggesting strong compatibility with AMX molecules, with sizes between 1.29 and 1.52 nm (Pezoti et al., 2016). The N_2 adsorption-desorption isotherm provides qualitative information on the adsorption process and the surface area of the materials (Yakout & El-deen, 2016). The isotherm profile also offers insight into the type of pore structure and helps to evaluate the type of pores (Handing Chen et al., 2017). Figure 4.2 displays a Type IV isotherm, which, according to the literature, suggests an H4-type hysteresis loop linked to slit-like

pores in both microporous and mesoporous structures (Calvo-muñoz et al., 2016). Pore development in activated carbon can be attributed to two main pathways: (i) chemical activation, where reactions between the carbon framework and potassium compounds lead to pore formation, and (ii) physical activation, where high temperature causes damage to the carbon structure, resulting in pore creation. In addition, pyrolysis at elevated temperatures (above 700 ℃) can eliminate the potassium compounds present in the carbon structure, leading to the formation of metallic substances that permeate the carbon matrix, facilitating the creation of micropores (Spessato et al., 2019).

Figure 4.3 shows SEM images of the biochar and PKSAC, illustrating the structural changes that occurred following KOH activation. The biochar surface (Figure 4.3a) exhibits a relatively rough and irregular morphology with limited visible porosity. Several pore openings are present; however, many of the pores appear partially blocked or poorly developed, indicating restricted accessibility to the internal pore structure. In contrast, the PKSAC surface (Figure 4.3b) displays a substantially more developed porous structure characterized by numerous interconnected pores distributed throughout the carbon matrix. The pore walls appear thinner and more uniformly developed than those observed in the biochar, indicating that KOH activation effectively removed portions of the carbon matrix and generated additional porosity. This enhanced pore development is consistent with the BET results, where the surface area increased from 91.38 to 798.35 m^2/g following activation. The improved pore structure facilitates the diffusion of AMX molecules into the internal adsorption sites and contributes to the enhanced adsorption performance of PKSAC.

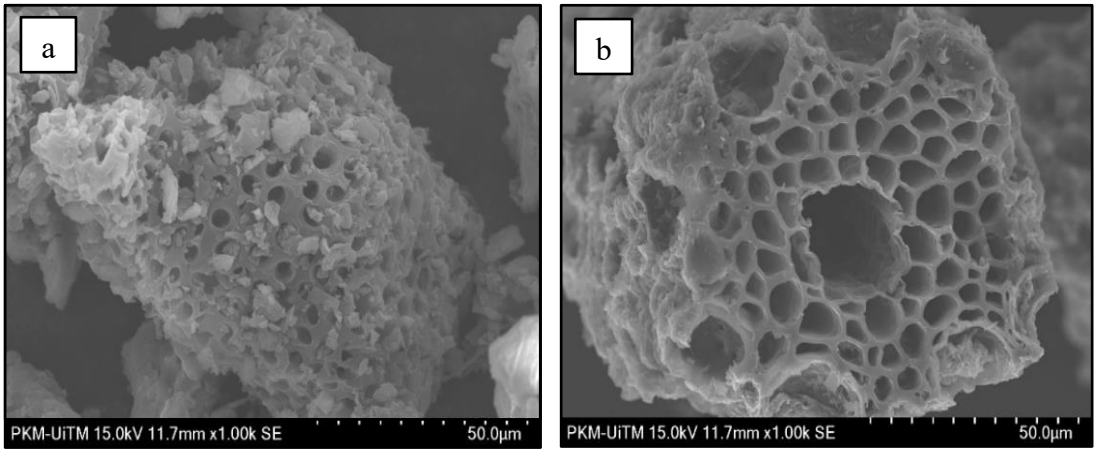

Figure 4.3 SEM Images of the (a) Biochar and (b) PKSAC

$$6KOH + 2C \rightarrow 2K + 3H_2\uparrow + 2K_2CO_3 \quad (4.1)$$

$$K_2CO_3 \rightarrow K_2O + CO_2\uparrow \quad (4.2)$$

$$CO_2 + C \rightarrow 2CO\uparrow \quad (4.3)$$

$$K_2CO_3 + 2C \rightarrow 2K + 3CO\uparrow \quad (4.4)$$

$$K_2O + C \rightarrow 2K + CO\uparrow \quad (4.5)$$

$$K_2CO_3 + H_2 \rightarrow 2K + H_2O + CO_2\uparrow \quad (4.6)$$

The chemical reactions involved in the KOH activation process are represented in Equations 4.1–4.6 (Cheng et al., 2020). During activation, KOH reacts with the carbon matrix to produce intermediate compounds such as K_2CO_3 and K_2O, together with gaseous products including H_2, CO, and CO_2. Although the activation process was conducted under an N_2 atmosphere, CO_2 can still be generated through the decomposition of carbonate intermediates and oxygen-containing species inherently present within the carbon structure (Nguyen et al., 2021). The evolution of these gaseous products removes carbon atoms from the carbon framework through gasification reactions, creating new pores and enlarging existing pores. Simultaneously, metallic potassium generated during activation can penetrate between the carbon layers, causing lattice expansion and structural distortion (Nguyen et al., 2021). Following cooling and washing, the metallic potassium is removed, leaving behind additional pore channels and voids. Consequently, both micropore and mesopore development are enhanced, resulting in the substantial increase in surface area and pore volume observed after KOH activation (Chen et al., 2018).

4.2.2.2 Surface Chemistry

Figure 4.4 presents the Fourier Transform Infrared (FTIR) spectra of biochar, PKSAC, and PKSAC after AMX adsorption, illustrating the changes in surface functional groups following KOH activation and adsorption. Palm kernel shell is primarily composed of cellulose, hemicellulose, and lignin, which contribute various oxygen-containing functional groups including hydroxyl, carbonyl, and ether functionalities (Jafari et al., 2023). The broad absorption band observed between 3000–3700 cm^{-1} corresponds to O–H stretching vibrations associated with hydroxyl and phenolic groups commonly found in lignocellulosic materials (Pamidimukkala & Soni, 2018). Following KOH activation, this band becomes more pronounced, indicating the

enrichment of oxygen-containing surface functionalities on the activated carbon surface (Opeoluwa et al., 2023). After AMX adsorption, a slight shift of the O–H band towards lower wavenumbers is observed, suggesting the involvement of hydroxyl groups in hydrogen-bonding interactions with AMX molecules (Cela-Dablanca et al., 2022).

The absorption peak located between 1600–1700 cm^{-1} is attributed to C=O stretching vibrations of carbonyl and carboxyl functional groups (Anastopoulos et al., 2020). Compared with biochar, the PKSAC spectrum exhibits a more distinct peak in this region, indicating the formation or enhancement of oxygen-containing functionalities during chemical activation (Rabia & Hussein, 2020). Following AMX adsorption, a further increase in the intensity of the C=O band is observed, suggesting the participation of carbonyl and carboxyl groups in the adsorption process. AMX contains several polar functional groups, including hydroxyl (-OH), amino ($-NH_2$), carboxyl (-COOH), and carbonyl (C=O) groups, which can interact with the oxygen-containing surface functionalities of PKSAC through hydrogen bonding and electrostatic interactions (Sharafinia et al., 2023).

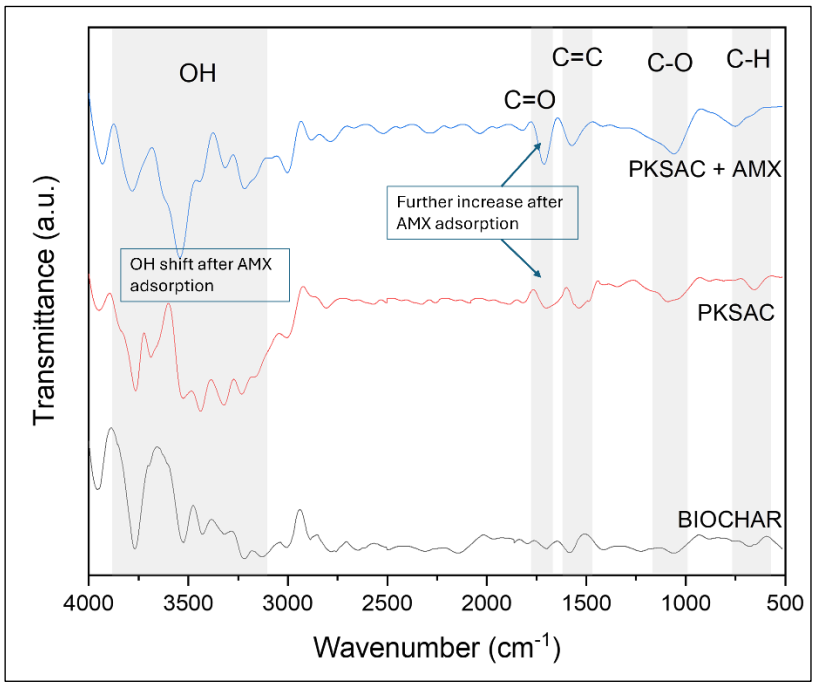

Figure 4.4 FTIR Spectra of Biochar and PKSAC Before and After AMX Adsorption

The peaks observed at 1500–1600 cm^{-1} and 1050–1085 cm^{-1} correspond to aromatic C=C stretching and C–O stretching vibrations, respectively (Jafari et al., 2023). The presence of aromatic C=C structures is mainly associated with lignin-derived carbon frameworks, while the C–O band is related to alcohol, phenolic, and ether groups (Rabia & Hussein, 2020). The persistence of these peaks after activation and adsorption indicates that the aromatic carbon framework remains intact while providing reactive surface sites for adsorption. In contrast, the aromatic C–H bending vibration observed between 680–750 cm^{-1} shows relatively minor changes after activation and adsorption, suggesting limited involvement in the adsorption process (Pamidimukkala & Soni, 2018)

Overall, the FTIR results primarily support the involvement of hydrogen bonding and electrostatic/polar interactions in AMX adsorption, as evidenced by the changes observed in the O–H and C=O regions (Limousy et al., 2016). Although aromatic interactions cannot be completely excluded due to the presence of aromatic structures in both PKSAC and AMX, direct evidence for π–π interactions from FTIR analysis is limited.

The XPS analysis provides further insight into the chemical transformations induced by KOH activation and the subsequent interactions between PKSAC and AMX. As shown in the survey spectra (Figure 4.5a), the oxygen-to-carbon ratio increases notably from biochar to PKSAC, confirming the successful introduction of oxygen-containing functional groups during activation. After adsorption, the oxygen content slightly decreases, indicating potential involvement of surface oxygen functionalities in binding with AMX (Spessato et al., 2019).

Deconvolution of the high-resolution C1s spectra (Figure 4.5b) reveals three primary carbon species: C=C (sp^2 hybridized carbon, aromatic structures), C–O (hydroxyl/ether groups), and COOH (carboxyl groups) (Ouyang et al., 2024). In the raw biochar, the surface is dominated by C=C (81.35%), with moderate C–O (14.97%) and minor COOH (3.88%) components. Upon KOH activation, the proportion of aromatic C=C bonds increase to 86.21%, while C–O decreases to 10.01% and COOH to 3.78%, suggesting structural rearrangement toward more graphitic domains and stabilization of hydroxyl functionalities (Spessato et al., 2019).

After AMX adsorption, a clear increase in the COOH contribution is observed (from 3.78% to 5.39%), alongside a slight decrease in C=C (to 85.11%) and C–O (to 9.50%) (Ouyang et al., 2024). These changes suggest surface oxidation and the

formation of new carboxyl-containing complexes during interaction with AMX, likely due to the involvement of electron-rich groups on PKSAC (Jafari et al., 2023).

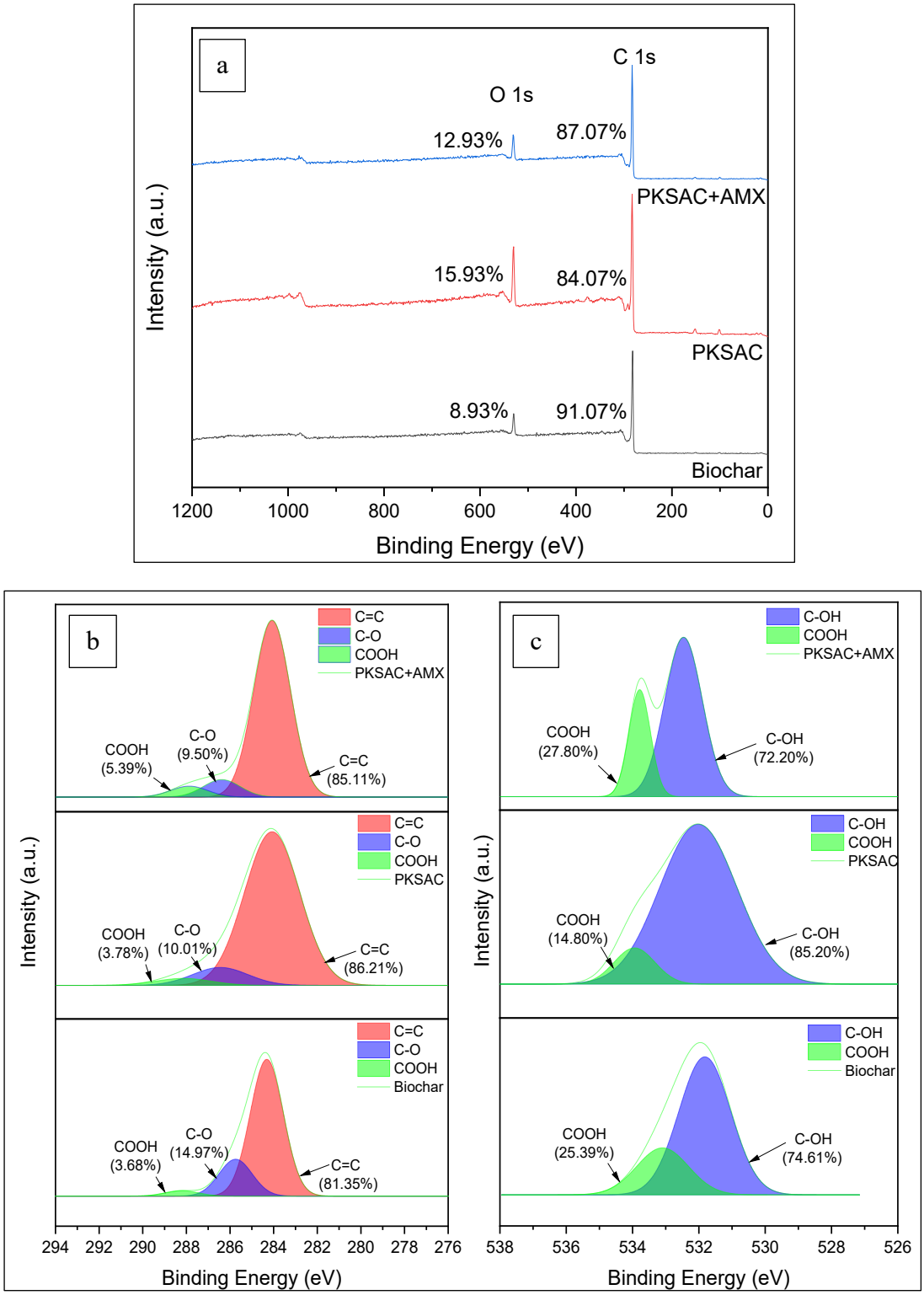

Figure 4.5 (a) XPS Survey Spectra of PKSAC and PKSAC+AMX; (b) High-Resolution C 1s Spectra; and (c) High-Resolution O 1s Spectra of PKSAC and PKSAC+AMX

Similarly, the O1s spectra (Figure 4.5c) show dominant contributions from C–OH and COOH species. KOH activation raises the C–OH fraction substantially (from 74.81% in biochar to 85.20% in PKSAC), while slightly reducing COOH content (from 25.39% to 14.80%), indicating the formation of hydroxyl-rich surfaces (Acosta et al., 2016)[167]. Following AMX adsorption, the proportion of COOH increases sharply to 27.80%, while C–OH decreases to 72.20%. This suggests that hydroxyl groups on PKSAC are actively involved in the adsorption process, primarily through hydrogen bonding and specific surface interaction with AMX molecules (Putra et al., 2009).

The observed shifts in oxygen-containing functionalities, especially the post-adsorption increase in COOH related signal and the concurrent decrease in C–OH which are consistent with the involvement of polar surface functional groups as primary active sites during adsorption (Shi et al., 2023). These experimental observations support a surface interaction-controlled adsorption mechanism predominantly governed by hydrogen bonding. Furthermore, the presence of sp^2-hybridized carbon (C=C) domains indicates structural compatibility for possible π–π interactions, although this contribution is inferred based on aromatic characteristics rather than directly isolated by XPS analysis (Pezoti et al., 2016).

4.3 Optimization of AMX Adsorption Condition using Response Surface Methodology (RSM)

The optimization process for AMX adsorption in this study comprises two main stages. Initially, ANOVA was employed to evaluate the statistical significance of each operating parameter. Subsequently, RSM regression model was utilized to compare experimental and predicted adsorption capacities. Finally, the interaction effects among the process variables were analyzed to understand their combined influence on adsorption efficiency.

4.3.1 Statistical Analysis and Regression Model of AMX Adsorption

BBD was applied to optimize the adsorption parameters, including adsorbent dosage (A), solution pH (B), and contact time (C), to maximize AMX removal efficiency, as shown in Table 4.2. The AMX removal performance ranged from 15.91

to 86.82% under different experimental conditions. The optimization process was conducted with the objective of maximizing AMX removal efficiency (%). Based on the developed quadratic model, the optimum adsorption conditions were determined to be 0.5 g adsorbent dosage, pH 4.0, and 50 minutes of contact time, resulting in a predicted AMX removal of 85.21%. The relationship between the process variables and predicted AMX removal is represented by the quadratic polynomial equation shown in Equation 4.7.:

$$Y = 34.81 + 17.74A - 4.18B + 16.35C - 5.20AB + 6.52AC - 8.86BC + 8.06A^2 + 9.46B^2 + 1.88C^2 \quad (4.7)$$

Where Y represents the predicted AMX removal response denotes the AMX removal response.

The optimum operating conditions were determined by numerical optimization using the Design Expert® software. Based on the developed quadratic model (Equation 4.5), the software predicted that the maximum AMX removal efficiency of 86.82% could be achieved at an adsorbent dosage of 0.5 g, solution pH of 4.0, and contact time of 50 minutes. Table 4.3 presents the ANOVA analysis of the proposed model. The BBD model for AMX removal by PKSAC demonstrated statistical significance with a p-value < 0.05, confirming the reliability of the model in describing the experimental observations.

Table 4.2
Experimental Design and Response for AMX Removal.

Run	**Factor**			**Response**	
	1	2	3	AMX Removal (%)	
	A: Adsorbent dosage (g)	B: pH	C: Time (min)	Predicted	Actual
1	**0.5**	**4**	**50**	**85.21**	**86.82**
2	0.3	7	50	34.81	35.63
3	0.3	7	50	34.81	30.94
4	0.5	10	50	59.20	59.14

5	0.1	7	90	37.72	37.93
6	0.3	4	10	26.25	24.84
7	0.5	7	90	85.99	84.64
8	0.1	10	50	35.86	34.24
9	0.3	7	50	34.81	37.52
10	0.1	4	50	36.09	36.14
11	0.3	4	90	85.18	84.91
12	0.1	7	10	14.56	15.91
13	0.5	7	10	38.75	38.54
14	0.3	7	50	34.81	36.13
15	0.3	7	50	34.81	33.84
16	0.3	10	90	48.33	49.73
17	0.3	10	10	36.86	37.12

The ANOVA analysis demonstrated that the developed quadratic model was highly significant, with a model p-value below 0.0001. The interaction terms AB (adsorbent dosage × pH), AC (adsorbent dosage × contact time), and BC (pH × contact time) were also statistically significant, as evidenced by their p-values of 0.0009, 0.0014, and <0.0001, respectively. These results indicate that the effect of one operating parameter on AMX removal was dependent on the level of another parameter, thereby confirming the presence of significant interaction effects among the studied variables (Aghababaei et al., 2017). The coefficient of determination (R^2 = 0.9947) indicated excellent agreement between the experimental and predicted responses, while the adjusted R^2 value (0.9878) further confirmed the reliability of the model. In addition, the non-significant lack-of-fit (p = 0.6100) demonstrated that the model adequately represented the experimental data. The signal-to-noise ratio of 39.60, which was substantially higher than the minimum desirable value of 4, indicated adequate precision and confirmed the suitability of the model for navigating the design space (Jawad & Surip, 2022)

Table 4.3
Analysis of Variance (ANOVA) for AMX Removal (%) by PKSAC

Source	Sum of Squares	df	Mean Square	F-value	p-value	
Model	7241.98	9	804.66	145.47	< 0.0001	Significant
A-Adsorbent dosage	2625.23	1	2625.23	474.59	< 0.0001	
B-pH	344.27	1	344.27	62.24	< 0.0001	
C-Time	2478.08	1	2478.08	447.99	< 0.0001	
AB	166.15	1	166.15	30.04	0.0009	
AC	144.96	1	144.96	26.21	0.0014	
BC	563.11	1	563.11	101.80	< 0.0001	
A²	217.61	1	217.61	39.34	0.0004	
B²	614.83	1	614.83	111.15	< 0.0001	
C²	21.39	1	21.39	3.87	0.0900	
Residual	38.72	7	5.53			
Lack of Fit	13.04	3	4.35	0.6774	0.6100	not significant
Pure Error	25.68	4	6.42			
Cor Total	7280.70	16				

R^2 = 0.9947

Adj-R^2 = 0.9878

The normal probability plot shown in Figure 4.6a demonstrates that most data points follow a straight-line pattern, with minimal deviation. As shown in Figure 4.6b, the agreement between predicted and experimental AMX removal percentages confirms the accuracy of the model. In general, the statistical model demonstrates high significance and a strong relationship between the input variables and the response (Wajid et al., 2022)

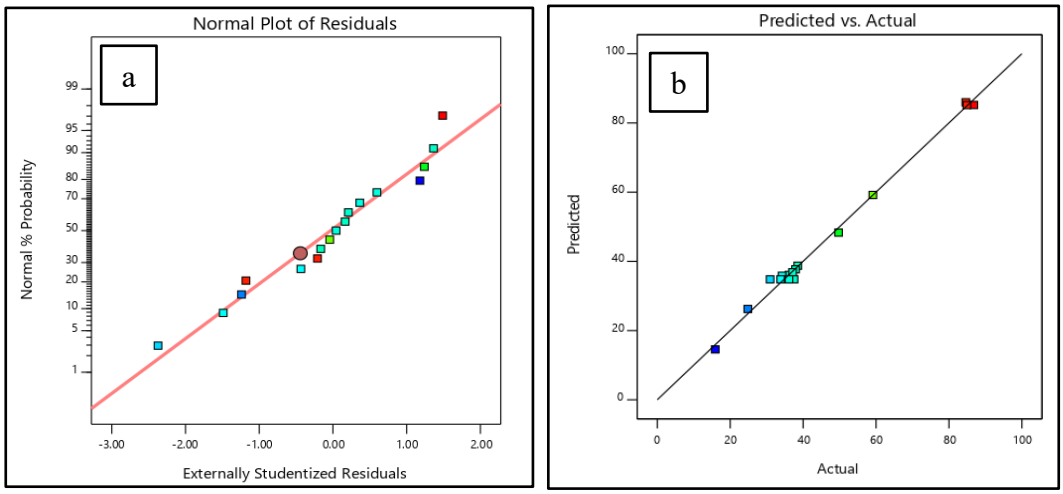

Figure 4.6 (a) Normal Probability Plot and (b) Experimental and Actual Removal of AMX (%)

4.3.2 Interactions Effect of Process Variables on the Response

The adsorption performance of AMX onto PKSAC was influenced by the combined effects of solution pH, adsorbent dosage, and contact time. The interactions among these variables were evaluated using contour plots generated from the Box–Behnken Design (BBD) model, as presented in Figure 4.7. The contour plots provide a graphical representation of the interaction effects between variables, while the statistical significance of these interactions is supported by the ANOVA results discussed in Section 4.3.1.

Figure 4.7a illustrates the interaction between adsorbent dosage and solution pH at a fixed contact time of 50 minutes. The curved contour lines indicate a significant interaction between adsorbent dosage (A) and pH (B), which is consistent with the ANOVA results where the AB interaction term was statistically significant ($p = 0.0009$). AMX removal increased substantially with increasing adsorbent dosage, particularly under acidic conditions. The highest removal efficiency was observed at an adsorbent dosage of approximately 0.5 g and pH 4.0. This behaviour can be attributed to the greater availability of adsorption sites at higher adsorbent dosages and the favourable surface charge conditions under acidic environments (Shi et al., 2023)

The pH_{PZC} profile of PKSAC is presented in Figure 4.7b. The ΔpH values increased from pH 2.0 to pH 4.0, indicating progressive protonation of the PKSAC surface (Pamidimukkala & Soni, 2018). Under acidic conditions, oxygen-containing

functional groups such as hydroxyl and carboxyl groups readily interact with H^+ ions, resulting in a more positively charged surface (Jafari et al., 2023). The maximum ΔpH observed at pH 4 suggests that protonation was most pronounced within this pH range. The pH_{PZC} value of 6.3 indicates that the PKSAC surface is positively charged at pH values below 6.3 and negatively charged at pH values above 6.3.

According to Table 4.4, AMX contains three ionizable functional groups, namely a carboxyl group (pKa_1 = 2.68), an amino group (pKa_2 = 7.49), and a phenolic hydroxyl group (pKa_3 = 9.63). Within the pH range of 4.0–7.0, AMX predominantly exists in its zwitterionic form, where the amino group remains protonated (NH_3^+) while the carboxyl group is deprotonated (COO^-) (Sharafinia et al., 2023). Under these conditions, adsorption is facilitated by hydrogen bonding and electrostatic interactions between the oxygen-containing functional groups on the PKSAC surface and the polar functional groups of AMX. At pH values above 7.49, the amino group gradually loses its proton, while the carboxyl group remains deprotonated, causing AMX to adopt a predominantly anionic form (Anastopoulos et al., 2020). Consequently, electrostatic repulsion between negatively charged PKSAC and anionic AMX molecules becomes more pronounced, resulting in lower adsorption efficiency (Chayid & Ahmed, 2015)

Table 4.4
Surface Charge of the PKSAC and AMX at Various pH Values.

pH	**PKSAC (pH_{PZC} = 6.3)**	**AMX Speciation***	**Potential interaction**
4.0 – 6.0	Net positively charged	Zwitterion ($AMX^{\pm}$) (NH_3^+ and COO^- present simultaneously)	Electrostatic interaction and hydrogen bonding
7.0	Net negatively charged	Zwitterion ($AMX^{\pm}$) (predominantly NH_3^+ and COO^-)	Electrostatic interaction and hydrogen bonding
8.0 –10.0	Net negatively charged	Anionic (AMX^-) (COO^- dominant, NH_2 neutral)	Electrostatic repulsion

* AMX pKa values: carboxyl group (pK_{a1} = 2.68), amine group (pK_{a2} = 7.49), and phenolic hydroxyl group (pK_{a3} = 9.63) (Shi et al., 2023)

The interaction between adsorbent dosage and contact time at a fixed pH of 4.0 is shown in Figure 4.7c. The contour lines exhibit noticeable curvature, indicating a significant interaction between adsorbent dosage (A) and contact time (C), which is supported by the significant AC interaction term obtained from ANOVA ($p = 0.0014$). The contour plot shows a positive gradient from the lower-left region to the upper-right region, demonstrating that AMX removal increased as both adsorbent dosage and contact time increased simultaneously. The improvement in adsorption performance can be attributed to the greater number of available adsorption sites at higher dosages and the longer interaction period that allows the adsorption process to approach equilibrium (Anastopoulos et al., 2020)

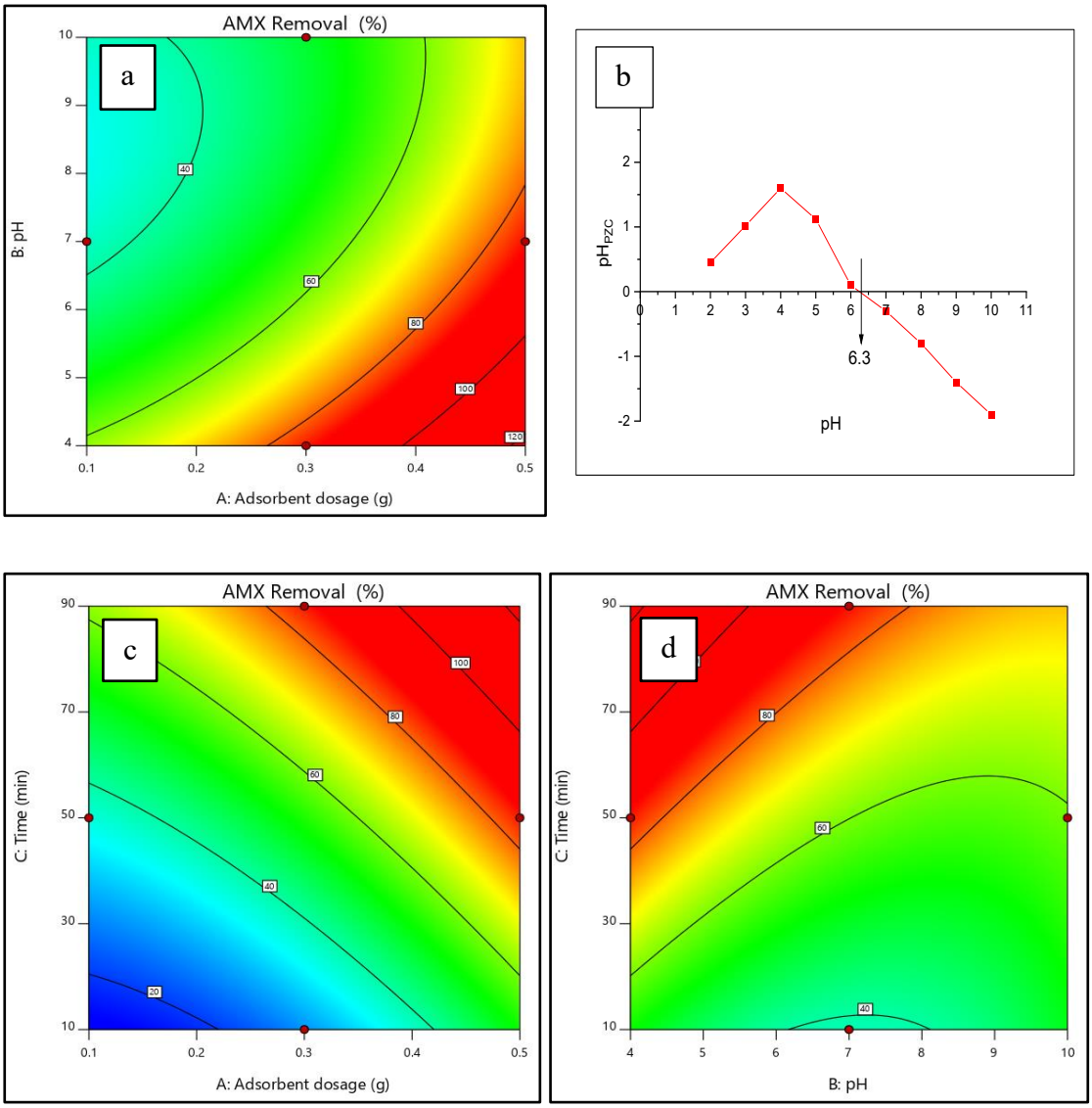

Figure 4.7 (a) pH_{PZC} of PKSAC and Contour Plot About the Interaction Between (b) pH and Adsorbent Dosage, (c) Time and Adsorbent Dosage, and (d) Time and pH.

Figure 4.7d presents the interaction between pH and contact time at a fixed adsorbent dosage. The pronounced curvature of the contour lines indicates a strong interaction between solution pH (B) and contact time (C). This observation is consistent with the ANOVA results, where the BC interaction term exhibited the highest F-value (101.80) and the lowest p-value ($p < 0.0001$) among all interaction terms. The contour plot demonstrates that AMX removal efficiency increased at lower pH values and longer contact times. The highest removal efficiency was observed in the region corresponding to pH 4.0–5.0 and contact times exceeding 70 minutes. In contrast, increasing the pH reduced adsorption performance despite prolonged contact durations, highlighting the dominant influence of solution pH on AMX adsorption (Chayid & Ahmed, 2015)

Overall, the contour plots generated using the BBD model demonstrate that the interaction effects among adsorbent dosage, pH, and contact time significantly influenced AMX removal by PKSAC. The curved contour patterns observed in Figures 4.7a, 4.7c, and 4.7d corroborate the statistically significant interaction terms identified in the ANOVA analysis, confirming that the effect of one variable was dependent on the level of another variable. Among the investigated interactions, the pH–contact time interaction (BC) exerted the strongest influence on AMX removal performance.

4.3.3 Numerical Optimization of AMX Adsorption

Following the evaluation of the regression model and interaction effects of the operating parameters, numerical optimization was performed using the desirability function approach available in Design Expert® software to determine the optimum conditions for AMX adsorption by PKSAC. The optimization objective was established to maximize AMX removal efficiency within the investigated experimental range. The factors considered during optimization were adsorbent dosage (0.1–0.5 g), solution pH (4.0–10.0), and contact time (10–90 minutes).

According to Table 4.5, the numerical optimization predicted that the optimum operating conditions for AMX adsorption were an adsorbent dosage of 0.49 g, solution pH of 4.12, and contact time of 59.29 minutes. Under these conditions, the model predicted an AMX removal efficiency of 90.85% with a desirability value of 1.000. The desirability value indicates excellent agreement between the optimization criteria and the predicted response, demonstrating the suitability of the developed quadratic model

for predicting AMX removal performance.

Table 4.5
Predicted Optimum Operating Conditions for AMX Adsorption by PKSAC Obtained Using the Desirability Function Approach.

Parameter	Optimization criterion	Predicted optimum value
Adsorbent dosage (g)	In range	0.494
pH	In range	4.121
Contact time (min)	In range	59.290
AMX removal (%)	Maximize	90.854
Desirability	Maximize	1.000

The desirability ramp plot shown in Figure 4.8 visually summarizes the optimum solution generated by the numerical optimization procedure. The optimized operating conditions obtained in this study are consistent with trends reported in previous studies on AMX adsorption using activated carbon-based adsorbents (Chayid & Ahmed, 2015). The optimum pH of approximately 4.0 supports enhanced adsorption due to favourable electrostatic interactions and hydrogen bonding between AMX molecules and oxygen-containing functional groups on the adsorbent surface. Similarly, the optimized contact time of approximately 60 minutes falls within the range commonly reported for biomass-derived activated carbons, indicating that sufficient interaction time is required to achieve near equilibrium adsorption (Wajid et al., 2022). These observations further support the validity and practical applicability of the optimization results obtained from the RSM model.

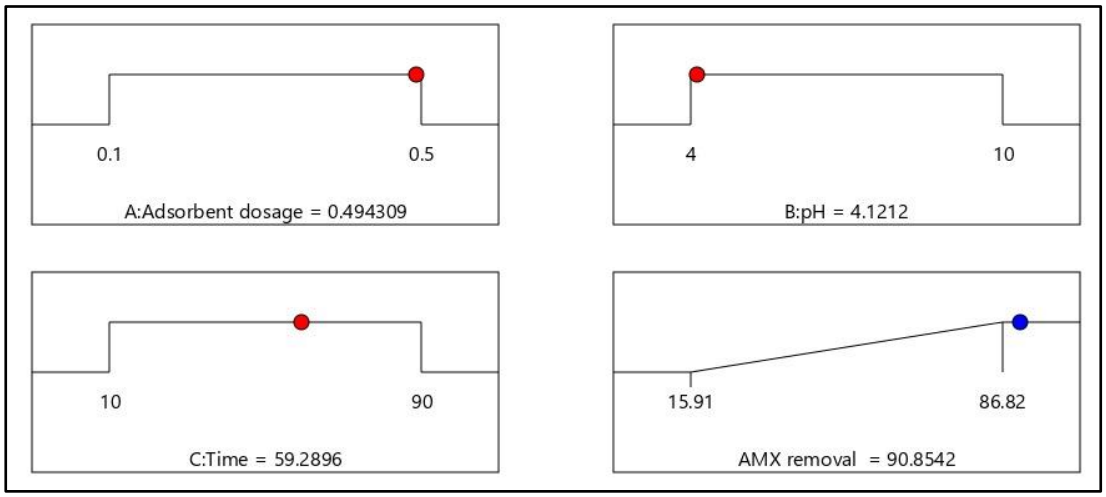

Figure 4.8 Desirability Ramp Plot Showing the Predicted Optimum Operating Conditions for AMX Adsorption by PKSAC Obtained from Numerical Optimization.

Furthermore, the optimized AMX removal efficiency (90.85%) was higher than the highest experimental AMX removal obtained during the Box–Behnken Design experiments (86.82%). This finding indicates that numerical optimization successfully identified a more favourable combination of operating conditions within the studied experimental region. For practical implementation, the predicted optimum conditions may be approximated to 0.5 g adsorbent dosage, pH 4.0, and 60 minutes contact time without significantly affecting the predicted adsorption performance.

4.4 Analysis of AMX Adsorption Performance

4.4.1 Adsorption Kinetics

The rate-controlling step and adsorption mechanism of AMX onto PKSAC were analysed using pseudo-first order (PFO), pseudo-second order (PSO), and Elovich kinetic models, as illustrated in Figure 4.9. The kinetic experiments were conducted using 0.5 g PKSAC prepared at an impregnation ratio of 1:3 in 300 mL of AMX solution at initial concentrations ranging from 100 to 400 ppm and a temperature of 25 ± 2 °C. The adsorption profiles indicate that equilibrium was achieved within approximately 7 hours of contact time, as evidenced by the plateau observed in all adsorption curves. For all initial AMX concentrations, adsorption followed a similar trend, characterised by rapid uptake during the initial stage followed by a slower adsorption rate as the

available adsorption sites gradually became occupied (Peng et al., 2014). Increasing the initial AMX concentration from 100 to 400 ppm resulted in higher adsorption capacities, increasing from 79.38 to 208.34 mg/g. This behaviour can be attributed to the greater concentration gradient between the solution and adsorbent surface, which enhances the driving force for mass transfer of AMX molecules from the aqueous phase to the adsorption sites (Yang et al., 2019).

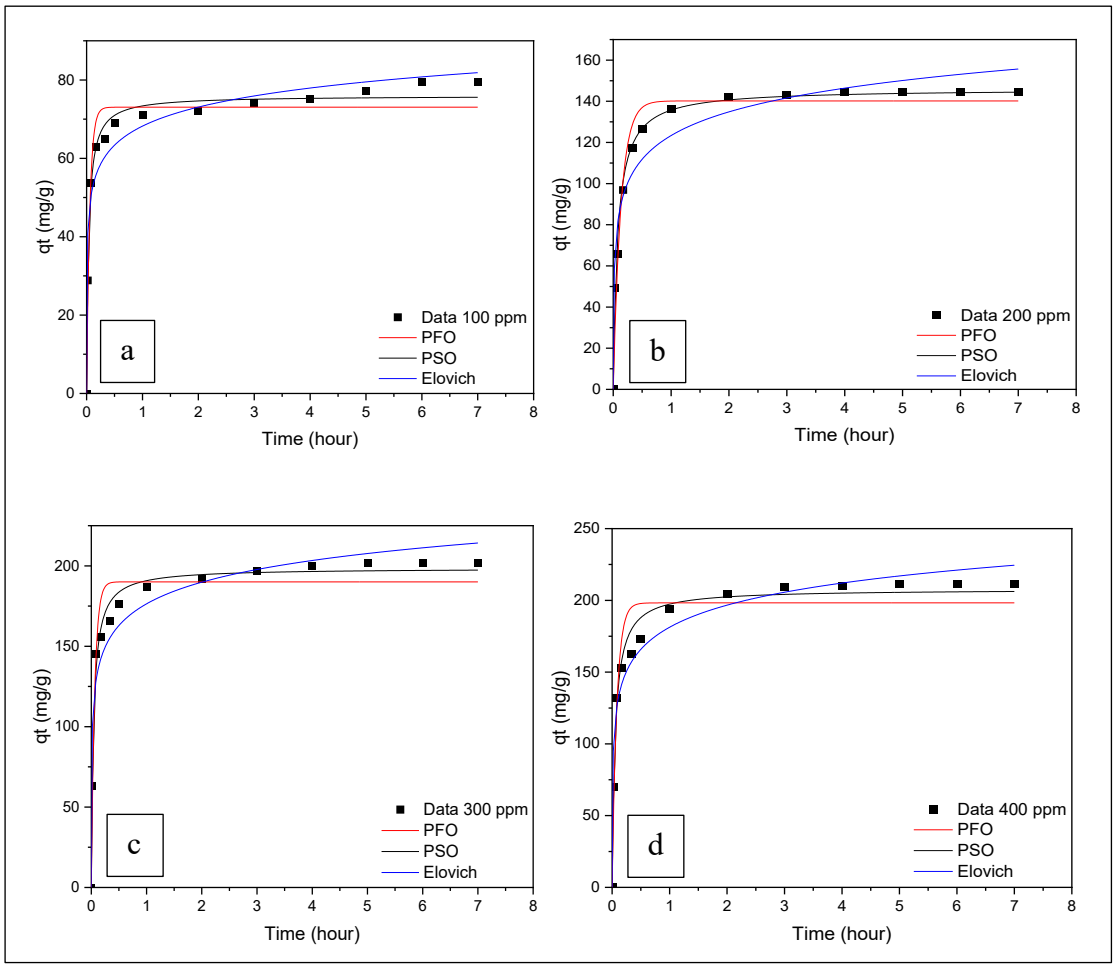

Figure 4.9. Adsorption Kinetic of AMX onto PKSAC by PSO, PSO and Elovich Kinetic Model Under (a) 100 ppm, (b) 200 ppm, (c) 300 ppm and (d) 400 ppm.

The kinetic parameters obtained from the PFO and PSO models are presented in Table 4.6, while the Elovich model parameters are summarised separately in Table 4.7. Among the evaluated models, the PSO model provided the best fit to the experimental data, with R^2 values ranging from 0.980 to 0.990, which were consistently higher than those obtained for the PFO model (0.927–0.957). In addition, the adsorption capacities predicted by the PSO model showed closer agreement with the experimental

values. The percentage error between experimental and calculated adsorption capacities ranged from 0.28–4.30% for the PSO model, compared with 2.88–7.96% for the PFO model. Furthermore, the PSO model exhibited lower RSS values than the PFO model across all concentrations, indicating superior fitting accuracy (Wajid et al., 2022).

The Elovich model parameters are presented separately because the model describes adsorption behaviour using the initial adsorption rate (α) and desorption constant (β), rather than predicting equilibrium adsorption capacity (qe) as in the PFO and PSO models (Shi et al., 2023). Although the Elovich model produced reasonable fits (R^2 = 0.927–0.954), its performance was inferior to that of the PSO model, as reflected by the lower R^2 values and substantially higher RSS values. This suggests that the Elovich model was less suitable for describing the adsorption kinetics of AMX onto PKSAC under the investigated conditions (Ouyang et al., 2024).

The good performance of the PSO model suggests that the adsorption rate was governed by interaction-controlled adsorption processes occurring at the adsorbent surface (Jang et al., 2018). Similar observations have been reported by Cheng (2020), who found that the PSO model provided the best representation of antibiotic adsorption onto biochar-based adsorbents (Cheng et al., 2020). The present findings are also consistent with the FTIR results discussed in Section 4.2.2.3, where increased intensities of hydroxyl (–OH) and carbonyl (C=O) functional groups were observed following adsorption. These oxygen-containing functional groups likely facilitated adsorption through hydrogen bonding and other surface interactions between PKSAC and AMX molecules, contributing to the observed kinetic behaviour (Chayid & Ahmed, 2015).

Table 4.6
PFO and PSO Kinetic Parameters of AMX by PKSAC.

Concentration (ppm)	$q_{e\ exp.}$ **(mg/g)**	**Model**	$q_{1_{e\ cal.}}$ **(mg/g)**	**Error (%)**	**Rate Constant ± SE (1/min)**	R^2	**RSS**
100	79.38	PFO	73.06 ± 1.66	7.96	17.79 ± 2.92 (k_1)	0.956	283.27
		PSO	75.97 ± 0.89	4.30	0.373 ± 0.04 (k_2)	0.990	64.61
200	144.33	PFO	140.18 ± 3.78	2.88	7.53 ± 1.14 (k_1)	0.952	1240.31
		PSO	146.00 ± 2.65	1.16	0.0903 ± 0.01 (k_2)	0.980	464.85
300	202.06	PFO	190.06 ± 4.40	5.94	16.46 ± 2.69 (k_1)	0.957	1972.37
		PSO	198.50 ± 2.52	1.76	0.1248 ± 0.01 (k_2)	0.989	495.49
400	208.34	PFO	200.25 ± 3.48	3.88	12.30 ± 2.69 (k_1)	0.927	888.51
		PSO	207.75 ± 3.48	0.28	0.0916 ± 0.01 (k_2)	0.982	888.51

Residual sum of squares (RSS); Standard Error (SE)

Table 4.7
Elovich Kinetic Parameters of AMX by PKSAC.

Concentration (ppm)	**α (mg/g min)**	**β (g/mg)**	**R^2**	**RSS**
100	$1.18\times10^5 \pm 1.21\times10^5$	0.0167	0.951	287.68
200	$2.76\times10^4 \pm 1.86\times 10^4$	0.0601 ±0.01	0.954	1181.81
300	$1.69\times10^5 \pm 1.75\times 10^5$	0.0514 ±0.01	0.943	2610.27
400	$1.98\times10^5 \pm 6.18\times 10^3$	12.30 ±2.48	0.927	3693.65

α=initial adsorption rate;

β=desorption constant related to surface coverage and adsorption energy

From a practical perspective, the relatively short equilibrium time of approximately 7 hours provides useful information for the design and scale-up of adsorption systems. Faster attainment of equilibrium reduces the required hydraulic retention time and reactor volume, thereby improving process efficiency and reducing operational costs (Bedia et al., 2018). The ability of PKSAC to achieve equilibrium within several hours, coupled with its relatively high adsorption capacity, highlights its potential applicability for the treatment of antibiotic-contaminated wastewater.

4.4.2 Adsorption Isotherms and the Effect of Temperature

Adsorption equilibrium studies were conducted to evaluate the adsorption behaviour of AMX onto PKSAC and to identify the most suitable isotherm model for describing the adsorption process. The equilibrium data were fitted using Langmuir, Freundlich, and Redlich–Peterson isotherm models, as shown in Figure 4.10, while the corresponding model parameters are summarized in Table 4.8.

The Langmuir and Redlich–Peterson models exhibited excellent agreement with the experimental data, with R^2 values ranging from 0.991–0.995 and 0.992–0.995, respectively. The Langmuir separation factor (R_L) remained between 0 and 1 at all investigated temperatures, confirming favourable adsorption of AMX onto PKSAC. In addition, the Redlich–Peterson exponent (g) ranged from 0.96–1.06, indicating that the adsorption behaviour approached Langmuir characteristics and suggesting that adsorption predominantly occurred as a monolayer on relatively homogeneous

adsorption sites (Jang et al., 2018). The close agreement between the Langmuir and Redlich–Peterson models further support this adsorption behaviour.

The maximum monolayer adsorption capacity (q_{max}) increased from 219.66 mg/g at 25 °C to 244.89 mg/g at 55 °C. This increase suggests that adsorption became more favourable at elevated temperatures, indicating an endothermic adsorption process (Haghighat et al., 2020). Higher temperatures may enhance the mobility of AMX molecules and facilitate diffusion into the pore structure of PKSAC, thereby improving access to available adsorption sites and increasing adsorption capacity (Wang & Guo, 2020).

From an adsorption process design perspective, the Langmuir model provides useful information because the q_{max} parameter represents the theoretical maximum adsorption capacity of the adsorbent (Ouyang et al., 2024). This parameter can be used to estimate adsorbent requirements, treatment capacity, and replacement frequency in practical wastewater treatment systems (Largitte & Pasquier, 2016). The relatively high q_{max} values obtained in this study indicate that PKSAC possesses considerable adsorption capacity for AMX removal and may reduce adsorbent consumption during large scale treatment applications (Ouyang et al., 2024).

Table 4.8
Isotherm Model Parameters (Langmuir, Freundlich, and Redlich–Peterson) for AMX Adsorption onto PKSAC at Different Temperatures.

Models	**Temperature (°C)**			
	25	35	45	55
Langmuir				
q_{max} **(mg/g)**	219.66	224.20	237.34	244.89
K_L **(L/mg)**	0.03	0.05	0.06	0.08
R_L	0.63 - 0.08	0.50 - 0.05	0.45 – 0.04	0.38 – 0.03
R^2	0.992	0.995	0.995	0.991
Freundlich				
K_F**(mg/g (L/mg)$^{1/n}$)**	18.12	22.88	27.98	31.82
n	2.50	2.70	2.86	3.03
R^2	0.951	0.933	0.926	0.934
Redlich-Peterson				
K_{RP} **(L/g)**	5.78	6.86	9.91	14.89
a_{RP} **(L/mg)**	0.04	0.03	0.05	0.11

g	0.97	1.06	1.03	0.96
R^2	0.992	0.994	0.995	0.992

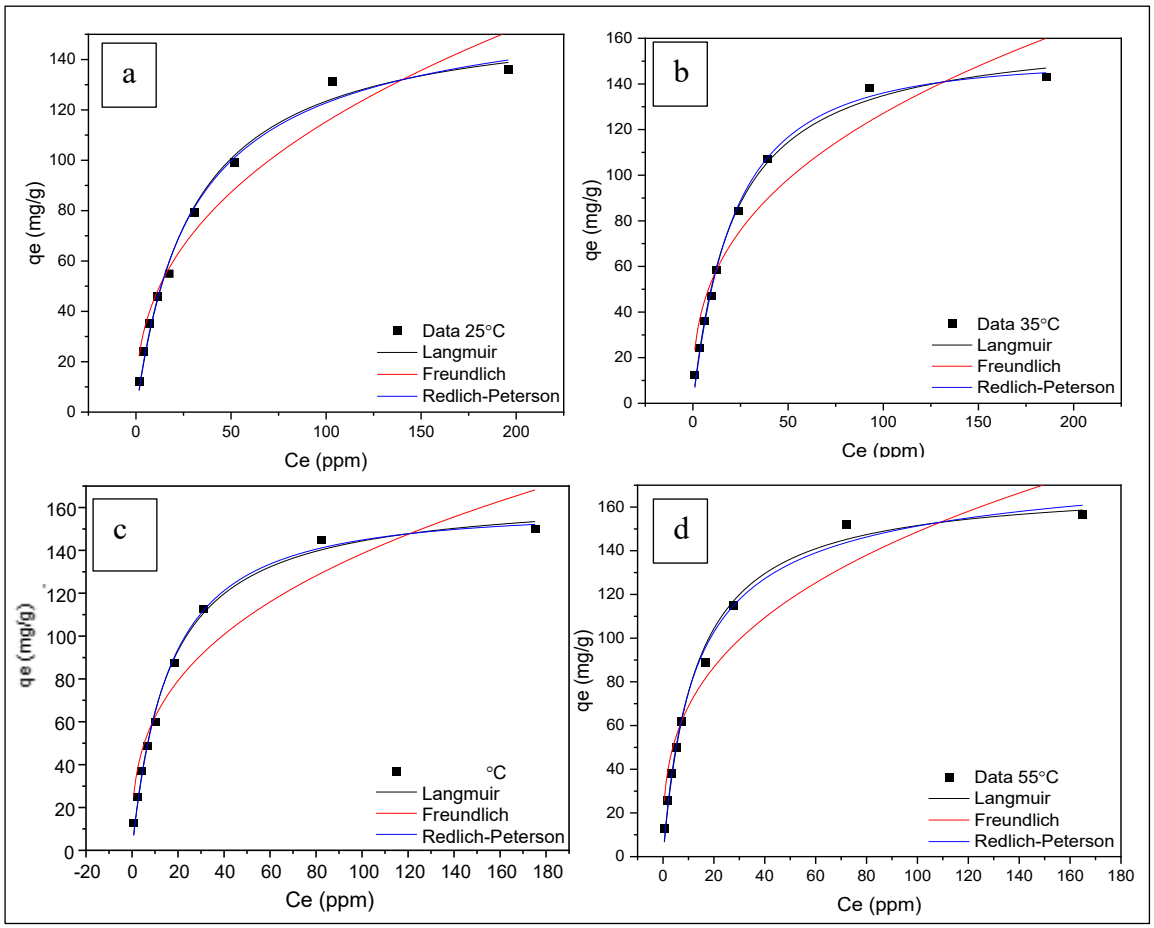

Figure 4.10 Langmuir, Freundlich, and Redlich–Peterson Isotherm Plots for AMX Adsorption onto PKSAC at (a) 25 ℃, (b) 35 ℃, (c) 45 ℃, and (d) 55 ℃.

The performance of an adsorbent is commonly assessed by comparing its Langmuir adsorption capacity and BET surface area (S_{BET}) with those reported in the literature. Table 4.9 presents a comparison between PKSAC, and several biomass-derived activated carbons used for AMX adsorption. To facilitate a fair comparison among studies, the adsorbent dosage used in this work was expressed as an adsorbent concentration of 5 g/L, corresponding to 0.5 g PKSAC in 100 mL of AMX solution.

As shown in Table 4.7, the PKSAC developed in this study achieved a q_{max} value of 219.66 mg/g despite having a BET surface area of 798.35 m^2/g, which was lower than those reported for phosphoric acid-activated olive stone carbon (1174 m^2/g),

microwave-assisted KOH-activated paper mill sludge carbon (1196 m^2/g), and microwave-prepared giant reed activated carbon (1065 m^2/g). Nevertheless, the adsorption capacity obtained in this study was substantially higher than that of olive stone-derived activated carbon (57.04 mg/g) and slightly higher than that of paper mill sludge-derived activated carbon (204.00 mg/g). Although giant reed-derived activated carbon exhibited a higher adsorption capacity (249.30 mg/g), its BET surface area was also considerably larger than that of PKSAC.

Table 4.9
Comparative Analysis of Maximum AMX Adsorption Capacities Across Various Adsorbents.

Activated carbon precursor	**Activation method**	**Experimental adsorption condition**			q_{max} **(mg/g)**	S_{BET} **(m^2/g)**	**Reference**
		Dosage (g/L)	pH	Temperature (°C)			
Palm kernel shell	KOH activation (700 °C, KOH:PKS = 1:3)	5	4	25	219.66	798.35	This study
Olive stone	H_3PO_4 chemical activation	1	Not adjusted	25	57.04	1174	(Limousy et al., 2016)
Paper mill sludge	Microwave-assisted KOH activation (800 °C, KOH:PS = 1:5)	0.0125-0.05	Not adjusted	25	204	1196	(Sousa et al., 2021)
Giant reed	KOH chemical activation	0.1	7	29	249.3	1065	(Chayid & Ahmed, 2015)

These observations indicate that adsorption performance cannot be explained solely by surface area (Jafari et al., 2023). The relatively high adsorption capacity achieved by PKSAC is likely attributed to the combined contribution of its pore structure and surface chemistry. FTIR analysis confirmed the presence of oxygen-containing functional groups, including hydroxyl, carbonyl, and ether groups, which can participate in hydrogen bonding and electrostatic interactions with AMX molecules

(Putra et al., 2009). Therefore, the adsorption performance of PKSAC is governed not only by the availability of adsorption sites but also by the nature of the surface functional groups involved in the adsorption process (Limousy et al., 2016).

4.4.3 Adsorption Energy in the PKSAC-AMX System

The adsorption of AMX onto PKSAC can be understood at the molecular level through the analysis of adsorption energy and energy gaps, which provide insights into the stability and reactivity of the interaction. This discussion integrates findings from DFT calculations with experimental data to elucidate the adsorption mechanisms involving specific functional groups of AMX (-COOH, -NH_2, and -OH) and the active hydroxyl groups on PKSAC.

4.4.3.1 Electron Density and Molecular Interactions in AMX Adsorption

XPS analysis suggests that the -OH and C=C groups on the PKSAC surface may enhance the adsorption of AMX. To further elucidate this adsorption behavior, theoretical DFT calculations were performed incorporating electron density distribution, electrostatic potential (ESP) mapping, molecular orbital analysis, and adsorption energy evaluations.

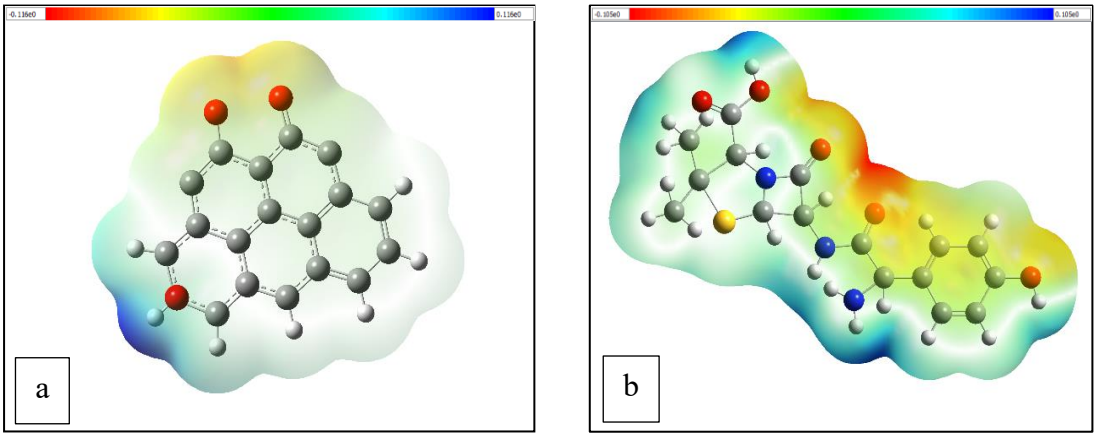

Figure 4.11 Electrostatic Potential (ESP) Maps of (a) PKSAC and (b) AMX

Figure 4.11 displays the ESP maps of PKSAC and AMX, providing insight into their surface charge distributions. The PKSAC surface exhibits red-shaded regions (Figure 4.11a), particularly around the oxygen containing functional groups including

hydroxyl moieties, indicating electron-rich regions with negative electrostatic potential. In contrast, AMX (Figure 4.11b) shows blue-shaded zones near certain oxygen and nitrogen atoms, corresponding to electron-deficient regions with positive electrostatic potential (Wei et al., 2022). This electrostatic complementarity between PKSAC and AMX supports the formation of hydrogen bonding interactions, while the optimized adsorption geometries confirm that AMX adsorption is governed mainly by specific noncovalent interactions, particularly hydrogen bonding assisted by electrostatic attraction rather than by covalent bonding or electron transfer (Spaltro et al., 2021).

Table 4.10
DFT Analysis of Energy Gap and Adsorption Energy for the Compounds.

Molecular fragment	**HOMO (E_H) (eV)**	**LUMO (E_L) (eV)**	**Energy gap (E_g) (eV)**	**Adsorption energy (kJ/mol)**	**Adsorption nature**
AMX	-3.61	-2.9	-	-	-
PKSAC-OH	-4.95	-4.89	-	-	-
PKSAC-OH: AMX-COOH	-5.23	-5.08	0.15	-118.67	Strong specific interaction (hydrogen bonding)
PKSAC-OH: AMX-NH_2	-5.5	-5.3	0.2	-102.89	Strong specific interaction (hydrogen bonding and electrostatic interactions)
PKSAC-OH: AMX-OH	-5.28	-5.07	0.21	-94.52	Strong hydrogen bond assisted adsorption

To visualize the orientation of the interactions, optimized adsorption geometries were generated for three interaction types: PKSAC–OH with AMX–COOH, AMX–NH_2, and AMX–OH (Figure 4.11). Among these, PKSAC–OH: AMX–COOH complex (Figure 4.11a) exhibits the most favorable hydrogen bonding orientation and interaction geometry. This configuration results in the highest adsorption energy (–118.67 kJ/mol) and the lowest HOMO–LUMO energy gap (0.15 eV), suggesting the strongest and most stable noncovalent surface interaction among the investigated systems (Table 4.10) (Spaltro et al., 2021). The interaction is dominated by hydrogen bonding, in which the

hydroxyl hydrogen of PKSAC acts as the hydrogen bond donor and the carbonyl oxygen on AMX serves as the hydrogen bond acceptor (Wei et al., 2022).

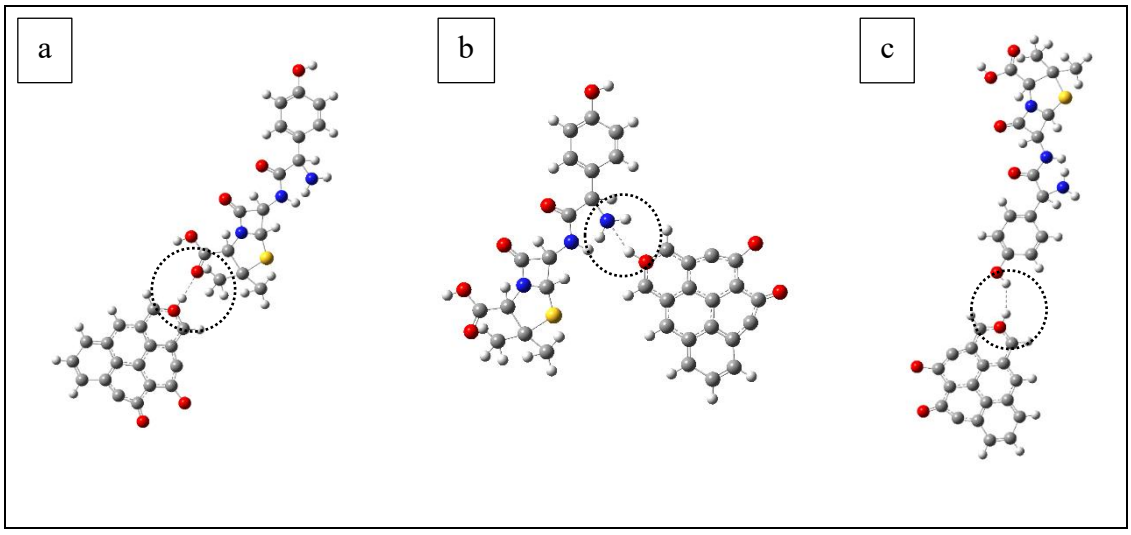

Figure 4.12 Molecular Interactions of (a) PKSAC-OH: AMX-COOH, (b) PKSAC-OH: AMX-NH_2 and (c) PKSAC-OH: AMX-OH

Figure 4.12b and 4.12c show similar but slightly weaker configurations involving AMX –NH_2 and AMX –OH functional groups, respectively. The interaction between PKSAC–OH and AMX–NH_2 has a slightly larger energy gap (0.20 eV) and lower adsorption energy (–102.89 kJ/mol), which can be attributed to less favorable hydrogen bonding orientation and donor acceptor strength compared to the carboxyl group (Antonelli et al., 2021). Similarly, the PKSAC–OH: AMX–OH complex (Figure 12c) exhibits the weakest interaction, reflected in the highest energy gap (0.21 eV) and lowest adsorption energy (–94.52 kJ/mol), likely due to the limited hydrogen-bonding capability between two hydroxyl groups with comparable polarity (Ajebli et al., 2022).

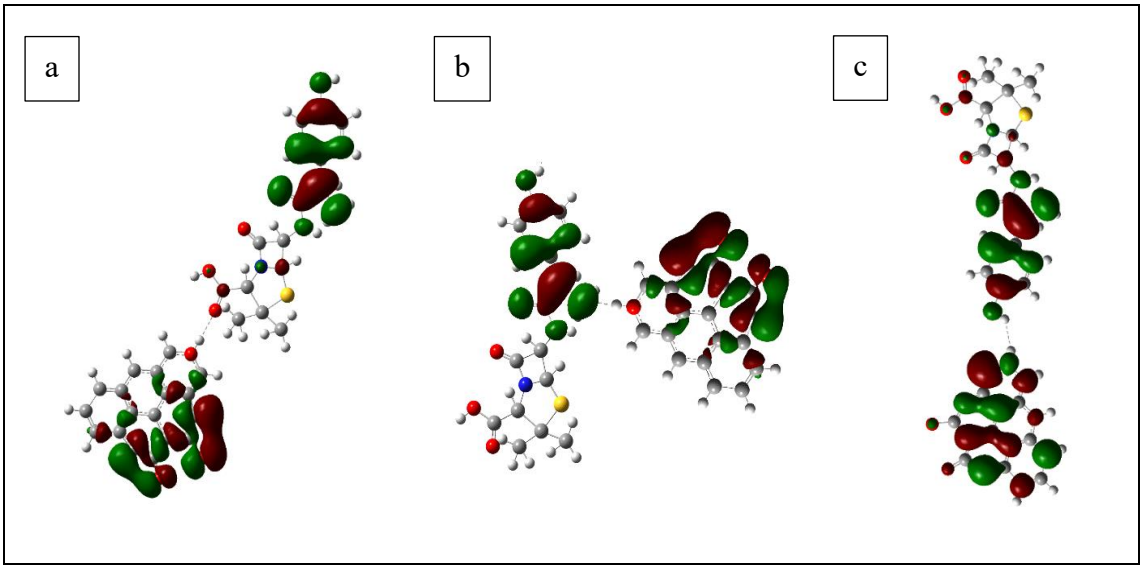

Figure 4.13 HOMO/LUMO Orbital Visualizations of the (a) PKSAC-OH: AMX-COOH, (b) PKSAC-OH: AMX-NH_2 and (c) PKSAC-OH: AMX-OH

Figure 4.13 shows the HOMO and LUMO orbital visualizations for three PKSAC-OH and AMX complexes. The red and green iso-surfaces represent the spatial distribution of frontier molecular orbitals (Antonelli et al., 2021). Although no direct HOMO and LUMO overlap is observed at the adsorption interface, this does not preclude strong binding. Instead, it indicates that AMX adsorption proceeds predominantly through strong noncovalent, interaction-controlled surface interaction, dominated by hydrogen bonding, and electrostatic complementarity rather than covalent orbital hybridization (Zhang et al., 2024). The relatively narrow energy gaps (0.15 to 0.21 eV) and significant adsorption energies (ranging from 94.52 to 118.67 kJ/mol) suggest strong and specific surface interactions arising from cooperative noncovalent forces, consistent with a physical adsorption mechanism governed by surface functionality (Wei et al., 2022).

This interpretation is further strengthened by the consistency between computational predictions and experimental observations. The ESP maps reveal that electron-rich regions on the PKSAC surface, particularly around oxygen-containing functional groups, together with electron-deficient zones on AMX, indicating favorable electrostatic complementarity between components (Spaltro et al., 2021). This charge complementarity reflects a strong tendency for hydrogen bonding and electrostatic interactions, rather than covalent bonding, consistent with the non-overlapping HOMO-LUMO orbitals at the adsorption interface (Antonelli et al., 2021).

This finding is corroborated by FTIR results, which show increased intensity in

the C=O region after AMX adsorption, indicating the involvement of PKSAC's oxygen-containing groups in interactions with AMX's polar sites. Similarly, XPS analysis reveals a decrease in surface –OH and C=C groups and an increase in COOH-related signals following adsorption, suggesting the participation of hydroxyl and carboxyl functionalities in surface interactions, particularly through hydrogen bonding (Limousy et al., 2016). The presence of aromatic (C=C) domains in PKSAC also indicates structural compatibility for possible π–π interactions involving aromatic moieties, although this contribution is inferred rather than directly isolated spectroscopically (Anastopoulos et al., 2020). These functional group changes align well with the DFT predicted strongest interaction, namely the PKSAC–OH: AMX–COOH pair, which exhibited the highest adsorption energy (–118.67 kJ/mol) and the lowest energy gap (0.15 eV), thereby further validating the computational model.

Moreover, this integrated approach aligns with findings from Zhang et al. [147], who reported high adsorption energy values (up to 1.837 eV) for tetracycline on modified biochar and attributed these values to noncovalent interactions facilitated by surface functional groups (Zhang et al., 2024). This study underscores the critical role of surface chemistry, particularly hydroxyl (OH), carboxyl (COOH), and amine (NH_2) groups, in promoting selective and strong adsorption of antibiotics (Ajebli et al., 2022). This reinforces the reliability of DFT in complementing and explaining experimental adsorption mechanisms in biochar systems.

4.4.3.2 Statistical Analysis of Energy Gap and Adsorption Energy

Figure 4.13 presents the scatter plot and linear regression analysis describing the relationship between the HOMO–LUMO energy gap and adsorption energy for the investigated PKSAC–AMX complexes. The statistical analysis was performed using simple linear regression implemented through the statsmodels library in Python 3.9.19, where adsorption energy was treated as the dependent variable and the HOMO–LUMO energy gap was treated as the independent variable. The corresponding regression statistics are summarized in Table 4.9.

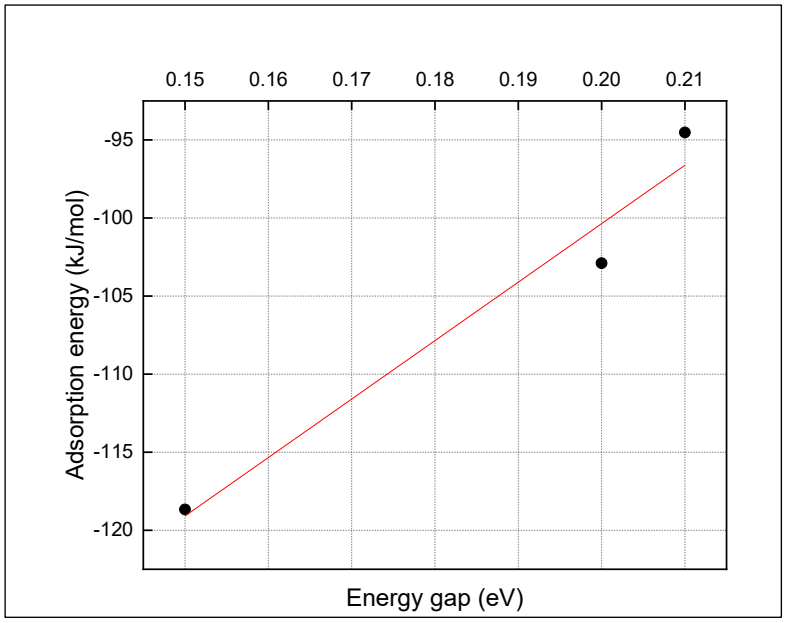

Figure 4.14 Scatter Plot with Linear Regression Showing the Relationship Between Energy Gap and Adsorption Energy.

As shown in Figure 4.14 and Table 4.11, the regression model produced a coefficient of determination (R^2) of 0.964, indicating that 96.4% of the variation in adsorption energy could be explained by variations in the HOMO–LUMO energy gap. The adjusted R^2 value of 0.927 further supports the existence of a strong linear relationship between the two variables. This trend suggests that the nature of the functional group interacting with the PKSAC–OH fragment may influence both the electronic properties and adsorption strength of the resulting adsorption complexes (Spaltro et al., 2021).

Despite the high R^2 value, the p-value obtained from the regression analysis was 0.122, which exceeds the conventional significance threshold of 0.05. Therefore, the relationship between the HOMO–LUMO energy gap and adsorption energy cannot be considered statistically significant at the 95% confidence level. This apparent discrepancy between the high R^2 value and non-significant p-value is likely attributed to the limited number of adsorption complexes included in the regression analysis. Consequently, the results should be interpreted as preliminary evidence of a correlation rather than definitive statistical proof of a causal relationship.

Table 4.11
Summary of Linear Regression Analysis Between Energy Gaps and Adsorption Energy.

Statistic	**Value**
$\boldsymbol{R^2}$	0.964
Adjusted $\boldsymbol{R^2}$	0.927
$\boldsymbol{F}$-statistics	26.44
$\boldsymbol{p}$-value	0.122
Standard Error	72.83

The regression trend indicates that smaller HOMO–LUMO energy gaps were generally associated with more negative adsorption energies, corresponding to stronger adsorption interactions (Wei et al., 2022). For example, the PKSAC–OH: AMX–COOH complex exhibited the lowest energy gap and the most favourable adsorption energy among the investigated systems. This observation suggests that electronic properties may influence adsorption strength by facilitating stronger interactions between AMX functional groups and the oxygen-containing surface functionalities of PKSAC (Antonelli et al., 2021).

4.5 Adsorption Mechanisms

Figure 4.15 illustrates the possible mechanisms contributing to the adsorption process of AMX onto PKSAC which is governed by a combination of physical and strong, interaction-controlled noncovalent surface interactions, as supported by DFT calculations and experimental observations. The adsorption process is primarily dominated by hydrogen bonding and electrostatic attraction, while π–π interactions may additionally contribute due to the presence of aromatic structures in both PKSAC and AMX (Antonelli et al., 2021). FTIR analysis (Figure 4.4) revealed significant changes in the PKSAC surface after AMX adsorption, particularly an increase in the C=O peak intensity, indicating the involvement of carbonyl-related functional groups in surface interactions (Shi et al., 2023). Similarly, XPS analysis (Figure 4.5) showed a decrease in C–OH and C=C groups and an increase in COOH-related signals, suggesting the

participation of hydroxyl and oxygen-containing groups during adsorption. The presence of C=C domains in PKSAC further indicates structural compatibility for potential π–π interactions, although this contribution is inferred rather than directly isolated spectroscopically (Sharafinia et al., 2023). The hydroxyl (-OH) and carboxyl (-COOH) groups on PKSAC serve as key interaction sites, forming strong hydrogen bonds with the polar functional groups of AMX (-NH_2, -COOH, and -OH) (Wajid et al., 2022). Among these, the PKSAC-OH and AMX-COOH interaction exhibits the highest binding energy (-118.67 kJ/mol), underscoring the significant role of the carboxyl group in adsorption. Additionally, HOMO-LUMO analysis indicates that a smaller energy gap for this interaction (0.15 eV) corresponds to enhanced adsorption stability and interaction strength (Thongpat et al., 2021).

Physical adsorption also plays an important role, with the high surface area (798.35 m^2/g) and hierarchical porosity of PKSAC providing abundant sites for AMX uptake (as evidenced through BET and SEM analyses). DFT-derived electron density and adsorption energy visualizations further support the presence of noncovalent surface interactions between AMX molecules and PKSAC, highlighting favorable interaction regions that contribute to adsorption without involving covalent orbital overlap (Antonelli et al., 2021). The combined contribution of physical adsorption and interaction-controlled surface interactions is influences by solution pH, where changes in the ionic form of AMX and the protonation state of surface functional groups on PKSAC modulate surface charge and thereby enhance electrostatic attraction under acidic conditions (Anastopoulos et al., 2020). This synergistic adsorption mechanism highlights the complementary roles of surface functionalization and structural properties of PKSAC in maximizing adsorption capacity, demonstrating its effectiveness as an adsorbent for pharmaceutical contaminants like AMX.

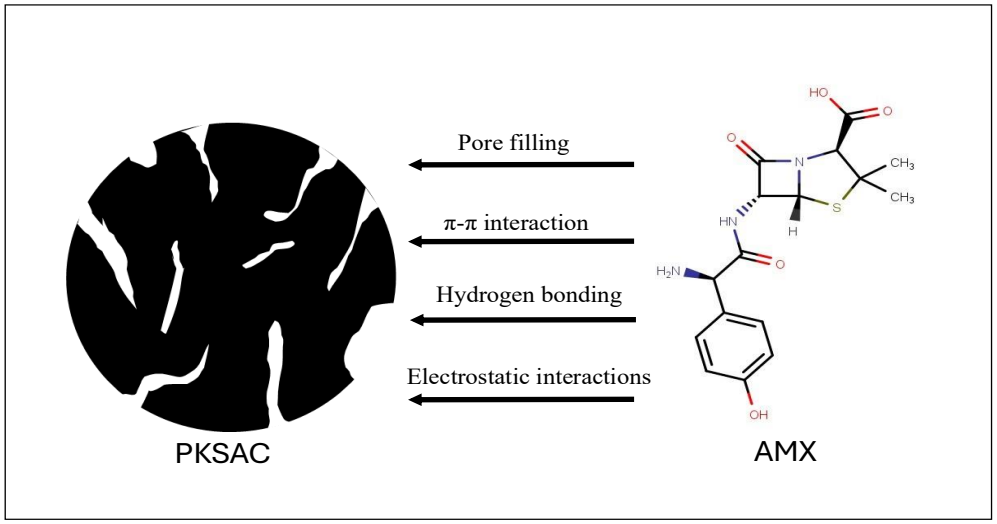

Figure 4.15 Proposed Mechanisms Governing AMX Adsorption onto PKSAC.

Table 4.12 summarizes the major findings obtained from characterization, optimization, kinetic, isotherm, and DFT analyses. Collectively, these results indicate that the adsorption of AMX onto PKSAC is governed by the combined effects of pore development, surface functionality, and interaction-controlled adsorption processes. The integration of experimental observations and computational modelling provides a comprehensive understanding of the adsorption mechanism, which is further illustrated in Figure 4.14.

Table 4.12
Summary of Evidence Supporting the Proposed Adsorption Mechanism of AMX onto PKSAC

Analysis	Key findings	Contribution to adsorption mechanism
BET	Surface area increased from 91.38 to 798.35 m^2/g	Enhanced accessibility of adsorption sites
SEM	Well-developed interconnected pores after KOH activation	Improved diffusion of AMX molecules
FTIR	Increased OH, C=O and C–O functionalities	Hydrogen bonding sites
XPS	Changes in C–OH, C=C and COOH signals after adsorption	Participation of oxygen-containing groups
pH_{PZC}	pHPZC = 6.3	Supports pH dependent electrostatic interactions

RSM	Highest removal at pH 4	Favourable electrostatic attraction under acidic conditions
Kinetic	PSO model best fit	Interaction-controlled adsorption process
Isotherm	Langmuir model best fit	Predominantly monolayer adsorption
DFT	PKSAC–OH : AMX–COOH showed strongest interaction	Hydrogen bonding identified as dominant interaction
HOMO-LUMO	Lowest energy gap (0.15 eV) for strongest complex	Greater adsorption stability

Overall, the combined evidence obtained from characterization, adsorption experiments, kinetic modelling, isotherm analysis and DFT calculations consistently indicates that AMX adsorption onto PKSAC is primarily governed by hydrogen bonding, supported by electrostatic interactions and facilitated by the porous structure generated during KOH activation.

CHAPTER 5
CONCLUSION AND RECOMMENDATIONS

5.1 Conclusion

KOH activation successfully transformed palm kernel shell biochar into a highly porous activated carbon with enhanced surface functionality. The BET surface area increased from 91.38 to 798.35 m^2/g, accompanied by the development of a hierarchical pore structure and the introduction of oxygen-containing functional groups. Characterization through BET, SEM, FTIR, XPS, and elemental analyses confirmed that the activation process substantially improved the physicochemical properties of the material, providing favorable adsorption sites for AMX removal.

The adsorption performance of PKSAC was subsequently optimized using RSM. Experimental optimization identified optimum conditions of 0.5 g adsorbent dosage, pH 4.0, and 50 minutes of contact time, resulting in a maximum AMX removal efficiency of 86.82%. Furthermore, numerical optimization using the desirability function predicted an optimum AMX removal efficiency of 90.85% at an adsorbent dosage of 0.494 g, pH 4.12, and contact time of 59.29 min, with a desirability value of 1.000. The optimized acidic condition is consistent with previous studies on AMX adsorption using activated carbon-based adsorbents, where enhanced adsorption was commonly observed due to favourable electrostatic interactions and hydrogen bonding between AMX molecules and oxygen-containing functional groups on the adsorbent surface. These findings demonstrate the effectiveness of RSM as both a predictive and optimization tool for adsorption processes and further support the validity of the optimized operating conditions identified in this study.

Adsorption equilibrium and kinetic investigations revealed important information regarding the adsorption behaviour of AMX onto PKSAC. The pseudo-second-order model provided the best description of the adsorption kinetics, indicating an interaction-controlled adsorption process. Equilibrium data were best represented by the Langmuir and Redlich–Peterson models, suggesting predominantly monolayer adsorption on relatively homogeneous adsorption sites. The increase in adsorption capacity with increasing temperature further indicated that the adsorption process was thermodynamically favorable at elevated temperatures.

The adsorption mechanism was elucidated through the integration of characterization results, adsorption studies, and DFT simulations. FTIR and XPS analyses demonstrated the participation of oxygen-containing functional groups during adsorption, while pH_{PZC} analysis highlighted the role of solution pH in governing surface charge interactions. DFT calculations identified the PKSAC–OH: AMX–COOH complex as the most favorable adsorption configuration, exhibiting the highest adsorption energy (−118.67 kJ/mol) and the lowest HOMO–LUMO energy gap (0.15 eV). Collectively, the findings indicate that hydrogen bonding is the dominant adsorption mechanism, supported by electrostatic interactions and facilitated by the porous structure generated through KOH activation.

5.2 Recommendations

Based on the findings and contributions of this study, several recommendations are proposed to guide future research and the practical deployment of PKSAC in environmental remediation applications.

Future studies should evaluate the performance of PKSAC in real wastewater systems. While the current research focused on synthetic AMX solutions, actual wastewater contains multiple coexisting contaminants, organic matter, and variable physicochemical conditions that may affect adsorption efficiency. Investigating PKSAC under such complex environmental matrices will provide a more realistic assessment of its practical viability in real-world treatment scenarios.

It is also recommended to investigate the adsorption performance of PKSAC in dynamic flow systems, such as continuous fixed-bed columns. Although batch experiments are valuable for mechanistic and equilibrium studies under controlled conditions, they do not capture the operational variability of industrial-scale systems. Column studies can offer essential insights into breakthrough behavior, saturation dynamics, and adsorbent regeneration potential, all of which are critical for process scale-up and long-term implementation.

Moreover, while this study utilized DFT to model molecular interactions between PKSAC and AMX, future computational work should explore the effects of competitive adsorption, solvation, and multi-contaminant systems. Further investigation into adsorption thermodynamics and electron density distributions could deepen the understanding of adsorbent selectivity and binding mechanisms, especially

in relation to specific surface functionalities.

Importantly, this study identified surface hydroxyl groups as main contributors to enhanced adsorption interactions. Given their demonstrated role in binding various functional groups on AMX, future research should investigate whether tailoring carbon adsorbents to enrich hydroxyl groups could improve performance across a wider spectrum of pharmaceutical and organic pollutants. This direction may offer a generalizable strategy for optimizing bio-based adsorbents for diverse environmental applications.

Finally, conducting a life cycle assessment (LCA) and cost-benefit analysis of PKSAC production and utilization is essential for evaluating its scalability and environmental impact. Integrating these environmental and economic assessments can support informed policymaking and promote the adoption of sustainable, biochar-based technologies in decentralized wastewater treatment systems.

REFERENCES

Acosta, R., Fierro, V., Martinez de Yuso, A., Nabarlatz, D., & Celzard, A. (2016). Tetracycline adsorption onto activated carbons produced by KOH activation of tyre pyrolysis char. *Chemosphere, 149, 168–176.* https://doi.org/10.1016/j.chemosphere.2016.01.093

Adzima, F., Nasir, M., Mangala Praveena, S., Aris, A. Z., Mangala, S., & Zaharin, A. (2019). Ecotoxicology and Environmental Safety Public awareness level and occurrence of pharmaceutical residues in drinking water with potential health risk : A study from Kajang (Malaysia). *Ecotoxicology and Environmental Safety*, *185*(August), 109681. https://doi.org/10.1016/j.ecoenv.2019.109681

Adzima, F., Nasir, M., Mangala, S., & Zaharin, A. (2019). Public awareness level and occurrence of pharmaceutical residues in drinking water with potential health risk : A study from Kajang (Malaysia). *Ecotoxicology and Environmental Safety*, *185*(August), 109681. https://doi.org/10.1016/j.ecoenv.2019.109681

Aghababaei, A., Ncibi, M. C., & Sillanpää, M. (2017). Optimized removal of oxytetracycline and cadmium from contaminated waters using chemically-activated and pyrolyzed biochars from forest and wood-processing residues. *Bioresource Technology*, *239*, 28–36. https://doi.org/10.1016/J.BIORTECH.2017.04.119

Ahmad, A. A., Alwahbi, A., Khatib, L. A. Al, & Dammag, H. (2024). Biomass-Based Activated Carbon. In *From Biomass to Biobased Products*.

Ahmad, I., Malak, H. A., & Abulreesh, H. H. (2021). Environmental antimicrobial resistance and its drivers : a potential threat to public health. *Journal of Global Antimicrobial Resistance*, *27*, 101–111. https://doi.org/10.1016/j.jgar.2021.08.001

Ahmed, M. B., Zhou, J. L., Ngo, H. H., Guo, W., Johir, M. A. H., & Sornalingam, K. (2017). Single and competitive sorption properties and mechanism of functionalized biochar for removing sulfonamide antibiotics from water. Chemical Engineering Journal, 311, 348–358.https://doi.org/10.1016/j.cej.2016.11.106

Ahmed, M. B., Zhou, J. L., Ngo, H. H., & Guo, W. (2015). Adsorptive removal of antibiotics from water and wastewater: Progress and challenges. *Science of the Total Environment*, *532*, 112–126. https://doi.org/10.1016/j.scitotenv.2015.05.130

Ahmed, M. J., & Theydan, S. K. (2012a). Adsorption of cephalexin onto activated carbons from Albizia lebbeck seed pods by microwave-induced KOH and K2CO3

activations. *Chemical Engineering Journal*, *211–212*, 200–207. https://doi.org/10.1016/j.cej.2012.09.089

Ahmed, M. J., & Theydan, S. K. (2012b). Physical and chemical characteristics of activated carbon prepared by pyrolysis of chemically treated date stones and its ability to adsorb organics. *Powder Technology*, *229*, 237–245. https://doi.org/10.1016/j.powtec.2012.06.043

Ajala, O. A., Akinnawo, S. O., Bamisaye, A., Adedipe, D. T., Adesina, M. O., Okon-Akan, O. A., Adebusuyi, T. A., Ojedokun, A. titi, Adegoke, K. A., & Bello, O. S. (2023). Adsorptive removal of antibiotic pollutants from wastewater using biomass/biochar-based adsorbents. *RSC Advances*, *13*, 4678–4712. https://doi.org/10.1039/D2RA06436G

Ajebli, S., Kaichouh, G., Khachani, M., Babas, H., Karbane, M. El, Warad, I., Safi, Z. S., Berisha, A., Mehmeti, V., Guenbour, A., Bellaouchou, A., & Zarrouk, A. (2022). The adsorption of Tenofovir in aqueous solution on activated carbon produced from maize cobs : Insights from experimental , molecular dynamics simulation , and DFT calculations. *Chemical Physics Letters*, *801*(May), 139676. https://doi.org/10.1016/j.cplett.2022.139676

Al-Qaim, F. F., Haider Mussa, Z., Yuzir, A., Abu Tahrim, N., Hashim, N., & Azman, S. (2018). Transportation of Different Therapeutic Classes of Pharmaceuticals to the Surface Water, Sewage Treatment Plant, and Hospital Samples, Malaysia. *Water*, *Lc*, 1–16. https://doi.org/10.3390/w10070916

Alardhi, S. M., Ali, N. S., Cata, N. M., Zendehboudi, S., Salih, I. K., Alrubaye, J. M., & Albayati, T. M. (2024). Separation techniques in different configurations of hybrid systems via synergetic adsorption and membrane processes for water treatment : A review. *Journal of Industrial and Engineering Chemistry*, *130*, 91–104. https://doi.org/10.1016/j.jiec.2023.09.051

Amarasiri, M., Sano, D., & Suzuki, S. (2020). Technology Understanding human health risks caused by antibiotic resistant bacteria (ARB) and antibiotic resistance genes (ARG) in water environments : Current knowledge and questions to be answered. *Environmental Science and Technology*, *50*(19), 2016–2059. https://doi.org/10.1080/10643389.2019.1692611

Anastopoulos, I., Pashalidis, I., Orfanos, A. G., & Manariotis, I. D. (2020). *Removal of caffeine , nicotine and amoxicillin from (waste) waters by various adsorbents . A review*. *261*(January). https://doi.org/10.1016/j.jenvman.2020.110236

Antonelli, R., Malpass, P., Gurgel, M., Gurgel, M., & Vieira, A. (2021). Fixed-Bed Adsorption of Cipro fl oxacin onto Bentonite Clay : Characterization , Mathematical Modeling , and DFT-Based Calculations. *Industrial & Engineering Chemistry Reseacrh*. https://doi.org/10.1021/acs.iecr.0c05700

Anuar, N. F., Iskandar Shah, D. R. S., Ramli, F. F., Md Zaini, M. S., Mohammadi,Nasrin Agha, Mohamad Daud, A. R., & Syed-Hassan, S. S. A. (2023). The removal of antibiotics in water by chemically modified carbonaceous adsorbents from biomass : A systematic review. *Journal of Cleaner Production*, *401*(November 2022), 136725. https://doi.org/10.1016/j.jclepro.2023.136725

Bagotia, N. (2025). Regeneration strategies for exhausted adsorbents used in water treatment - A critical review. *Journal of Water Process Engineering*, *69*(November 2024), 106560. https://doi.org/10.1016/j.jwpe.2024.106560

Batuman, O., Britt-ugartemendia, K., Kunwar, S., Yilmaz, S., Fessler, L., Redondo, A., Chumachenko, K., Chakravarty, S., & Wade, T. (2024). The Use and Impact of Antibiotics in Plant Agriculture : A Review. *Phytopathology*, *114*(5), 885–909.

Bedia, J., Peñas-Garzón, M., Gómez-Avilés, A., Rodriguez, J. J., & Belver, C. (2018). A Review on the Synthesis and Characterization of Biomass-Derived Carbons for Adsorption of Emerging Contaminants from Water. *Journal of Carbon Research*, *4*(4), 63. https://doi.org/10.3390/c4040063

Bedia, J., Peñas-Garzón, M., Gómez-Avilés, A., Rodriguez, J. J., & Belver, C. (2020). Review on Activated Carbons by Chemical Activation with FeCl3. *C — Journal of Carbon Research*, *6*(2), 21. https://doi.org/10.3390/c6020021

Belay, W. Y., Getachew, M., Tegegne, B. A., Teffera, Z. H., Dagne, A., Zeleke, T. K., Abebe, R. B., Gedif, A. A., Fenta, A., Yirdaw, G., Tilahun, A., & Aschale, Y. (2024). Mechanism of antibacterial resistance , strategies and next-generation antimicrobials to contain antimicrobial resistance : a review. *Pharmacology*, *August*, 1–26. https://doi.org/10.3389/fphar.2024.1444781

Bobate, S., Mahalle, S., Dafale, N. A., & Bajaj, A. (2023). Emergence of environmental antibiotic resistance : Mechanism , monitoring and management. *Environmental Advances*, *13*(August), 100409. https://doi.org/10.1016/j.envadv.2023.100409

Calvo-muñoz, E. M., García-mateos, F. J., & Rosas, J. M. (2016). *Biomass Waste carbon Materials as adsorbents for cO 2 capture under Post-combustion conditions*. *3*(May), 1–14. https://doi.org/10.3389/fmats.2016.00023

Chandrasekaran, A., Patra, C., Narayanasamy, S., & Subbiah, S. (2020). Adsorptive

removal of Ciprofloxacin and Amoxicillin from single and binary aqueous systems using acid-activated carbon from Prosopis juliflora. *Environmental Research*, *188*(June), 109825. https://doi.org/10.1016/j.envres.2020.109825

Chayid, M. A., & Ahmed, M. J. (2015). Amoxicillin adsorption on microwave prepared activated carbon from Arundo donax Linn: Isotherms, kinetics, and thermodynamics studies. *Journal of Environmental Chemical Engineering*, *3*(3), 1592–1601. https://doi.org/10.1016/j.jece.2015.05.021

Chen, Haiyang, Jing, L., Teng, Y., & Wang, J. (2018). Characterization of antibiotics in a large-scale river system of China : Occurrence pattern , spatiotemporal distribution and environmental risks. *Science of the Total Environment*, *618*, 409–418. https://doi.org/10.1016/j.scitotenv.2017.11.054

Chen, Handing, Chen, X., Qin, Y., Wei, J., & Liu, H. (2017). Bioresource Technology Effect of torrefaction on the properties of rice straw high temperature pyrolysis char : Pore structure , aromaticity and gasification activity. *Bioresource Technology*, *228*, 241–249. https://doi.org/10.1016/j.biortech.2016.12.074

Chen, J., Li, H., Li, J., Chen, F., Lan, J., & Hou, H. (2021). Efficient removal of tetracycline from water by tannic acid-modified rice straw-derived biochar:Kinetics and mechanisms. *Journal of Molecular Liquids*, *340*, 117237. https://doi.org/10.1016/j.molliq.2021.117237

Chen, T., Luo, L., Deng, S., Shi, G., Zhang, S., Zhang, Y., Deng, O., Wang, L., Zhang, J., & Wei, L. (2018). Sorption of tetracycline on H3PO4 modified biochar derived from rice straw and swine manure. *Bioresource Technology*, *267*(July), 431–437. https://doi.org/10.1016/j.biortech.2018.07.074

Cheng, D., Ngo, H. H., Guo, W., Chang, S. W., Nguyen, D. D., Zhang, X., Varjani, S., & Liu, Y. (2020). Feasibility study on a new pomelo peel derived biochar for tetracycline antibiotics removal in swine wastewater. *Science of the Total Environment*, *720*, 137662. https://doi.org/10.1016/j.scitotenv.2020.137662

Clara, M., Rosa, L., Maugeri, A., Favara, G., Mastra, C. La, Magnano, R., Lio, S., Barchitta, M., & Agodi, A. (2025). The Impact of Wastewater on Antimicrobial Resistance : A Scoping Review of Transmission Pathways and Contributing Factors. *Antibiotics*, 1–29.

Collignon, P. J., & McEwen, S. A. (2019). One Health — Its Importance in Helping to Better Control Antimicrobial Resistance. *Tropical Medicine and Infectious Disease*. https://doi.org/10.3390/tropicalmed4010022

Cuerda-Correa, E. M., Alexandre-Franco, M., & Fernández-González, C. (2019). Advanced Oxidation Processes for the Removal of Antibiotics From Water. An Overview. *Water*, *12*(1), 102. https://doi.org/10.3390/w12010102

Cuong, N. Van, Tuan, B., Doan, K., Phu, H., Van, N. T. B., Be, V., Guy, H., Carrique-, J., & Choisy, M. (2021). Effects of prophylactic and therapeutic antimicrobial uses in scale chicken flocks. *Zoonoses Public Health*, *November 2020*, 483–492. https://doi.org/10.1111/zph.12839

Darweesh, T. M., & Ahmed, M. J. (2017). Batch and fixed bed adsorption of levofloxacin on granular activated carbon from date (Phoenix dactylifera L.) stones by KOH chemical activation. *Environmental Toxicology and Pharmacology*, *50*, 159–166. https://doi.org/https://doi.org/10.1016/j.etap.2017.02.005

DasSharma, D., Samanta, S., S, D. N. K., & Halder, G. (2020). A mechanistic insight into enrofloxacin sorptive affinity of chemically activated carbon engineered from green coconut shell. *Journal of Environmental Chemical Engineering*, *8*(5), 104140. https://doi.org/https://doi.org/10.1016/j.jece.2020.104140

Dhingra, S., Rahman, N. A. A., Peile, E., & Rahman, M. (2020). Microbial Resistance Movements : An Overview of Global Public Health Threats Posed by Antimicrobial Resistance , and How Best to Counter. *Frontiers in Public Health*, *8*(November), 1–22. https://doi.org/10.3389/fpubh.2020.535668

Ejraei, A., Ali, M., & Ziarati, A. (2019). Wastewater treatment using a hybrid system combining adsorption , photocatalytic degradation and membrane fi ltration processes. *Journal of Water Process Engineering*, *28*(August 2018), 45–53. https://doi.org/10.1016/j.jwpe.2019.01.003

Gao, Y., Yue, Q., Gao, B., & Li, A. (2020). Insight into activated carbon from different kinds of chemical activating agents : A review. *Science of the Total Environment*, *746*.

García-ávila, F., Zambrano-jaramillo, A., Velecela-garay, C., Coronel-sánchez, K., & Valdiviezo-gonzalez, L. (2024). Effectiveness of membrane technologies in removing emerging contaminants from wastewater: Reverse Osmosis and Nanofiltration. *Water Cycle*. https://doi.org/10.1016/j.watcyc.2024.12.004

Gaynes, R. (2017). The Discovery of Penicillin — New Insights After More Than 75 Years of Clinical Use. *Emerging Infectious Diseases*, *23*(5).

Geng, X., Lv, S., Yang, J., Cui, S., & Zhao, Z. (2021). Carboxyl-functionalized biochar derived from walnut shells with enhanced aqueous adsorption of

sulfonamide antibiotics. *Journal of Environmental Management*, *280*. https://doi.org/10.1016/j.jenvman.2020.111749

Grenni, P., Ancona, V., & Caracciolo, A. B. (2018). Ecological effects of antibiotics on natural ecosystems: A review. *Microchemical Journal*. https://doi.org/10.1016/j.microc.2017.02.006

Gusti, Y. (2025). Carbon-Based adsorbents for heavy metal removal in Wastewater : Green technology or environmental Burden ? *Environmental Nanotechnology, Monitoring & Management*, *23*(January), 101051. https://doi.org/10.1016/j.enmm.2025.101051

Hafizuddin, M. S., Lee, C. L., Chin, K. L., H'ng, P. S., Khoo, P. S., & Rashid, U. (2021). Fabrication of highly microporous structure activated carbon via surface modification with sodium hydroxide. *Polymers*, *13*(22), 1–16. https://doi.org/10.3390/polym13223954

Haghighat, G. A., Saghi, M. H., Anastopoulos, I., Javid, A., Roudbari, A., Talebi, S. S., Ghadiri, S. K., Giannakoudakis, D. A., & Shams, M. (2020). Aminated graphitic carbon derived from corn stover biomass as adsorbent against antibiotic tetracycline: Optimizing the physicochemical parameters. *Journal of Molecular Liquids*, *313*. https://doi.org/10.1016/j.molliq.2020.113523

Haque, A., Rogerson, L., Deb, N., Haruna, S., Ahn, J., Johnston, T. V, Sze, C., Lin, K., Chong, L., Na, L., Ji, M., & Ku, S. (2024). Sustainable management and valorization of antibiotic waste. *Chemical Engineering Journal*, *498*(June). https://doi.org/10.1016/j.cej.2024.155372

Hazra, M., & Durso, L. M. (2022). Performance Efficiency of Conventional Treatment Plants and Constructed Wetlands towards Reduction of Antibiotic Resistance. *Antibiotics*.

Heard, M. J., Barton, C. E., Frost, V., & Hongo, R. A. (2021). Sourcing Antibiotic-Resistant Escherichia Coli in Aquatic Ecosystems: A Combined Laboratory and Field Module. *Journal of Microbiology and Biology Education*, *22*(3). https://doi.org/10.1128/jmbe.00207-21

Hoseinzadeh, R., Mohd, W., Wan, A., Sahu, J. N., & Arami-niya, A. (2013). Journal of Analytical and Applied Pyrolysis The effects of a microwave heating method on the production of activated carbon from agricultural waste : A review. *Journal of Analytical and Applied Pyrolysis*, *100*, 1–11. https://doi.org/10.1016/j.jaap.2012.12.019

Huang, A., Yan, M., Lin, J., Xu, L., Gong, H., & Gong, H. (2021). A review of processes for removing antibiotics from breeding wastewater. *International Journal of Environmental Research and Public Health*, *18*(9). https://doi.org/10.3390/ijerph18094909

Huang, H., Tang, J., Gao, K., He, R., Zhao, H., & Werner, D. (2017a). Characterization of KOH modified biochars from different pyrolysis temperatures and enhanced adsorption of antibiotics. *RSC Advances*, *7*(24), 14640–14648. https://doi.org/10.1039/c6ra27881g

Huang, S., Yu, J., Li, C., Zhu, Q., Zhang, Y., Lichtfouse, É., & Marmier, N. (2022). The Effect Review of Various Biological, Physical and Chemical Methods on the Removal of Antibiotics. *Water*, *14*(19), 3138. https://doi.org/10.3390/w14193138

Huat, S., Yee, C., Chin, J., Nai, P., Yek, Y., Chung, C., Swee, C., Yein, K., Keey, R., & Shiung, S. (2022). Removal of heavy metals using activated carbon from microwave steam activation of palm kernel shell. *Environmental Advances*, *9*(March), 100272. https://doi.org/10.1016/j.envadv.2022.100272

Hussain, M., Riaz, A., Zeb, H., Ali, A., Mujahid, R., Ahmad, F., & Shahzad, M. (2025). Paving the path to water security : The role of advanced adsorbents in wastewater treatment. *Journal of Water Process Engineering*, *71*(February), 107333. https://doi.org/10.1016/j.jwpe.2025.107333

Jafari, K., Heidari, M., Fatehizadeh, A., Dindarloo, K., Alipour, V., & Rahmanian, O. (2023). Extensive Sorption of Amoxicillin by Highly Efficient Carbon-Based Adsorbent From Palm Kernel: Artificial Neural Network Modeling. In *Heliyon*. https://doi.org/10.1016/j.heliyon.2023.e18635

Jais, F. M., Ibrahim, S., Chee, C. Y., & Ismail, Z. (2021). High removal of crystal violet dye and tetracycline by hydrochloric acid assisted hydrothermal carbonization of sugarcane bagasse prepared at high yield. *Sustainable Chemistry and Pharmacy*, *24*(June), 100541. https://doi.org/10.1016/j.scp.2021.100541

Jang, H. M., Yoo, S., Choi, Y.-K., Park, S., & Kan, E. (2018). Adsorption isotherm, kinetic modeling and mechanism of tetracycline on Pinus taeda-derived activated biochar. *Bioresource Technology*, *259*, 24–31. https://doi.org/10.1016/j.biortech.2018.03.013

Jawad, A. H., & Surip, S. N. (2022). Diamond & Related Materials Upgrading low rank coal into mesoporous activated carbon via microwave process for methylene blue dye adsorption : Box Behnken Design and mechanism study. *Diamond & Related*

Materials, *127*(May), 109199. https://doi.org/10.1016/j.diamond.2022.109199

Kamalesh, R., Karishma, S., Saravanan, A., & Yaashikaa, P. R. (2024). Sustainable Chemistry for the Environment Emerging breakthroughs in membrane filtration techniques and their application in agricultural wastewater treatment : Reusability aspects. *Sustainable Chemistry for the Environment*, *8*(November), 100183. https://doi.org/10.1016/j.scenv.2024.100183

Khader, E. H., Muslim, S. A., Cata, N. M., Ali, N. S., & Salih, I. K. (2024). Recent advances in photocatalytic advanced oxidation processes for organic compound degradation: A review. *Desalination and Water Treatment*, *318*(March), 100384. https://doi.org/10.1016/j.dwt.2024.100384

Kovalakova, P., Cizmas, L., Mcdonald, T. J., Marsalek, B., Feng, M., & Sharma, V. K. (2020). Chemosphere Occurrence and toxicity of antibiotics in the aquatic environment : A review. *Chemosphere*, *251*, 126351. https://doi.org/10.1016/j.chemosphere.2020.126351

Kraemer, S. A., Ramachandran, A., & Perron, G. G. (2019). Antibiotic Pollution in the Environment : From Microbial Ecology to Public Policy. *Microorganisms*, 1–24.

Krasucka, P., Pan, B., Sik Ok, Y., Mohan, D., Sarkar, B., & Oleszczuk, P. (2021). Engineered biochar – A sustainable solution for the removal of antibiotics from water. *Chemical Engineering Journal*, *405*(June 2020), 126926. https://doi.org/10.1016/j.cej.2020.126926

Kumar, M., Jaiswal, S., Sodhi, K. K., Shree, P., Singh, D. K., Agrawal, P. K., & Shukla, P. (2019). Antibiotics bioremediation: Perspectives on its ecotoxicity and resistance. In *Environment International* (Vol. 124, pp. 448–461). Elsevier Ltd. https://doi.org/10.1016/j.envint.2018.12.065

Kumar, U., Kuntail, J., Kumar, A., Prakash, R., Pai, M. R., & Sinha, I. (2022). In-situ H2O2 production for tetracycline degradation on Ag/s-(Co3O4/NiFe2O4) visible light magnetically recyclable photocatalyst. *Applied Surface Science*, *589*(December 2021), 153013. https://doi.org/10.1016/j.apsusc.2022.153013

Largitte, L., & Pasquier, R. (2016). Chemical Engineering Research and Design A review of the kinetics adsorption models and their application to the adsorption of lead by an activated carbon. *Chemical Engineering Research and Design*, *109*, 495–504. https://doi.org/10.1016/j.cherd.2016.02.006

Larsson, D. G. J., & Flach, C. (2021). Antibiotic Resistance in the Environment. *Nature Reviews Microbiology*, *20*(5), 257–269. https://doi.org/10.1038/s41579-021-

00649-x

Lean, E., Weng, C., Takada, H., Seki, K., Takei, A., & Suzuki, S. (2021). Antibiotic residues from aquaculture farms and their ecological risks in Southeast Asia : a case study from Malaysia. *Ecosystem Health and Sustainability*, *7*(1), 1–18. https://doi.org/10.1080/20964129.2021.1926337

Lee, B., Cheen, C., Shuaib, M., Saheed, M., Show, P., Chang, J., Chuan, T., Shiung, S., & Ching, J. (2020). Conventional and emerging technologies for removal of antibiotics from wastewater. *Journal of Hazardous Materials*, *400*(April), 122961. https://doi.org/10.1016/j.jhazmat.2020.122961

Li, B., Huang, Y., Wang, Z., Li, J., Liu, Z., & Fan, S. (2021). Enhanced adsorption capacity of tetracycline on tea waste biochar with KHCO3 activation from aqueous solution. *Environmental Science and Pollution Research*, *28*(32), 44140–44151. https://doi.org/10.1007/s11356-021-13817-6

Li, H., Hu, J., Yao, L., Shen, Q., An, L., & Wang, X. (2020). Ultrahigh adsorbability towards different antibiotic residues on fore-modified self-functionalized biochar: Competitive adsorption and mechanism studies. *Journal of Hazardous Materials*, *390*. https://doi.org/10.1016/j.jhazmat.2020.122127

Li, M., Wang, S., Gao, H., Yin, Z., Chen, C., Yang, H., Fang, L., Angadi, V. J., Yi, Z., & Li, D. (2022). Selective Removal of Antibiotics Over $MgAl_2O_4/C_3N_4/YMnO_3$ Photocatalysts: Performance Prediction and Mechanism Insight. *Journal of the American Ceramic Society*, *106*(4), 2420–2442. https://doi.org/10.1111/jace.18946

Lim, A. H., Ab Rahman, N., Hashim, H., Kamal, M., Velvanathan, T., Chok, M. C. F., & Sivasampu, S. (2023). Impact of COVID-19 Pandemic on Antibiotic Utilisation in Malaysian Primary Care Clinics: An Interrupted Time Series Analysis. *Antibiotics*, *12*(4). https://doi.org/10.3390/antibiotics12040659

Lim, A. H., Ab Rahman, N., Nasarudin, S. N. S., Velvanathan, T., Fong, M. C. C., Mohamad Yahaya, A. H., & Sivasampu, S. (2024). A comparison between antibiotic utilisation in public and private community healthcare in Malaysia. *BMC Public Health*, *24*(1), 1–8. https://doi.org/10.1186/s12889-023-17579-3

Limousy, L., Ghouma, I., Ouederni, A., & Jeguirim, M. (2016). Amoxicillin removal from aqueous solution using activated carbon prepared by chemical activation of olive stone. *Environmental Science and Pollution Research*. https://doi.org/10.1007/s11356-016-7404-8

Liu, H., Liu, Y., Li, X., Zheng, X., Feng, X., & Yu, A. (2022). Adsorption and Fenton-like Degradation of Ciprofloxacin Using Corncob Biochar-Based Magnetic Iron–Copper Bimetallic Nanomaterial in Aqueous Solutions. *Nanomaterials*, *12*(4). https://doi.org/10.3390/nano12040579

Liu, P., Liu, W.-J., Jiang, H., Chen, J.-J., Li, W.-W., & Yu, H.-Q. (2012). *Modification of bio-char derived from fast pyrolysis of biomass and its application in removal of tetracycline from aqueous solution*. *121*, 235–240. https://doi.org/10.1016/j.biortech.2012.06.085

Low, K., Chai, L., Lee, C., Zhang, G., Zhang, R., Vahab, V., & Bong, C. (2021). Prevalence and risk assessment of antibiotics in riverine estuarine waters of Larut and Sangga Besar River , Perak*. *Journal of Oceanology and Limnology*, *39*(1), 122–134.

Luo, B., Huang, G., Yao, Y., An, C., Zhang, P., & Zhao, K. (2021). Investigation into the influencing factors and adsorption characteristics in the removal of sulfonamide antibiotics by carbonaceous materials. *Journal of Cleaner Production*, *319*(August), 128692. https://doi.org/10.1016/j.jclepro.2021.128692

Lv, M., Zhang, D., Niu, X., Ma, J., Lin, Z., & Fu, M. (2022). Insights into the fate of antibiotics in constructed wetland systems : Removal performance and mechanisms. *Journal of Environmental Management*, *321*(August), 116028. https://doi.org/10.1016/j.jenvman.2022.116028

Ma, Y., Li, M., Li, P., Yang, L., Wu, L., Gao, F., Qi, X., & Zhang, Z. (2021). Hydrothermal synthesis of magnetic sludge biochar for tetracycline and ciprofloxacin adsorptive removal. *Bioresource Technology*, *319*(September 2020), 124199. https://doi.org/10.1016/j.biortech.2020.124199

Mackuľak, T. s, Cernanský, S., Fehér, M., & Gál, M. (2019). Pharmaceuticals , drugs , and resistant microorganisms — environmental impact on population health Macku Tomá s Lucia Biro. *Environmental Science & Health*, 40–48. https://doi.org/10.1016/j.coesh.2019.04.002

Maged, A., Dissanayake, P. D., Yang, X., Pathirannahalage, C., Bhatnagar, A., & Ok, Y. S. (2021). New mechanistic insight into rapid adsorption of pharmaceuticals from water utilizing activated biochar. *Environmental Research*, *202*, 111693. https://doi.org/https://doi.org/10.1016/j.envres.2021.111693

Mahtab, T., Jyoti, A., Khusro, A., Redwan, B. M., Zidan, M., Mitra, S., Bin, T., Dhama, K., Hossain, K., Gajdács, M., Umar, M., Sahibzada, K., Hossain, J., & Koirala, N.

(2021). Antibiotic resistance in microbes : History , mechanisms , therapeutic strategies and future prospects. *Journal of Infection and Public Health*, *14*, 1750–1766. https://doi.org/10.1016/j.jiph.2021.10.020

Mandal, S., Natarajan, S., Mani, P., & Pankajakshan, A. (2020). Post-Synthetic Modification of Metal–Organic Frameworks Toward Applications. *Advanced Functional Materials*, *31*(4). https://doi.org/10.1002/adfm.202006291

Mangala Praveena, S., Norashikin, S., Shaifuddin, M., Sukiman, S., Adzima, F., Nasir, M., Hanafi, Z., Kamarudin, N., Hanidza, T., Ismail, T., & Aris, A. Z. (2018). Pharmaceuticals residues in selected tropical surface water bodies from Selangor (Malaysia): Occurrence and potential risk assessments. *Science of the Total Environment*, *642*, 230–240. https://doi.org/10.1016/j.scitotenv.2018.06.058

Mangala Praveena, S., Zahirah, M., Rashid, M., Adzima, F., Nasir, M., Yee, S., & Aris, A. Z. (2019). *Occurrence and potential human health risk of pharmaceutical residues in drinking water from Putrajaya (Malaysia)*. https://doi.org/10.1016/j.ecoenv.2019.05.051

Mangla, D., Annu, Sharma, A., & Ikram, S. (2022). Critical review on adsorptive removal of antibiotics: Present situation, challenges and future perspective. *Journal of Hazardous Materials*, *425*(October 2021), 127946. https://doi.org/10.1016/j.jhazmat.2021.127946

Manyi-Loh, C., Mamphweli, S., Meyer, E., & Okoh, A. (2018). Antibiotic Use in Agriculture and Its Consequential Resistance in Environmental Sources : Potential Public Health Implications. *Molecul*. https://doi.org/10.3390/molecules23040795

Meng, Q., Zhang, Y., Meng, D. Di, Liu, X., Zhang, Z., Gao, P., Lin, A., & Hou, L. (2020). Removal of sulfadiazine from aqueous solution by in-situ activated biochar derived from cotton shell. *Environmental Research*, *191*, 110104. https://doi.org/https://doi.org/10.1016/j.envres.2020.110104

Mohamad, Z. A., Bakon, S. K., Jamilan, M. A., Daud, N., Ciric, L., Ahmad, N., & Muhamad, N. A. (2022). Prevalence of Antibiotic-Resistant Bacteria and Antibiotic-Resistant Genes and the Quantification of Antibiotics in Drinking Water Treatment Plants of Malaysia: Protocol for a Cross-Sectional Study. *Jmir Research Protocols*, *11*(11), e37663. https://doi.org/10.2196/37663

Mostafapour, F. K., Balarak, D., & Chandrika, K. (2022). Degradation of Amoxicillin in Aqueous Solution by Nano-MgO/Uv Photocatalytic Process. *International Journal of Life Science and Pharma Research*.

https://doi.org/10.22376/ijpbs/lpr.2020.10.3.p60-66

Muteeb, G., Rehman, T., Shahwan, M., & Aatif, M. (2023). Origin of Antibiotics and Antibiotic Resistance , and Their Impacts on Drug Development : A Narrative Review. *Pharmaceuticals*, 1–54.

Ngo, T. H., Tran, H. Le, Nakada, N., Tanaka, H., & Huynh, T. H. (2021). Occurrence of pharmaceutical and personal care products in Cau River, Vietnam. *Environmental Science and Pollution Research*, 12082–12091.

Nguyen, H., You, S., & Hosseini-bandegharaei, A. (2017). Mistakes and inconsistencies regarding adsorption of contaminants from aqueous solutions : A critical review. *Water Research*, *120*, 88–116. https://doi.org/10.1016/j.watres.2017.04.014

Nguyen, V. T., Nguyen, T. B., Huang, C. P., Chen, C. W., Bui, X. T., & Dong, C. Di. (2021). Alkaline modified biochar derived from spent coffee ground for removal of tetracycline from aqueous solutions. *Journal of Water Process Engineering*, *40*(December 2020), 101908. https://doi.org/10.1016/j.jwpe.2020.101908

Nicolaou, K. C., & Rigol, S. (2018). A brief history of antibiotics and select advances in their synthesis. *The Journal of Antibiotics*, *71*(2), 153–184. https://doi.org/10.1038/ja.2017.62

Opeoluwa, S., Kayode, G., Ajani, A. O., Afolabi, T. J., Okeowo, I. O., & Adetoro, R. (2023). Optimization and Isothermal Studies of Antibiotics Mixture Biosorption From Wastewater Using Palm Kernel , Chrysophyllum albidum , and Coconut Shells Biocomposite. *Avicenna Journal of Environmental Health Engineering Avicenna*, *10*(1), 44–56. https://doi.org/10.34172/ajehe.2023.5316

Ouyang, E., Zhang, R., Fu, W. J., Zhao, R., Yang, H., Xiang, H., & He, W. (2024). Facile Synthesis of Bamboo Biochar for Efficient Adsorption of Quinolone Antibiotics: Effects and Mechanisms. *ACS Omega*. https://doi.org/10.1021/acsomega.4c07479

Pamidimukkala, P. S., & Soni, H. (2018). Efficient removal of organic pollutants with activated carbon derived from palm shell: Spectroscopic characterisation and experimental optimisation. *Journal of Environmental Chemical Engineering*, *6*(2), 3135–3149. https://doi.org/10.1016/j.jece.2018.04.013

Pego, M., Carvalho, J., & Guedes, D. (2019). Surface modifications of activated carbon and its impact on application. *Surface Review and Letters*, *26*(1), 1–10. https://doi.org/10.1142/S0218625X1830006X

Peng, L., Ren, Y., Gu, J., Qin, P., Zeng, Q., Shao, J., Lei, M., & Chai, L. (2014). Iron improving bio-char derived from microalgae on removal of tetracycline from aqueous system. *Environmental Science and Pollution Research*, *21*(12), 7631–7640. https://doi.org/10.1007/s11356-014-2677-2

Pezoti, O., Cazetta, A. L., Bedin, K. C., Souza, L. S., Martins, A. C., Silva, T. L., Santos Júnior, O. O., Visentainer, J. V., & Almeida, V. C. (2016). NaOH-activated carbon of high surface area produced from guava seeds as a high-efficiency adsorbent for amoxicillin removal: Kinetic, isotherm and thermodynamic studies. *Chemical Engineering Journal*, *288*, 778–788. https://doi.org/10.1016/j.cej.2015.12.042

Phoon, B. L., Ong, C. C., Mohamed Saheed, M. S., Show, P.-L. L., Chang, J.-S. S., Ling, T. C., Lam, S. S., & Juan, J. C. (2020). Conventional and emerging technologies for removal of antibiotics from wastewater. *Journal of Hazardous Materials*, *400*, 122961. https://doi.org/https://doi.org/10.1016/j.jhazmat.2020.122961

Polianciuc, S. I., Gurzău, A. E., Kiss, B., Ștefan, M. G., & Loghin, F. (2020). Antibiotics in the environment : causes and consequences. *Medicine and Pharmacy Reports*, *93*(3), 231–240. https://doi.org/10.15386/mpr-1742

Prasannamedha, G., Kumar, P. S., Mehala, R., Sharumitha, T. J., & Surendhar, D. (2021). Enhanced adsorptive removal of sulfamethoxazole from water using biochar derived from hydrothermal carbonization of sugarcane bagasse. *Journal of Hazardous Materials*, *407*, 124825. https://doi.org/https://doi.org/10.1016/j.jhazmat.2020.124825

Premarathna, K. S. D., Rajapaksha, A. U., Sarkar, B., Kwon, E. E., Bhatnagar, A., Ok, Y. S., & Vithanage, M. (2019). Biochar-based engineered composites for sorptive decontamination of water: A review. *Chemical Engineering Journal*, *372*, 536–550. https://doi.org/10.1016/j.cej.2019.04.097

Putra, E. K., Pranowo, R., Sunarso, J., Indraswati, N., & Ismadji, S. (2009). Performance of activated carbon and bentonite for adsorption of amoxicillin from wastewater: Mechanisms, isotherms and kinetics. *Water Research*, *43*(9), 2419–2430. https://doi.org/10.1016/j.watres.2009.02.039

Rabia, B., & Hussein, M. Z. (2020). Ecofriendly Approach for Treatment of Heavy-Metal-Contaminated Water Using Activated Carbon of Kernel Shell of Oil Palm. *Materials*, 11–13.

Rahman, N. A., Teng, C. L., & Sivasampu, S. (2016). Antibiotic Prescribing in Public

and Private Practice: A Cross-Sectional Study in Primary Care Clinics in Malaysia. *BMC Infectious Diseases*, *16*(1). https://doi.org/10.1186/s12879-016-1530-2

Ripanda, A., Rwiza, M. J., Charles, E., Hossein, M., Said, M., El, A., Mahmoud, D., Murthy, H. C. A., Bakari, R., Ali, S., Vuai, H., & Machunda, R. L. (2025). Ecological consequences of antibiotics pollution in sub-Saharan Africa : Understanding sources , pathways , and potential implications. *Emerging Contaminants*, *11*(2), 100475. https://doi.org/10.1016/j.emcon.2025.100475

Saboor, F. H., Nasirpour, N., Shahsavari, S., & Kazemian, H. (2022). The Effectiveness of MOFs for the Removal of Pharmaceuticals From Aquatic Environments: A Review Focused on Antibiotics Removal. *Chemistry - An Asian Journal*, *17*(4). https://doi.org/10.1002/asia.202101105

Salam, A., Al-amin, Y., Salam, M. T., & Pawar, J. S. (2023). Antimicrobial Resistance : A Growing Serious Threat for Global. *Healthcare*, 1–20.

Sargazi, G., Afzali, D., Mostafavi, A., & Kazemian, H. (2020). A Novel Composite Derived From a Metal Organic Framework Immobilized Within Electrospun Nanofibrous Polymers: An Efficient Methane Adsorbent. *Applied Organometallic Chemistry*, *34*(3). https://doi.org/10.1002/aoc.5448

Sayin, F., Akar, S. T., & Akar, T. (2021). From green biowaste to water treatment applications: Utilization of modified new biochar for the efficient removal of ciprofloxacin. *Sustainable Chemistry and Pharmacy*, *24*(May), 100522. https://doi.org/10.1016/j.scp.2021.100522

Shamsuddin, S., Akkawi, M. E., Zaidi, S. T. R., Ming, L. C., & Manan, M. M. (2016). Antimicrobial drug use in primary healthcare clinics: a retrospective evaluation. *International Journal of Infectious Diseases*, *52*, 16–22. https://doi.org/10.1016/j.ijid.2016.09.013

Sharafinia, S., Rashidi, A., Tabarkhoon, F., Dehghan, F., Tabarkhoon, F., & Bazmi, M. (2023). Effective adsorption of amoxicillin by using UIO-66@ Cr-MIL-101 nanohybrid: isotherm, kinetic, thermodynamic, and optimization by central composite design. *Scientific Reports*, *13*(1), 22689. https://doi.org/10.1038/s41598-023-49393-7

Sharma, N., Yadav, A., Yadav, S., Panghal, P., Singh, S., Deep, A., & Kumar, S. (2024). Biomass-based adsorbents for wastewater remediation : A systematic review on removal of emerging contaminants. *Microchemical Journal*, *207*(August), 111880. https://doi.org/10.1016/j.microc.2024.111880

Shirani, Z., Song, H., & Bhatnagar, A. (2020). Efficient removal of diclofenac and cephalexin from aqueous solution using Anthriscus sylvestris-derived activated biochar. *Science of The Total Environment*, *745*, 140789. https://doi.org/10.1016/J.SCITOTENV.2020.140789

Singh, A., Chaurasia, D., Khan, N., Singh, E., & Bhargava, P. C. (2023). Efficient mitigation of emerging antibiotics residues from water matrix : Integrated approaches and sustainable technologies. *Environmental Pollution*, *328*(March), 121552. https://doi.org/10.1016/j.envpol.2023.121552

Sinthuchai, D., Boontanon, S. K., Boontanon, N., & Polprasert, C. (2016). Evaluation of removal efficiency of human antibiotics in wastewater treatment plants in Bangkok, Thailand. *Water Science & Technology*, 182–191. https://doi.org/10.2166/wst.2015.484

Sosa-Hernandez, J. E., Rodas-zuluaga, L. I., Itzel, Y. L., Melchor-martínez, E. M., Aghalari, Z., Salas, D., & Parra-saldívar, R. (2021). Case Studies in Chemical and Environmental Engineering Sources of antibiotics pollutants in the aquatic environment under SARS-CoV-2 pandemic situation. *Case Studies in Chemical and Environmental Engineering*, *4*. https://doi.org/10.1016/j.cscee.2021.100127

Sousa, É., Rocha, L., Jaria, G., Gil, M. V., Otero, M., Esteves, V. I., & Calisto, V. (2021). Optimizing microwave-assisted production of waste-based activated carbons for the removal of antibiotics from water. *Science of the Total Environment*, *752*, 141662. https://doi.org/10.1016/j.scitotenv.2020.141662

Spaltro, A., Pila, M. N., Colasurdo, D. D., Noseda, E., Rom, G., Simonetti, S., & Ruiz, D. L. (2021). Removal of paracetamol from aqueous solution by activated carbon and silica . Experimental and computational study. *Journal of Contaminant Hydrology*, *236*(November 2020). https://doi.org/10.1016/j.jconhyd.2020.103739

Spessato, L., Bedin, K. C., Cazetta, A. L., Souza, I. P. A. F., Duarte, V. A., Crespo, L. H. S., Silva, M. C., Pontes, R. M., & Almeida, V. C. (2019). KOH-super activated carbon from biomass waste : Insights into the paracetamol adsorption mechanism and thermal regeneration cycles. *Journal of Hazardous Materials*, *371*(February), 499–505. https://doi.org/10.1016/j.jhazmat.2019.02.102

Subari, S. N. M., Osman, R., & Saim, N. (2017). Occurrence, source apportionment and environmental risk assessment of pharmaceuticals in Klang river, Malaysia. *Pertanika Journal of Science and Technology*, *25*, 119–128. https://api.semanticscholar.org/CorpusID:119092263

Sultana, M., Hasan, M., Sabrin, M., Rahaman, H., & Alam, N. (2022). A review on experimental chemically modified activated carbon to enhance dye and heavy metals adsorption. *Cleaner Engineering and Technology*, *6*, 100382. https://doi.org/10.1016/j.clet.2021.100382

Taheran, M., Naghdi, M., Brar, S. K. K., Knystautas, E. J. J., Verma, M., Ramirez, A. A. A., Surampalli, R. Y. Y., & Valero, J. R. R. (2016). Adsorption study of environmentally relevant concentrations of chlortetracycline on pinewood biochar. *Science of the Total Environment*, *571*, 772–777. https://doi.org/10.1016/j.scitotenv.2016.07.050

Theamwong, N., Intarabumrung, W., Sangon, S., Aintharabunya, S., Ngernyen, Y., Hunt, A. J., & Supanchaiyamat, N. (2021). Activated carbons from waste Cassia bakeriana seed pods as high-performance adsorbents for toxic anionic dye and ciprofloxacin antibiotic remediation. *Bioresource Technology*, *341*(July), 125832. https://doi.org/10.1016/j.biortech.2021.125832

Thongpat, W., Taweekun, J., & Maliwan, K. (2021). Synthesis and characterization of microporous activated carbon from rubberwood by chemical activation with KOH. *Carbon Letters*, *0123456789*. https://doi.org/10.1007/s42823-020-00224-z

Tian, C., Huang, W., Wei, Z., Chen, L., Dong, Y., Ji, S., Zhang, X., Nong, G., Wang, S., & Xu, J. (2023). Photocatalytic Degradation of Different Antibiotics Using TiO_2–carbon Composites: A Case Study of Tetracycline and Ciprofloxacin. *New Journal of Chemistry*, *47*(42), 19646–19656. https://doi.org/10.1039/d3nj02748a

Tiryaki, B., Yagmur, E., Banford, A., & Aktas, Z. (2014). Comparison of activated carbon produced from natural biomass and equivalent chemical compositions. *Journal of Analytical and Applied Pyrolysis*, *105*, 276–283. https://doi.org/10.1016/j.jaap.2013.11.014

Turk Sekulic, M., Boskovic, N., Milanovic, M., Grujic Letic, N., Gligoric, E., & Pap, S. (2019). An insight into the adsorption of three emerging pharmaceutical contaminants on multifunctional carbonous adsorbent: Mechanisms, modelling and metal coadsorption. *Journal of Molecular Liquids*, *284*, 372–382. https://doi.org/10.1016/j.molliq.2019.04.020

Ullah, S., Shoaib, S., Shah, A., Altaf, M., Hossain, I., El, M. E., Kallel, M., El-bahy, Z. M., Najam, T., & Altaf, M. (2024). Activated carbon derived from biomass for wastewater treatment : Synthesis , application and future challenges. *Journal of Analytical and Applied Pyrolysis*, *179*(March), 106480.

https://doi.org/10.1016/j.jaap.2024.106480

Wahyu, M., Kim, S., Roddick, F., Xie, Z., & Fan, L. (2025). Journal of Water Process Engineering A review of the recent advancements in adsorption technology for removing antibiotics from hospital wastewater. *Journal of Water Process Engineering*, *70*(January), 106960. https://doi.org/10.1016/j.jwpe.2025.106960

Wajid, S., Shah, A., Rehman, M., Arslan, M., Abbasi, S. A., Hayat, A., Anwar, S., Iqbal, S., & Afzal, M. (2022). Response Surface Methodology for Optimization of Operational Parameters To Remove Ciprofloxacin from Contaminated Water in the Presence of a Bacterial Consortium. *Acs Omega*. https://doi.org/10.1021/acsomega.2c02448

Wan, S., Hua, Z., Sun, L., Bai, X., & Liang, L. (2016). Biosorption of nitroimidazole antibiotics onto chemically modified porous biochar prepared by experimental design: Kinetics, thermodynamics, and equilibrium analysis. *Process Safety and Environmental Protection*, *104*, 422–435. https://doi.org/10.1016/j.psep.2016.10.001

Wang, H., Lou, X., Hu, Q., & Sun, T. (2021). Adsorption of antibiotics from water by using Chinese herbal medicine residues derived biochar: Preparation and properties studies. *Journal of Molecular Liquids*, *325*, 2–10. https://doi.org/10.1016/j.molliq.2020.114967

Wang, J., & Guo, X. (2020). Adsorption isotherm models : Classification , physical meaning , application and solving method. *Chemosphere*, *258*, 127279. https://doi.org/10.1016/j.chemosphere.2020.127279

Wang, J., & Zhuan, R. (2020). Degradation of antibiotics by advanced oxidation processes : An overview. *Science of the Total Environment*, *701*, 135023. https://doi.org/10.1016/j.scitotenv.2019.135023

Wang, K., Li, J., & Zhang, G. (2019). Ag-Bridged Z-Scheme 2D/2D Bi5FeTi3O15/g-C3N4 Heterojunction for Enhanced Photocatalysis: Mediator-Induced Interfacial Charge Transfer and Mechanism Insights. *Acs Applied Materials & Interfaces*, *11*(31), 27686–27696. https://doi.org/10.1021/acsami.9b05074

Wee, S. Y., Haron, D. E. M., Aris, A. Z., Yusoff, F. M., & Praveena, S. M. (2020). Active pharmaceutical ingredients in Malaysian drinking water: consumption, exposure, and human health risk. *Environmental Geochemistry and Health*, *42*(10), 3247–3261. https://doi.org/10.1007/s10653-020-00565-8

Wei, M., Marrakchi, F., Yuan, C., Cheng, X., Jiang, D., Zafar, F. F., Fu, Y., & Wang,

S. (2022b). Adsorption modeling, thermodynamics, and DFT simulation of tetracycline onto mesoporous and high-surface-area NaOH-activated macroalgae carbon. *Journal of Hazardous Materials*, *425*, 127887. https://doi.org/10.1016/J.JHAZMAT.2021.127887

Wen, C., Liu, T., Wang, D., Wang, Y., Chen, H., Luo, G., Zhou, Z., Li, C., & Xu, M. (2023). Biochar as the effective adsorbent to combustion gaseous pollutants : Preparation , activation , functionalization and the adsorption mechanisms. *Progress in Energy and Combustion Science*, *99*(April 2022), 101098. https://doi.org/10.1016/j.pecs.2023.101098

Wu, Y., Cheng, H., Pan, D., Zhang, L., Li, W., Song, Y., Bian, Y., Jiang, X., & Han, J. (2021). Potassium hydroxide-modified algae-based biochar for the removal of sulfamethoxazole: Sorption performance and mechanisms. *Journal of Environmental Management*, *293*, 112912. https://doi.org/10.1016/j.jenvman.2021.112912

Xia, M., Li, A., Zhu, Z., Zhou, Q., & Yang, W. (2013). Factors influencing antibiotics adsorption onto engineered adsorbents. *Journal of Environmental Sciences (China)*, *25*(7), 1291–1299. https://doi.org/10.1016/S1001-0742(12)60215-0

Xiong, W., Sun, Y., Ding, X., Wang, M., & Zeng, Z. (2015). Selective Pressure of Antibiotics on ARGs and Bacterial Communities in Manure-Polluted Freshwater-Sediment Microcosms. *Frontiers in Microbiology*, *6*. https://doi.org/10.3389/fmicb.2015.00194

Xu, D., Gao, Y., Lin, Z., Gao, W., Zhang, H., Karnowo, K., Hu, X., Sun, H., Syed-Hassan, S. S. A., & Zhang, S. (2020). Application of Biochar Derived From Pyrolysis of Waste Fiberboard on Tetracycline Adsorption in Aqueous Solution. *Frontiers in Chemistry*, *7*(February), 1–11. https://doi.org/10.3389/fchem.2019.00943

Yahya, M. A., Mansor, M. H., Amani, W., & Wan, A. (2018). *A brief review on activated carbon derived from agriculture by-product A Brief Review on Activated Carbon Derived From Agriculture By-Product*. *030023*(June).

Yakout, S. M., & El-deen, G. S. (2016). Characterization of activated carbon prepared by phosphoric acid activation of olive stones. *Arabian Journal of Chemistry*, *9*, S1155–S1162. https://doi.org/10.1016/j.arabjc.2011.12.002

Yang, J., Dai, J., Wang, L., Ge, W., Xie, A., He, J., & Yan, Y. (2019). Ultrahigh adsorption of tetracycline on willow branche-derived porous carbons with tunable

pore structure: Isotherm, kinetics, thermodynamic and new mechanism study. *Journal of the Taiwan Institute of Chemical Engineers*, *96*, 473–482. https://doi.org/10.1016/j.jtice.2018.12.017

Yang, Q., Wu, P., Liu, J., Rehman, S., Ahmed, Z., Ruan, B., & Zhu, N. (2020a). Batch interaction of emerging tetracycline contaminant with novel phosphoric acid activated corn straw porous carbon: Adsorption rate and nature of mechanism. *Environmental Research*, *181*, 108899. https://doi.org/https://doi.org/10.1016/j.envres.2019.108899

Yang, Q., Wu, P., Liu, J., Rehman, S., Ahmed, Z., Ruan, B., & Zhu, N. (2020b). Batch interaction of emerging tetracycline contaminant with novel phosphoric acid activated corn straw porous carbon: Adsorption rate and nature of mechanism. In *Environmental Research* (Vol. 181). https://doi.org/10.1016/j.envres.2019.108899

Yin, S., Gao, L., Fan, X., Gao, S., Zhou, X., & Jin, W. (2024). Performance of sewage sludge treatment for the removal of antibiotic resistance genes : Status and prospects. *Science of the Total Environment*, *907*(August 2023), 167862. https://doi.org/10.1016/j.scitotenv.2023.167862

Yuan, M., Li, C., Zhang, B., Wang, J., Zhu, J., Ji, J., & Ma, Y. (2021). A mild and one-pot method to activate lignin-derived biomass by using boric acid for aqueous tetracycline antibiotics removal in water. *Chemosphere*, *280*(May), 130877. https://doi.org/10.1016/j.chemosphere.2021.130877

Zakaria, B. S., & Dhar, B. R. (2022). A Review of Stand-Alone and Hybrid Microbial Electrochemical Systems for Antibiotics Removal From Wastewater. *Processes*, *10*(4), 714. https://doi.org/10.3390/pr10040714

Zhang, J., Liu, C., Wu, Y., Li, X., Zhang, J., Liang, J., & Li, Y. (2024). Adsorption of tetracycline by polycationic straw : Density functional theory calculation for mechanism and machine learning prediction for. *Enviromental Pollution*, *340*(August 2023). https://doi.org/10.1016/j.envpol.2023.122869

Zhang, X., Gang, D. D., Zhang, J., Lei, X., Lian, Q., Holmes, W. E., Zappi, M. E., & Yao, H. (2022). Insight into the activation mechanisms of biochar by boric acid and its application for the removal of sulfamethoxazole. *Journal of Hazardous Materials*, *424*, 127333. https://doi.org/https://doi.org/10.1016/j.jhazmat.2021.127333

Zhou, Y., Liu, X., Xiang, Y., Wang, P., Zhang, J., Zhang, F., Wei, J., Luo, L., Lei, M., & Tang, L. (2017). Modification of biochar derived from sawdust and its

application in removal of tetracycline and copper from aqueous solution: Adsorption mechanism and modelling. *Bioresource Technology*, *245*(September), 266–273. https://doi.org/10.1016/j.biortech.2017.08.178

Zulfiqar, N., Nadeem, R., & Musaimi, O. Al. (2024). Photocatalytic Degradation of Antibiotics via Exploitation of a Magnetic Nanocomposite: A Green Nanotechnology Approach Toward Drug-Contaminated Wastewater Reclamation. *Acs Omega*. https://doi.org/10.1021/acsomega.3c08116

APPENDICES

APPENDIX A

Calibration curve of Amoxicillin

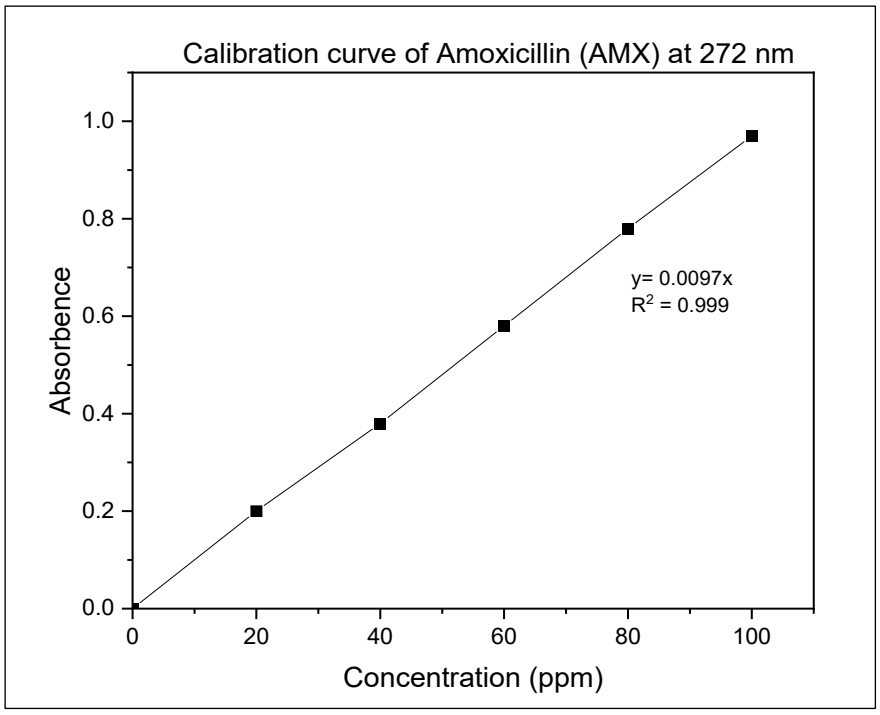

APPENDIX B

DFT analysis of AMX by using Gaussian

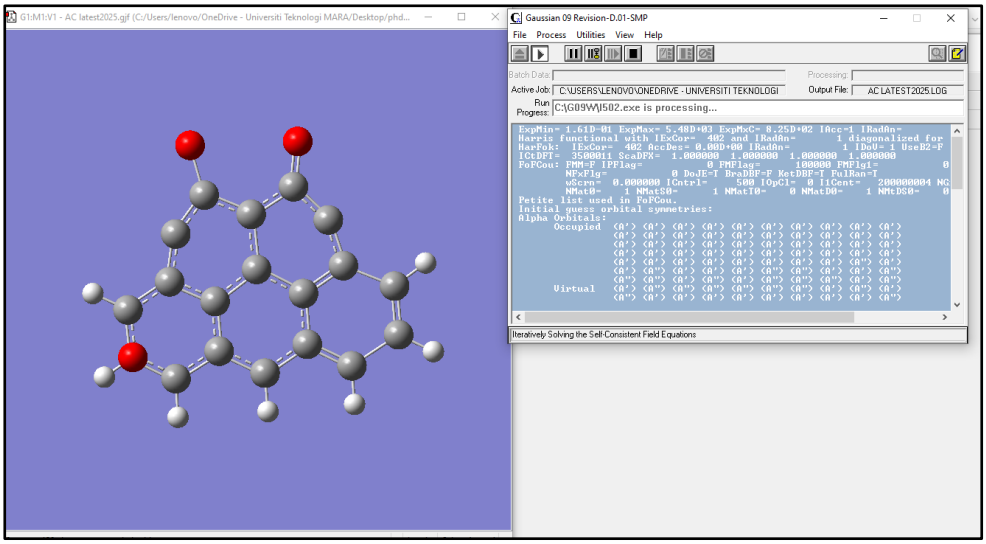

AUTHOR'S PROFILE



Nur Faradila binti Anuar earned her Bachelor of Chemical Engineering (Hons.) from Universiti Kuala Lumpur MICET, Master of Science from Universiti Malaya, and PhD in Chemical Engineering from Universiti Teknologi MARA. Her doctoral research focused on the development of KOH-modified palm kernel shell activated carbon for amoxicillin removal from water, integrating adsorption studies with advanced tools such as Response Surface Methodology and Density Functional Theory. Her expertise includes biomass valorization, surface chemistry, adsorption kinetics, and molecular simulation. She is currently involved in multidisciplinary research on sustainable materials and green water treatment technologies.

LIST OF PUBLICATION:

Anuar, N. F., Shah, D. R. S. I., Ramli, F. F., Zaini, M. S. M., Mohammadi, N. A., Daud, A. R. M., & Syed-Hassan, S. S. A. (2023). The removal of antibiotics in water by chemically modified carbonaceous adsorbents from biomass: A systematic review. *Journal of Cleaner Production*, *401*, 136725.

Anuar, N. F., Shah, D. R. S. I, Rahmat, N., Long, X., & Syed-Hassan, S. S. A., "Optimization and mechanistic insights into amoxicillin adsorption by KOH-modified palm kernel shell biochar: Experimental, Box-Behnken response surface methodology, and density functional theory analysis," *Chem. Eng. Res. Des.*, vol. 223, no. January, pp. 797–812, 2025, doi: 10.1016/j.cherd.2025.10.038.

Shah, D. R. S. I., Ramli, F. F., Anuar, N. F., Daud, W. M. A. W., & Aghamohammadi, N. (2024). A systematic review on employing thermochemical techniques for the production of exceptionally efficient biochar from discarded disposable diapers (D3). *Journal of Analytical and Applied Pyrolysis*, *180*, 106527.

Shah, D. R. S. I., Anuar, N. F., Daud, W. M. A. W., Alias, A. B., & Aghamohammadi, N. (2025). Mechanistic exploration and optimization of amoxicillin adsorption using discarded disposable diapers (D3) activated carbon: A multi-analytical approach. *Journal of Industrial and Engineering Chemistry*.

Shah, D. R. S. I, Anuar, N. F., Jaafar, M. I., Daud, W. M. A. W., & Aghamohammadi, N. (2025). Towards a greener future of sustainable and circular practices in resource recovery from discarded disposable diaper (D3): a systematic review and meta-analysis. *Journal of Material Cycles and Waste Management*, 1-22.